Response of the Southern Ocean circulation to changes in global climate

Adele K. Morrison

Research School of Earth Sciences,
The Australian National University, Canberra, Australia

March 2014

A thesis submitted for the degree of Doctor of Philosophy of
The Australian National University

THE AUSTRALIAN
LIBRARY
NATIONAL UNIVERSITY

Except where otherwise indicated, this thesis is my own original work.

Adele K. Morrison
March, 2014

Acknowledgements

Andy Hogg was an amazing supervisor. He was forever patient when progress was slow and never failed to make time for a question or chat. I am extremely grateful for his encouragement to continue with academia, despite my protest. I don't believe I could have found a better supervisor.

It was a pleasure to collaborate with Matt England and Oleg Saenko on the final two chapters of my thesis. Their enthusiasm for the research and attention to detail helped the projects progress smoothly and simply.

I am grateful to Ross Griffiths for nurturing and sustaining the friendly and welcoming GFD group; it has been a thoroughly enjoyable place to work over the last fours years, and no doubt I will miss the lunch, coffee and Friday beer routines. Thanks to everyone in the GFD group, with special mention to Kial, Marshall, Isa, Kate and Chris for all the fun, beer and adventures.

Abstract

The Southern Ocean circulation plays a central role in the dynamics of past and future global climate change. However, due to a scarcity of observations and the difficulty of accurately modelling the Southern Ocean, we lack a comprehensive understanding of how the circulation responds to change. The energetic eddy field directly impacts the response of the circulation, but the small scale of the eddies has generally been below the resolution of numerical ocean models. This thesis makes use of two high resolution idealised ocean models to investigate the role of eddies in modifying the response of the Southern Ocean circulation to changing wind stress and surface buoyancy forcing.

The simulations demonstrate that the eddy field is significant in the dynamical response, but that the impact on different aspects of the circulation is complex and subtle. The Antarctic Circumpolar Current (ACC) transport increases only weakly in response to enhanced Southern Ocean wind stress, due to the enhanced eddy field, which efficiently eliminates momentum input. In contrast, the eddy field only partially compensates wind-driven increases in the upper overturning circulation, resulting in a moderate overturning increase in response to enhanced westerly winds. Southern Ocean heat uptake is also shown to be dependent on changes in the eddy field. Mid-depth warming occurs primarily due to a decrease in the upward eddy heat flux, associated with reduced isopycnal temperature gradients in a warmer climate. However, increased wind stress may reduce the mid-depth heat uptake; a transient cooling trend arises from the wind-driven enhancement of the vertical eddy heat flux.

The uncoupled idealised models also permit an in-depth analysis of the response of the Southern Ocean overturning to changes in surface buoyancy forcing. A suite of buoyancy forcing perturbations show that mid-latitude heat and freshwater fluxes may be as significant as wind stress in altering the strength of the upper overturning circulation. Analysis of the transient model response to a range of surface buoyancy forcing perturbations also indicates that recent observations are consistent with a slowdown of the lower overturning cell.

In summary, this thesis has refined our understanding of how the large scale Southern Ocean circulation responds to atmospheric change and the role of the eddy field in modifying that response. This work provides a basis to interpret the more complicated response of coupled and coarse resolution models.

Contents

Acknowledgements v

Abstract vii

Preface xi

1 Introduction 1
- 1.1 Southern Ocean circulation 1
  - 1.1.1 Mean state 1
  - 1.1.2 Sensitivity to surface forcing 4
- 1.2 Glacial-interglacial cycles and the Southern Ocean 6
- 1.3 Anthropogenic climate change and the Southern Ocean 7
- 1.4 Research orientation 8

2 Sensitivity of the Southern Ocean overturning circulation to surface buoyancy forcing 11
- 2.1 Introduction 11
- 2.2 Model 12
- 2.3 Results 15
- 2.4 Discussion 17

3 On the relationship between Southern Ocean overturning and ACC transport 21
- 3.1 Introduction 21
- 3.2 Numerical model and experiments 23
- 3.3 Results 25
  - 3.3.1 Mean state and eddy kinetic energy 25
  - 3.3.2 Overturning response 26
  - 3.3.3 ACC response 27
- 3.4 Discussion and conclusions 29

4 The role of vertical eddy flux in Southern Ocean heat uptake 33
- 4.1 Introduction 33
- 4.2 Numerical Model 35
- 4.3 Mean Vertical Heat Transport 36
- 4.4 Response to Idealised Climate Change Scenarios 37
  - 4.4.1 Surface Warming 37

4.4.2 Enhanced Southern Wind Stress 39
4.4.3 Combined Warming and Enhanced Wind Stress 40
4.5 Discussion and Conclusions 40

5 Southern Ocean surface cooling in response to a warming perturbation in an eddy permitting ocean model 43
5.1 Introduction 43
5.2 Numerical model 45
5.3 Surface response to buoyancy forcing perturbations 48
5.3.1 Freshwater perturbations 48
5.3.2 Warming perturbations 49
5.4 Heat and salt budgets 50
5.4.1 Methods 50
5.4.2 Freshwater perturbations 53
5.4.3 Warming perturbations 55
5.5 Response of the lower overturning cell 57
5.5.1 Overturning transport 57
5.5.2 Abyssal temperature and salinity 59
5.6 Comparison to observations 60
5.7 Discussion and summary 62

6 Conclusions 67
6.1 Summary 67
6.2 Future directions 68
6.2.1 Ocean-atmosphere coupling 68
6.2.2 Detecting change in the Southern Ocean overturning 68
6.2.3 How eddy saturated is the ocean? 69
6.2.4 Improved observations 70

Preface

The main body of this thesis is comprised of four chapters (2-5), each of which is a manuscript written for journal publication. These manuscripts have reached various stages in the review process, as outlined below. Except where referenced, the material presented in this thesis is entirely based on my own work, with the coauthors involved in interpretation of results and editing.

Chapter 2: Morrison, A. K., A. McC. Hogg, and M. L. Ward, 2011: Sensitivity of the Southern Ocean overturning circulation to surface buoyancy forcing. *Geophysical Research Letters*, **38**, L14602.

Chapter 3: Morrison, A. K., and A. McC. Hogg, 2013: On the relationship between Southern Ocean overturning and ACC transport. *Journal of Physical Oceanography*, **43**, 140-148.

Chapter 4: Morrison, A. K., O. A. Saenko, A. McC. Hogg, and P. Spence, 2013: The role of vertical eddy flux in Southern Ocean heat uptake. *Geophysical Research Letters*, **40**, 5445-5450.

Chapter 5: Morrison, A. K., M. H. England, and A. McC. Hogg, 2014: Southern Ocean surface cooling in response to a warming perturbation in an eddy permitting ocean model. *Journal of Climate*, Submitted.

Chapter 1

Introduction

The Southern Ocean overturning circulation provides a unique pathway for the deep water masses of the global ocean to return to the surface, creating a mechanism for the transfer of carbon and heat between the deep ocean and the atmosphere (Marshall and Speer, 2012). The strength of upwelling in the Southern Ocean controls the release of CO_2 from the ocean and is therefore central to the dynamics of past (Sigman et al., 2010) and future (Takahashi et al., 2012) global climate change. Evidence suggests that the atmospheric CO_2 changes at the heart of the cyclic glacial-interglacial transitions over the last million years were driven by physical changes in the rate of Southern Ocean upwelling (Skinner et al., 2010). Meanwhile, present-day absorption of carbon and heat by the Southern Ocean is a significant mitigating influence on the rate of anthropogenic atmospheric warming (Sabine et al., 2004; Levitus et al., 2012). Yets the pathways, volume transport and controlling forcing of the Southern Ocean circulation remain poorly understood compared with other regions of the world's oceans. The remoteness and severity of the environment has led to a paucity of observations, both spatially and temporally, while the computational burden of resolving the small scale eddy field has slowed numerical modelling progress.

This introductory chapter reviews our current understanding (prior to the results of this thesis) of the large scale circulation in the Southern Ocean and the role it plays in global climate. Section 1.1 introduces the Southern Ocean circulation: the different components and their sensitivity to changing atmospheric forcing, and some of the open questions and challenges in the field. Sections 1.2 and 1.3 provide motivational background for the research in this thesis, addressing the dynamical role of the Southern Ocean overturning circulation in glacial-interglacial cycles and anthropogenic climate change.

1.1 Southern Ocean circulation

1.1.1 Mean state

The unblocked circumpolar passage around Antarctica permits two unique features of the global ocean circulation, shown schematically in Figure 1.1. One is the world's largest ocean current - the eastward flowing Antarctic Circumpolar Current (ACC) - with a volume transport of $\sim$140 Sv (1 Sv = 10^6 m^3s^{-1}; Cunningham et al., 2003). The other is the upwelling limb of the meridional (north-south) overturning circulation, which transports deep waters formed around Antarctica and in the North Atlantic back to the surface.

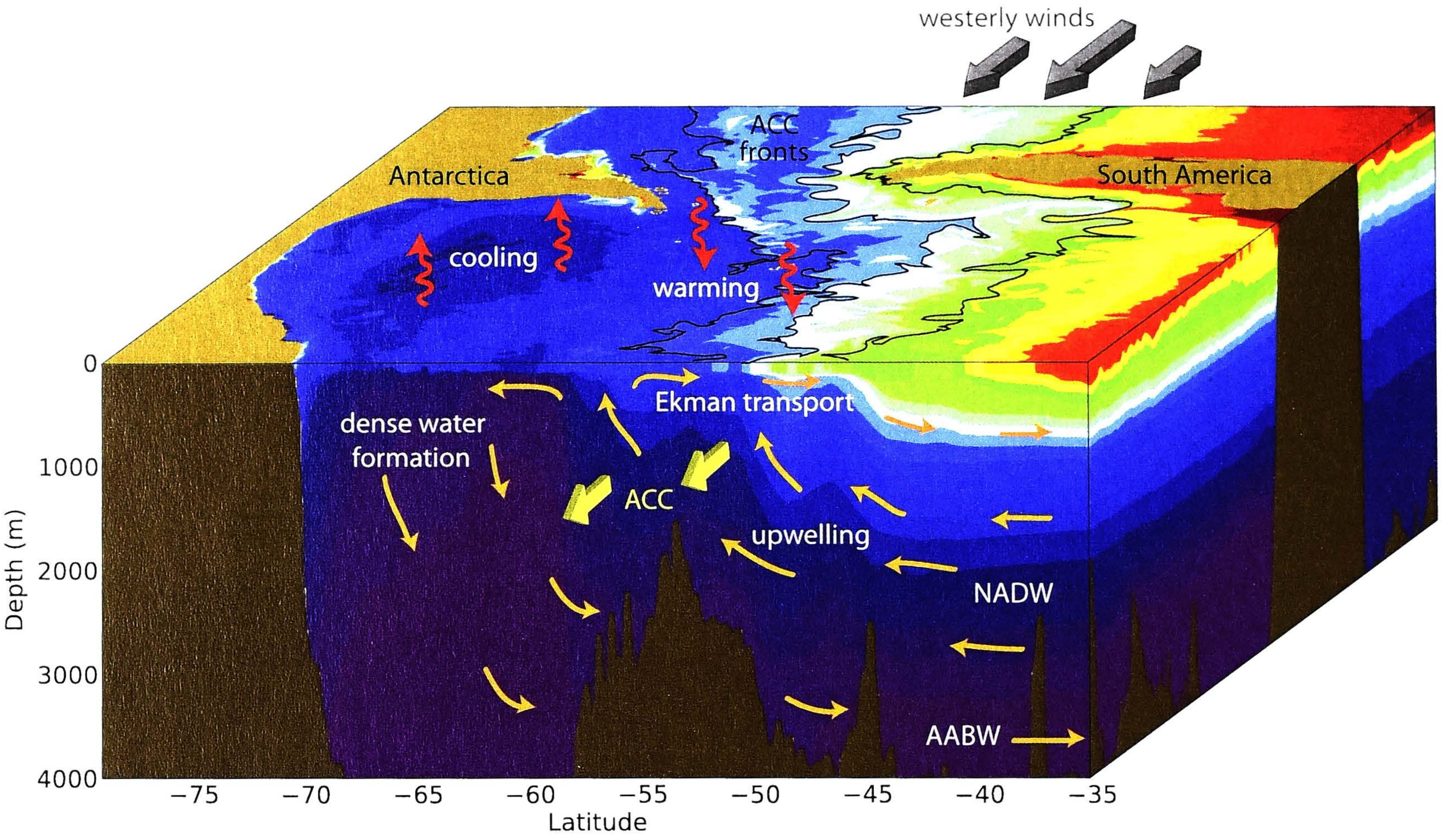

Figure 1.1: Schematic of the large scale Southern Ocean circulation. Isopycnal layers (colour shows ocean density) tilt up towards Antarctica on the left, linked to the zonal Antarctic Circumpolar Current (ACC; yellow arrows and black streamlines) through a thermal wind balance. Upwelling modified North Atlantic Deep Water (NADW) splits at the surface into the two branches of the meridional overturning circulation. Warming and freshening permits northward Ekman transport in the surface layer to close the upper cell, while dense water formation near the coast of Antarctica replenishes the lower cell with Antarctic Bottom Water (AABW). [Figure constructed from data sourced from a global MOM4 simulation run by Paul Spence.]

The strongly tilted density layers (isopycnals) in the Southern Ocean are central to both the ACC and the overturning circulation. A combination of strong westerly winds and surface heat and freshwater fluxes set the mean stratification. The winds drive a thin Ekman layer, which, due to the rotation of the Earth, transports water northward in the upper few hundred metres of the ocean. The northward movement of the surface waters tilts up the isopycnals in the south, so that modified North Atlantic Deep Water (NADW) outcrops at the surface. The available potential energy stored in the tilted isopycnals is released into mesoscale eddies - coherent vortices roughly 10–50 km in size - through a process known as baroclinic instability. The eddy field acts to oppose the wind-driven steepening of the isopycnals and the resulting isopycnal slopes are primarily a balance between the competing effects of the Ekman and eddy-driven contributions. Latitudinally varying heat and freshwater fluxes at the surface also contribute to setting the mean stratification in the Southern Ocean.

South of the wind stress maximum, the latitudinal variation in wind stress creates a divergence in the surface Ekman transport, which draws up modified NADW from below. Deep water upwells southward and approximately adiabatically along the sloping isopycnals (i.e. with little mixing across density layers until it reaches the surface). Below the level of the shallowest topography in the unblocked passage (occurring at Drake Passage - the gap between Antarctica and South America), the southward flow may be sustained by zonal (east-west) pressure gradients across the topography. Above the Drake Passage sill, upwelling is only possible through the mass flux induced by the eddy field, which occurs via zonal variations in the thickness of isopycnal layers, giving rise to the necessary pressure gradients to drive the meridional flow (Speer et al., 2000b). If the meridional transports are integrated along lines of latitude (known as a zonally averaged framework), two separate Southern Ocean overturning cells are clear, with the upwelling waters dividing into two branches at the surface (Figure 1.1). The upper cell returns lighter water masses, after warming and freshening at the surface, northward towards the equator in the upper Ekman layer. Sea ice forming polynyas around Antarctica modify the upwelled waters entering the abyssal cell, returning cold, dense Antarctic Bottom Water (AABW) northward along the bottom topography.

Viewed in three dimensional space, observations suggest that the global overturning circulation is rather more complicated and interconnected than what is implied by the simplified zonally averaged picture (Lumpkin and Speer, 2007; Marshall and Speer, 2012; Talley, 2013). In this framework, the two overturning cells are intrinsically connected. After upwelling in the Southern Ocean, modified NADW flows primarily southward (not northward) at the surface to form bottom water around Antarctica and fill the abyss of the Indian and Pacific basins as AABW. The deep water formation regions in the North Atlantic are fed primarily from water masses most recently upwelled in the Southern Ocean from the AABW pathway via the Indian and Pacific basins, instead of the direct NADW pathway. Rather than the two nearly independent overturning cells that appear in the zonal-average framework, the new global conceptual picture more closely resembles a single loop, linking all ocean basins and deep water formation regions. However, while our understanding of the dynamical controls on the overturning remains far from complete, progress can be made through attempts to first understand the overturning in a simplified framework.

The upwelling is distributed around the Southern Ocean and, despite its importance for global climate, has a transport of roughly one fifth the magnitude of the ACC transport. Assuming evenly distributed circumpolar upwelling and a net transport of 30 Sv, the mean vertical velocity is only ~50 m/yr. With present measurement techniques, it is impossible to directly measure such small velocities against the large background noise of the eddy field, which may induce transient vertical velocities of up to 200 m/day (Rivas et al., 2008). Knowledge of the pathways and transport of the overturning circulation has therefore been inferred from indirect methods, such as tracing of water mass properties (e.g. temperature, salinity, oxygen) in hydrographic sections. However, the scarcity of measurements results in large uncertainties in the observational transport estimates of ~30-60% (Talley, 2008). The necessity of resolving eddies, due to their central role in the upwelling above topography, has also slowed progress in numerical modelling of the Southern Ocean overturning circulation.

The Antarctic Circumpolar Current arises through a thermal wind balance with the meridional density gradient. That is, the strength of the ACC transport is directly related to the slope of the isopycnals in the Southern Ocean (Rintoul et al., 2001). Satellite observations and high resolution idealised numerical models have illustrated the complex structure of the ACC (e.g. surface streamlines in Figure 1.1). The energetic Southern Ocean eddy field splits the current into multiple jets that divide and merge along the circumpolar path.

1.1.2 Sensitivity to surface forcing

The significance of the Southern Ocean for global climate arises largely due to the capacity of the ocean circulation to respond to changes in external forcing. However, the dynamics of how the circulation responds to forcing perturbations is uncertain. The sensitivity of the Southern Ocean overturning to changing wind stress and buoyancy fluxes is one of the largest unknowns in solving the puzzle of glacial-interglacial transitions, as well as in predicting the extent of future climate change.

The upper overturning circulation in the Southern Ocean is commonly considered to be wind-driven, due to the central role of the divergent surface Ekman transport in driving upwelling (Toggweiler and Samuels, 1993; Marshall and Speer, 2012). In this simple view, uniform increases in wind stress enhance the divergence and therefore the rate of upwelling. Coarse resolution modelling studies support this theory, showing overturning increasing in proportion to westerly wind stress (Saenko et al., 2005). However, over the last decade, models that partially resolve the eddy field, known as eddy permitting models, have shown that the response of the eddy field to changing wind stress complicates the simple wind-driven theory (Hallberg and Gnanadesikan, 2006; Farneti et al., 2010). Eddies act to relax the isopycnal tilt, effectively providing a southward mass transport in the surface layers of the Southern Ocean. As the wind stress increases, the eddy field increases approximately linearly (Hallberg and Gnanadesikan, 2006; Abernathey et al., 2011; Meredith et al., 2012), causing an increase in the southward transport, which opposes the wind-driven increase in the northward Ekman transport. Therefore in the presence of eddies, the overturning sensitivity to wind stress is decreased. This phenomenon is termed *eddy compensation*. Extrapolating from the results of coarse resolution and eddy permitting studies, it has been hypothesised that, in eddy resolving models or the real ocean, wind-driven increases in the southward eddy transport may exactly counteract increases in the northward Ekman transport (Hallberg and Gnanadesikan, 2006; Farneti et al., 2010). Such perfect eddy compensation would yield the upper overturning cell completely insensitive to changes in wind stress.

Nearly all sensitivity studies of the upper overturning circulation have focused on the response to wind stress changes, due to the wind-driven overturning hypothesis of Toggweiler and Samuels (1995). However, air-sea fluxes of heat and precipitation in the mid-latitudes also play a critical role in the overturning dynamics by allowing the conversion of dense upwelled water masses into the lighter water masses of the Ekman layer (Speer et al., 2000b). While it has been proposed that changing mid-latitude buoyancy fluxes may have played a significant role in driving the enhanced overturning and outgassing following the Last Glacial Maximum (Watson and Naveira Garabato, 2006), the idea has not been extensively tested.

There is some confusion over the influence of wind stress on the lower overturning cell. The proposed theory of Toggweiler et al. (2006) for the Southern Ocean control on the glacial-interglacial atmospheric CO_2 variability relied on an enhancement of the lower overturning cell with increased or southerly shifted westerly winds. Several numerical modelling studies have demonstrated an increase in the lower overturning cell in response to enhanced westerly winds, but have failed to produce the required control on atmospheric CO_2 (Menviel et al., 2008; Tschumi et al., 2008; D'Orgeville et al., 2010). Recent theoretical scaling arguments predict the opposite: that the strength of the lower cell decreases as wind stress increases (Nikurashin and Vallis, 2012). An analysis of the third Coupled Model Intercomparison Project (CMIP3) models also suggests that stronger wind stress would weaken the abyssal overturning in the Southern Ocean (Saenko et al., 2012). Meanwhile Stewart and Thompson (2012) find that, although the abyssal overturning is relatively insensitive to the midlatitude westerlies, there may be a strong dependence on the weaker polar easterlies. In their model, increases in the easterly wind stress near the coast of Antarctica reduce eddy activity over the continental slope, thereby increasing the dominance of the mean wind-driven component of the overturning. While the sensitivity of the lower overturning circulation to changing wind stress remains unclear, a solution for the Southern Ocean control on the atmospheric CO_2 concentration could lie with the dynamics of the upper overturning cell. Lauderdale et al. (2013) ran a series of Southern Ocean simulations with varying wind stress and buoyancy forcing and found a linear relationship between the strength of the upper overturning cell and atmospheric CO_2.

Furthermore, buoyancy forcing is a more prominent controlling factor on the sensitivity of the abyssal overturning circulation. Sea ice formation on Antarctic shelves creates cold, salty shelf waters, which descend the continental slope to form Antarctic Bottom Water. Modelling studies with increases in either atmospheric CO_2 or melting of Antarctic ice sheets respond with a reduction in the volume and density of dense water production (e.g. Stouffer et al., 2007; Swingedouw et al., 2008; Menviel et al., 2010). In many models this reduction in deep water formation leads to a dramatic shut down of the lower overturning cell. However, the air-sea heat and freshwater flux thresholds which may result in a shutdown of the lower overturning cell in the real ocean are unknown, due to the inaccessibility of the Antarctic dense water formation regions and the difficulty of modelling the small-scale convective structures.

Finally, the transport of the ACC may be influenced by any factor that can change the tilt of the Southern Ocean isopycnals. Local surface heat and freshwater flux perturbations may change the density structure of the water column and therefore the ACC transport (Gent et al., 2001; Hogg, 2010). Reorganisation of the deep ocean stratification through changes in remote (e.g. Northern Hemisphere) forcing also affects ACC transport (Fučkar and Vallis, 2007). However, models and observations indicate that ACC transport is only weakly sensitive to changes in wind stress (Meredith and Hogg, 2006; Hallberg and Gnanadesikan, 2006; Farneti et al., 2010; Jones et al., 2011). The limited sensitivity of the ACC transport is thought to be a result of the near linear response of the eddy kinetic energy to increasing wind stress. As the enhanced wind stress acts to steepen isopycnals, a more active eddy field opposes by flattening the isopycnals. This mechanism is known as *eddy saturation* (distinct from eddy compensation, which refers to limiting of the overturning sensitivity).

1.2 Glacial-interglacial cycles and the Southern Ocean

Pockets of gas trapped in Antarctic and Greenland ice cores reveal a striking pattern in the history of atmospheric CO_2 (Figure 1.2; Petit et al., 1997). Cold glacial periods with low atmospheric CO_2 are terminated by rapid warming and enhanced atmospheric CO_2, with a cyclic period of roughly 100,000 years. The regularity of the glacial-interglacial transitions, without an obvious trigger or dynamical sequence, has confounded scientists for decades (e.g. Siegenthaler and Wenk, 1984; Sigman and Boyle, 2000; Broecker, 2009; Fischer et al., 2010).

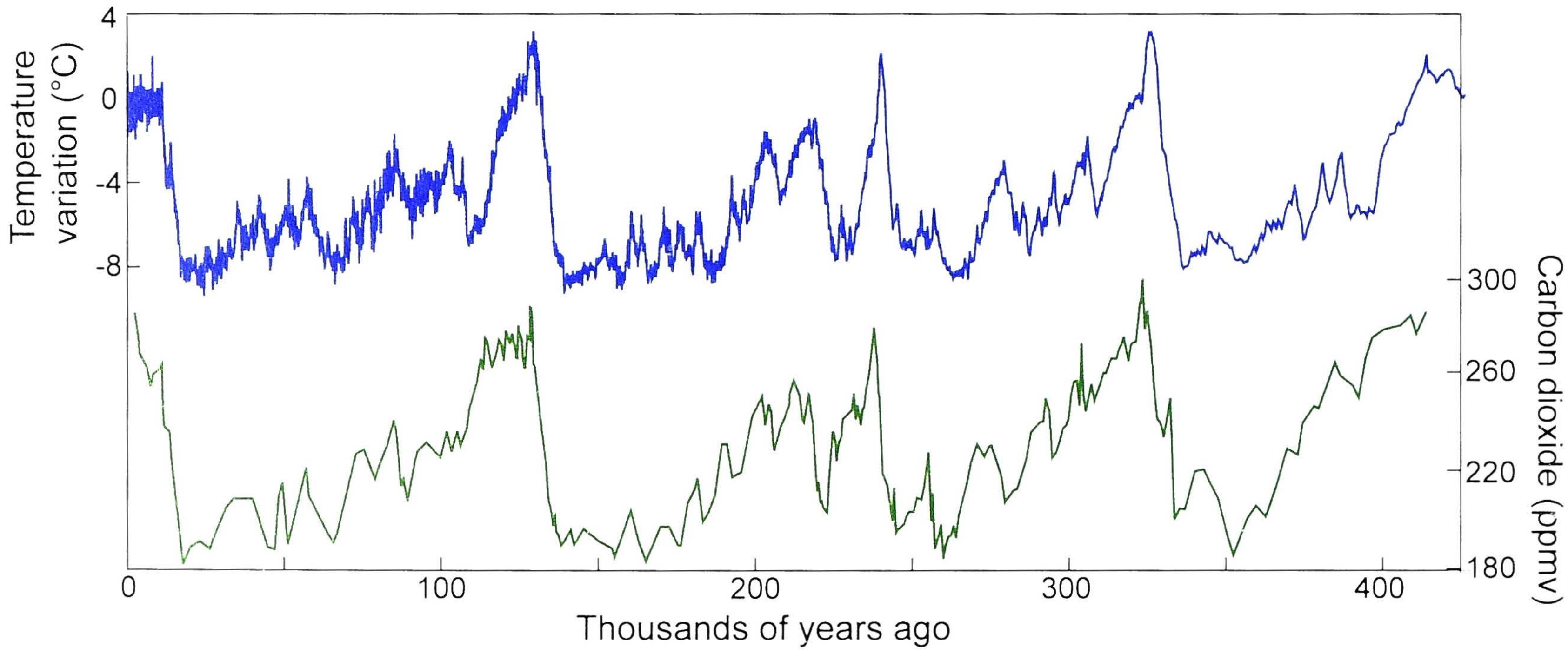

Figure 1.2: Data from the Vostok ice core in Antarctica, showing the last four glacial cycles (from Petit et al., 1997). a) Variation in Antarctic temperature relative to preindustrial climate. b) Atmospheric CO_2 concentration. Note that the time axis is reversed.

A major breakthrough came from the record of atmospheric radiocarbon, ^{14}C, over the last glacial cycle (Hughen et al., 2006). ^{14}C is formed in the atmosphere through the interaction of cosmic rays with nitrogen and decays with a half-life of ~6000 years. As the Earth warmed over the last 20,000 years (since the Last Glacial Maximum) and atmospheric CO_2 increased, the atmospheric ^{14}C concentration simultaneously decreased. The drop in ^{14}C implicates glacial carbon storage in the deep ocean, resulting in an isolated aged carbon reservoir. Skinner et al. (2010) located a deep Southern Ocean water mass with a corresponding glacial-interglacial history of ^{14}C, providing observational evidence that the interglacial rise in atmospheric CO_2 is closely linked to Southern Ocean upwelling rates.

Debate is ongoing about the relative roles of upwelling from the upper or lower overturning cells and whether the changes in upwelling were primarily wind or buoyancy driven. As outlined in Section 1.1.2, Toggweiler et al. (2006) proposed that atmospheric CO_2 increased as a result of enhanced upwelling and outgassing from the lower cell, driven by increased or southerly shifted westerly winds. They argue that only changes in the lower overturning cell can be important, because the upwelled carbon is drawn from depths >2000 m. Yet paleoceanographic models have failed to demonstrate a link between the strength of the lower overturning cell and atmospheric CO_2 concentration (Menviel et al., 2008; Tschumi et al., 2008; D'Orgeville et al., 2010). Furthermore, recent theory and coupled model analyses suggest that the lower overturning cell actually scales inversely with westerly wind stress (Nikurashin and Vallis, 2012; Saenko et al., 2012). An alternative hypothesis is that carbon outgassing increased following the Last Glacial Maximum due to an enhancement of the upper overturning cell, driven either by increased wind stress or increased heat and freshwater fluxes in the midlatitudes (Watson and Naveira Garabato, 2006). The question of how the abyssal carbon (at depths >2000 m) enters the upwelling limb of the upper overturning cell (usually <2000 m) may be solved by either increased interior vertical mixing (Watson and Naveira Garabato, 2006) or a wind-driven deepening of the upper cell (Barker et al., 2010; Nikurashin and Vallis, 2012). Further support for outgassing driven by changes in the upper cell, rather than the lower cell, is provided by the recent modelling study of Lauderdale et al. (2013), which found a linear relationship between the strength of the upper overturning cell and atmospheric CO_2.

1.3 Anthropogenic climate change and the Southern Ocean

There is a strong signature of human-induced climate change in the Southern Ocean. The warming trend is more intense and deep-reaching compared with the global average, due to the connection between the surface and deep ocean provided by the overturning circulation (Gille, 2008; Purkey and Johnson, 2010). Freshening also extends through the water column to the abyssal water masses (Durack and Wijffels, 2010; Purkey and Johnson, 2013).

The fast timescale of the Southern Ocean changes indicate that they have likely been driven by changes in the local forcing. Due to changes in both atmospheric ozone and CO_2 forcing, the westerly winds have strengthened and shifted southward (Thompson and Solomon, 2002; Marshall, 2003). Climate models predict that this trend will likely continue in the future, despite ozone recovery (Bracegirdle et al., 2013). Surface air temperatures have increased (Chapman and Walsh, 2007). It is likely that precipitation over far southern latitudes has also increased due to an amplified hydrological cycle (Durack et al., 2012) and positive trend in the Southern Annular Mode (Karoly, 2003). Freshwater input into the Southern Ocean from Antarctic ice sheet melt is also accelerating (Rignot et al., 2011).

Due to the uncertainty in the sensitivity of the Southern Ocean circulation, it remains unclear what effect these forcing changes will have on the ACC and overturning circulation. An observational analysis of recent changes in the zonally averaged isopycnal slopes in the Southern Ocean concluded that there have been no detectable changes in the ACC transport to date (Böning et al., 2008). Several studies have suggested that the upper overturning circulation may have increased in response to enhanced westerly winds, using indirect observations including an inverse calculation of atmospheric CO_2 history (Le Quéré et al., 2007), trends in ship-based pCO_2 measurements (Takahashi et al., 2012) and spatial patterns of change in ocean chlorofluorocarbon concentrations (Waugh et al., 2013). While the individual uncertainty in each of these methods prohibits a conclusive result, the agreement between them adds plausibility to the hypothesis that the upper overturning cell may be strengthening due to climate change. Changes in the upper overturning circulation may have severe implications for the rate of global warming. The oceans have absorbed 30% of the additional CO_2 that humans have released into the atmosphere over the period 1960-2008 (Le Quere et al., 2009). Around half of that CO_2 has been absorbed south of 30°S (Takahashi et al., 2012), due to the overturning of water masses by the Southern Ocean circulation. Enhanced upwelling would likely increase the outgassing of natural carbon from the deep ocean, offsetting the uptake of anthropogenic carbon in the short term (Le Quéré et al., 2007; Takahashi et al., 2012). The resultant increase in atmospheric CO_2 and temperature could lead to a positive feedback, driving further increases in the strength of upwelling and outgassing in the Southern Ocean.

Observations of the abyssal Southern Ocean indicate that Antarctic Bottom Water is warming (Purkey and Johnson, 2010; Kouketsu et al., 2011) and freshening (Purkey and Johnson, 2013). Kawano et al. (2010) inferred that the warming may be linked to a change in the transport of the lower overturning circulation, since the observed warming pattern is concentrated on AABW pathways and depth levels. Kouketsu et al. (2011) also hypothesised a reduction in transport of the lower overturning cell, based on the correlation in their ocean reanalysis data between the abyssal warming and AABW transport. However, actual transport observations are too scarce and uncertain to conclusively show a change in the lower overturning cell (Shimada et al., 2012). It remains possible that the remote changes in AABW properties may be caused by temperature and salinity changes at the formation regions, or enhanced deep mixing, rather than reduced volume fluxes.

1.4 Research orientation

The research presented in this thesis has been able to contribute to long-standing questions in the field through the use of an idealised, high resolution ocean modelling approach. While many previous studies have used more comprehensive models, such as the global coupled models used for the Intergovernmental Panel on Climate Change (IPCC) reports, the computational demand of incorporating many different climate system elements restricts the resolution of such models and thereby introduces the need for parameterisation of the eddy field. Smaller domain, high resolution uncoupled ocean models have the advantage of explicitly resolving the eddy field, which has an order one effect on the response of the Southern Ocean circulation. Although the exact quantitative response of the Southern Ocean circulation can not be determined using idealised models, the dynamical insights gained through these methods have significantly advanced progress in understanding the Southern Ocean circulation and its role in global climate.

The first two chapters are a sensitivity analysis of the upper overturning circulation in the Southern Ocean in response to changing atmospheric forcing. Chapter 2 investigates the influence of midlatitude buoyancy forcing on the strength of the upper overturning cell. In Chapter 3, the extent of eddy compensation and eddy saturation are examined under a range of wind stress perturbations and model resolutions.

The final two chapters seek to explain elements of the temperature changes that have been observed in the Southern Ocean in recent decades, through an improved understanding of the changes in ocean circulation. Chapter 4 presents an investigation of possible mechanisms affecting the accelerated mid-depth heat uptake in the Southern Ocean midlatitudes. The role of eddies and changes in the upper overturning circulation in modifying both wind and surface warming driven changes in heat content are assessed. Chapter 5 brings attention to observations of recent sea surface temperature cooling south of 50°S in the Southern Ocean. The observations are compared to the transient response of an idealised model to surface warming and freshwater perturbations and a possible ocean-driven mechanism is put forward to explain the cooling trend.

Chapter 2

Sensitivity of the Southern Ocean overturning circulation to surface buoyancy forcing

Abstract

The sensitivity of the Southern Ocean overturning to altered surface buoyancy forcing is investigated in a series of eddy-permitting, idealised simulations. The modelled response indicates that heat and freshwater fluxes in the Southern Hemisphere mid-latitudes may play a significant role in setting the strength of the overturning circulation. Enhanced buoyancy fluxes act to increase the meridional overturning up to a limit approaching the wind-driven Ekman transport. The sensitivity of the overturning to surface buoyancy forcing is strongly dependent on the relative locations of the wind stress profile, buoyancy forcing and upwelling region. The numerical simulations provide support for the hypothesis that changes in upwelling during deglaciations may have been driven by changes in heat and freshwater fluxes, instead of, or in addition to, changes in wind stress.

2.1 Introduction

The southern limb of the oceanic meridional overturning circulation plays a key role in the Earth's response to climate change. The rise in atmospheric CO_2 at glacial-interglacial transitions has been attributed to outgassing of enhanced upwelling water masses in the Southern Ocean (Skinner et al., 2010), while subducting water masses currently represent a significant fraction of the global anthropogenic CO_2 sink (Gruber et al., 2009). Despite the significance of the Southern Ocean overturning to past and future climate change, the dynamics and sensitivity to forcing changes are poorly understood.

The upper cell of the Southern Ocean meridional overturning is commonly considered to be a wind-driven circulation, with dense waters upwelling along steeply tilted isopycnals, driven by divergent Ekman transport at the surface (Toggweiler and Samuels, 1993). Coarse resolution modelling studies support this theory, showing overturning increasing in proportion to westerly wind stress (Saenko et al., 2005). More recently, investigations into the response of the overturning to changing wind stress in eddy-permitting models have revealed the significance of the eddy field to the overturning dynamics; increases in

Ekman transport are at least partially compensated by increases in opposing eddy-induced transport, implying only a weak sensitivity of the net residual overturning transport to wind stress (Hallberg and Gnanadesikan, 2006; Viebahn and Eden, 2010; Farneti et al., 2010). The focus of these modelling studies has been on the effect of wind stress forcing on the overturning, while very little modelling work has examined the response of the overturning to changes in surface buoyancy forcing.

Air-sea fluxes of heat and precipitation over the Antarctic Circumpolar Current (ACC) region are necessary for the conversion of dense upwelled water masses into lighter waters at the surface (Speer et al., 2000b). Theoretical frameworks, based on zonally averaged representations of the meridional overturning circulation (Marshall and Radko, 2003; Radko and Kamenkovich, 2011), show the magnitude of the overturning increasing linearly with the net buoyancy flux supplied to the surface mixed layer. While the effect of mid-latitude buoyancy fluxes on the overturning has not been extensively tested in an eddy-permitting numerical model, coarse resolution simulations have highlighted the link between southern hemisphere mid-latitude freshwater forcing and the formation of deep water in the North Atlantic (Saenko et al., 2003). It has also been proposed that the increase in atmospheric CO_2, observed at the end of the last glacial maximum, was a result of increased upwelling in the Southern Ocean, driven by an increased surface buoyancy flux (Watson and Naveira Garabato, 2006). In addition, observational studies have shown that heat and freshwater fluxes into the Southern Ocean have increased over the past few decades (Böning et al., 2008) and modelling studies suggest that this trend will continue with future climate change (Bracegirdle et al., 2008). However, due to the sparse coverage of flux data in the Southern Ocean and the difficulties of investigating buoyancy forcing in coupled climate models, the dependence of the meridional overturning on surface buoyancy forcing has not been fully explored.

In this paper we investigate the dependence of the overturning on surface buoyancy forcing in the mid-latitudes through a series of eddy-permitting, idealised simulations of the Southern Ocean.

2.2 Model

We use GOLD, the primitive equation, isopycnal layered ocean model of Hallberg and Gnanadesikan (2006), which is a recent adaptation of the Hallberg Isopycnal Model (Hallberg, 1995). The idealised domain is a zonally reentrant, 40° wide sector of the Southern Ocean with a simple Drake Passage-like sill (Figure 2.1a). A Mercator grid, with grid size decreasing towards the southern boundary, is employed at two different horizontal resolutions ($1/4^\circ$ and $1/8^\circ$), resulting in square grid cells of size 14 km ($1/4^\circ$) and 7 km ($1/8^\circ$) at 60°S. The latitudinal extent is from 70°S to the equator. A sponge of width 2° at the equator relaxes the density stratification to observational data (Levitus, 2010) at the northern boundary with a decay timescale of 1 day. This allows an effective parameterisation of North Atlantic Deep Water (NADW) formation, without constraining

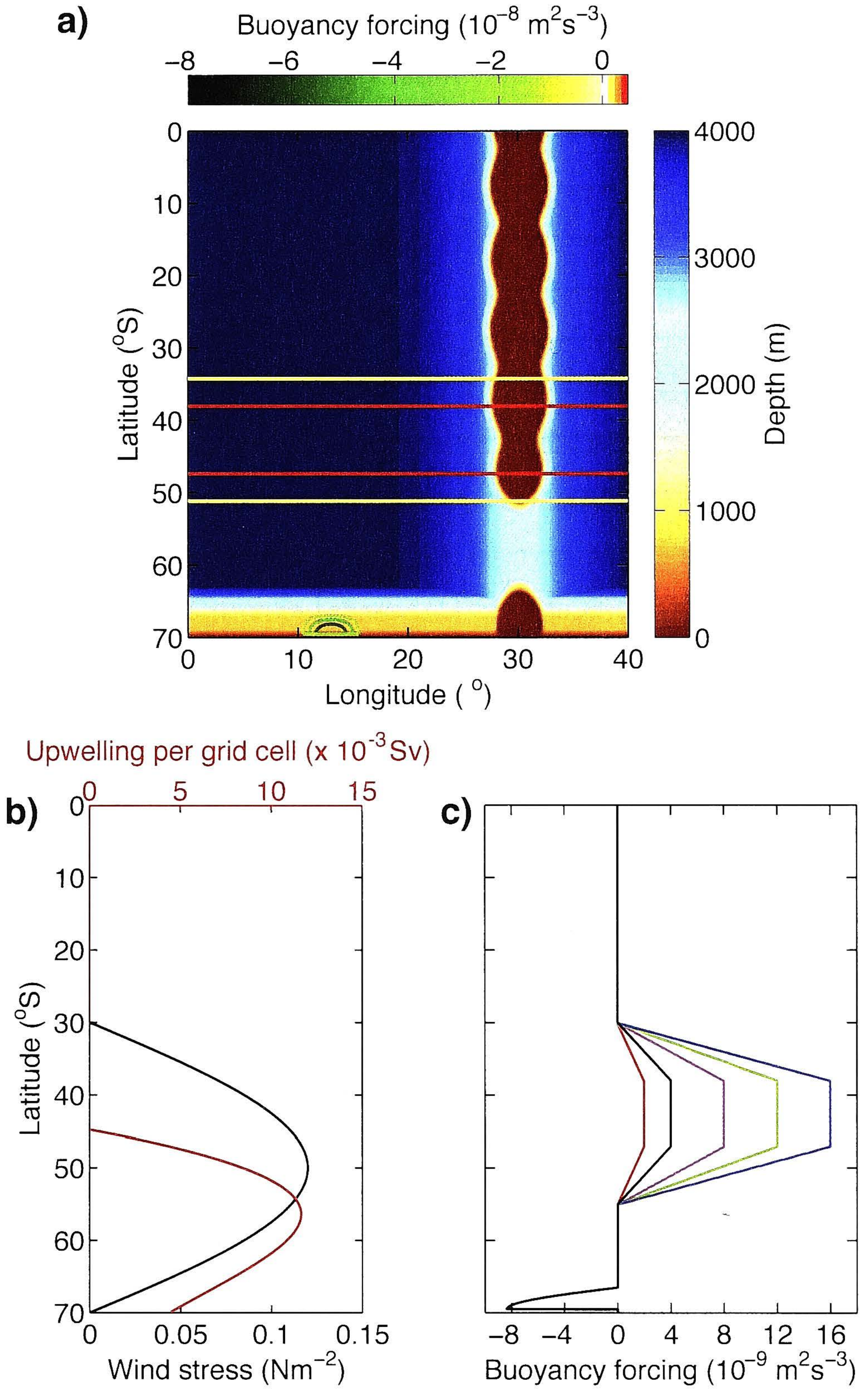

Figure 2.1: (a) Bathymetry, with spatial distribution of buoyancy forcing shown in contours. (b) Zonally averaged wind stress (black) and theoretical zonally integrated Ekman-induced upwelling in each meridional grid cell (red). (c) Zonally averaged buoyancy forcing (control in black, perturbations in colour).

incoming velocities. Bathymetry consists of an Antarctic shelf and Drake Passage-like sill, providing an unblocked circumpolar passage down to 2500 m below the surface, with a maximum ocean depth of 4000 m. A three layer bulk mixed layer is used, in addition to nine interior constant density layers (shown in Figure 2.2a). Biharmonic viscosity with an additional Smagorinsky component provides numerical closure. Biharmonic coefficients are set to 2×10^{11} m^4 s^{-1} ($1/4°$) and 2×10^{10} m^4 s^{-1} ($1/8°$). A weak diapycnal diffusivity of 10^{-6} m^2 s^{-1} in the interior ensures a largely adiabatic circulation. The control cases are spun up for ~120 years (Figure 2.2c). Perturbations from the end of the control spin-up are allowed to reach equilibrium (~30 years), and 25 year averages after these spin-up times were used for the results presented in this paper.

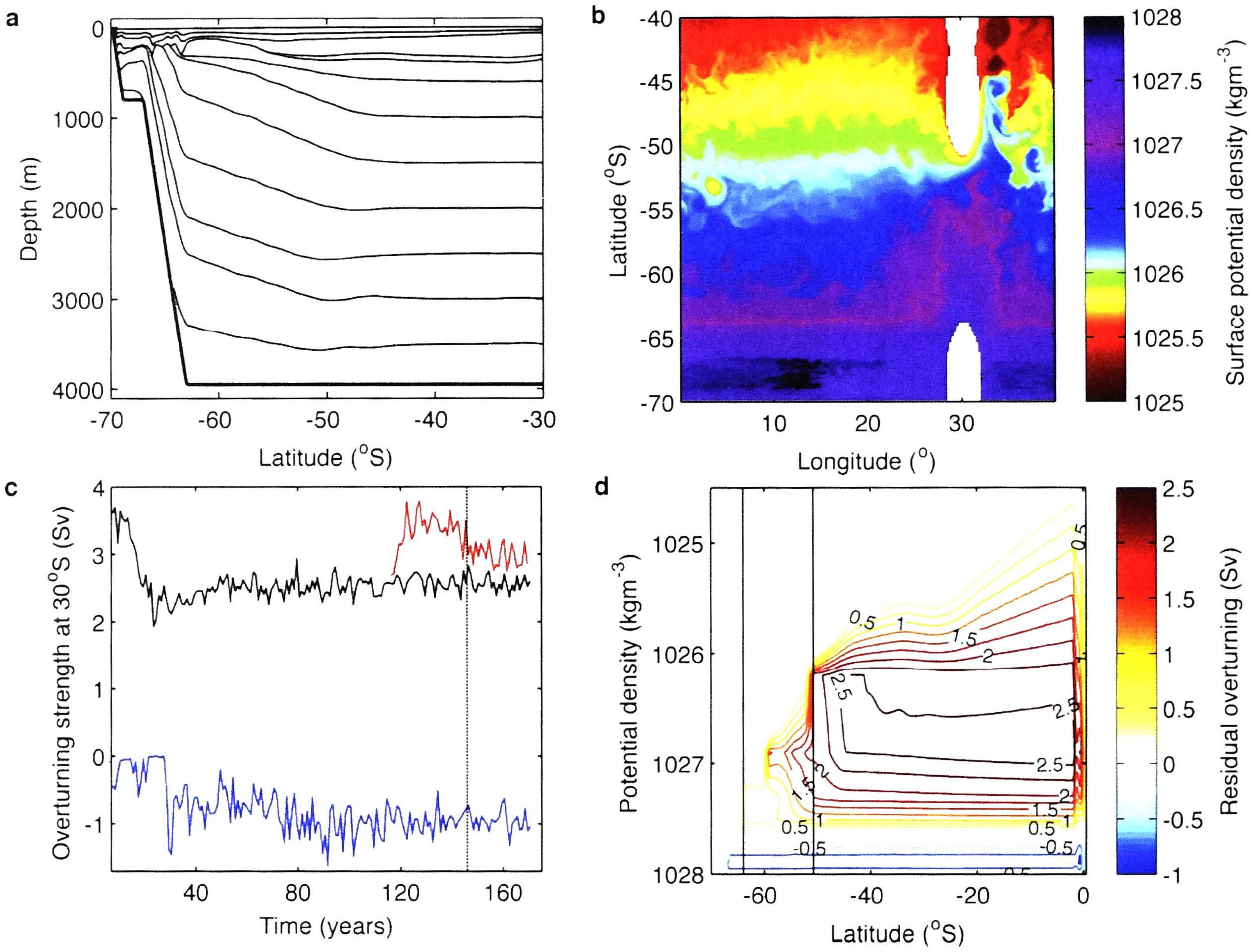

Figure 2.2: (a) Zonally and temporally averaged isopycnal layers for the 1/8° control simulation. (b) Snapshot of surface potential density for the 1/8° control simulation. (c) Timeseries of 1/8° overturning spinup. The maximum of the upper (lower) cell in the control run at 30°S is shown in black (blue), with the buoyancy forcing perturbation 16×10^{-9} m^2 s^{-3} shown in red. The vertical line indicates the point after which the 25 year averages were calculated. (d) Residual overturning streamfunction in density space for the 1/8° control simulation. Positive values (red) indicate clockwise transports, while negative values (blue) indicate anti-clockwise transports. The vertical black lines show the extent of the unblocked circumpolar passage (above the sill). Horizontal sections of the streamfunction imply adiabatic transport along isopycnal layers. Since the isopycnals are strongly tilted in the south, this also indicates upwelling.

The modelled residual overturning is forced by zonally and temporally invariant, sinusoidal winds, with a maximum of 0.12 N m^{-2} at 50°S (Figure 2.1b). The idealised buoyancy forcing used in the model (Figure 2.1a,c) is based on net heat and freshwater surface fluxes derived from several observational and reanalysis products. Sparse data coverage (and loosely constrained reanalyses) over the Southern Ocean is no impediment to this study, as our framework tests the sensitivity of the overturning to forcing changes, rather than simulating the exact structure and magnitude of the overturning. The region of mid-latititude positive buoyancy forcing (ie. acting to decrease the density of surface waters) in the control run has a magnitude of 4×10^{-9} m^2 s^{-3}, incorporating both heat and freshwater fluxes. The region of negative buoyancy forcing has a zonal average peaking at -8×10^{-9} m^2 s^{-3}, but is spatially localised (a necessary condition for the formation of an Antarctic Bottom Water cell in this model). We use a fixed, non-interactive buoyancy flux, to allow precise control of surface buoyancy forcing and an increased ability to isolate dynamical processes.

2.3 Results

The surface forcing generates a Southern Ocean-like state (Figure 2.2) with tilted isopycnals, an energetic eddy field with associated fronts and jets and two overturning cells which broadly resemble observations (Speer et al., 2000b). The lower Antarctic Bottom Water cell is driven principally by the negative buoyancy forcing near the southern boundary. The ACC transport in the model is 108 Sv in the 1/4° runs and 91 Sv in the 1/8° runs. The upper meridional overturning cell simulates the upwelling of NADW in the latitudes unblocked by bathymetry. Scaled up to the full width of the Southern Ocean, the transports of the upper and lower cells in Figure 2.2d would be 23 Sv and 9 Sv respectively. The meridional overturning in the model is largely adiabatic in the interior, with diapycnal transport occurring predominantly in the mixed layers, as allowed by the surface buoyancy forcing and diapycnal eddy transports.

As the mid-latitude surface buoyancy forcing is increased, so does the overturning in the upper cell (Figure 2.3), while the lower overturning cell is unaffected. Due to the adiabatic nature of the overturning, the changes in a single profile of the streamfunction (as shown in Figure 2.3a) are representative of the changes in the structure of the entire overturning cell. When surface buoyancy forcing is weak, the modelled overturning is substantially less than the magnitude of the wind-driven Ekman transport (Figure 2.3b). At progressively larger values of buoyancy forcing, the overturning approaches a limit close to the value of the Ekman transport (offset by the opposing eddy-induced transport). The simulated 1/8° overturning is less sensitive to buoyancy forcing than the overturning in the 1/4° model. Though it may appear that the reduced sensitivity in the 1/8° model is a result of eddy compensation, this is not the case; the eddy kinetic energy (EKE) is nearly insensitive to buoyancy forcing. In the 1/8° model, a doubling of buoyancy forcing increases EKE by less than 5%, whereas a doubling of wind stress increases EKE by more than 100%.

Increased buoyancy forcing results in an expected lightening of surface waters and an associated southward shift in the location of isopycnal layer outcropping (Figure 2.4a). The structure of the overturning in the interior remains largely unchanged and therefore the upwelling region also shifts southward, following the movement of the outcropping. Note that the data shown in Figure 2.4a indicates roughly the latitude of the northern edge of the upwelling, which is spread over a $5^\circ - 8^\circ$ latitude band. The limiting behaviour seen in Figure 2.4a arises due to the restricted range of the mid-latitude buoyancy forcing. There is nearly no change in the latitude of outcropping south of 50° - 55°S (Figure 2.4b). Therefore the upwelling shifts southward only so far as the mid-latitude buoyancy perturbations extend. The reduced surface density at high latitudes in the 1/8° model (as indicated by

Figure 2.4 and the 25% reduction in ACC transport compared with the 1/4° model) may be linked to an enhancement of the eddy field at higher resolution. EKE is around 40% higher in the 1/8° model and the increased eddy field acts to reduce the tilt of isopycnal layers near the surface, resulting in more southerly outcropping in the higher resolution case.

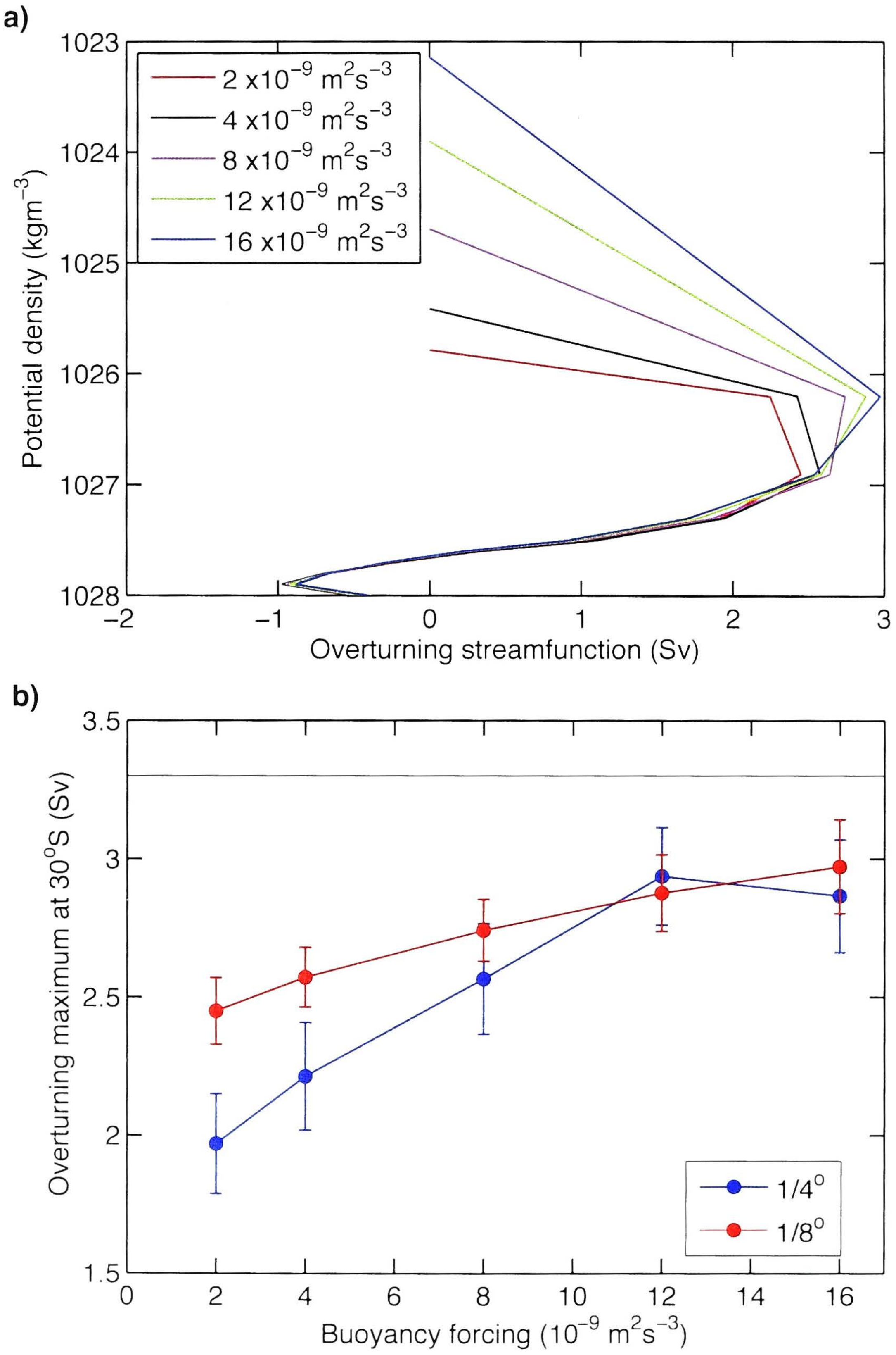

Figure 2.3: (a) Transects of the overturning streamfunction (such as shown in Figure 2.2d) at 30°S for a range of buoyancy forcing perturbations, run at 1/8° resolution. The upper (lower) overturning cell is represented by positive (negative) streamfunction values. (b) Maximum of the overturning streamfunction at 30°S for varied surface buoyancy forcing and resolution. The error bars show the standard deviation of 1 year overturning averages from the 25 year mean. The horizontal black line indicates the maximum of the analytically calculated Ekman transport.

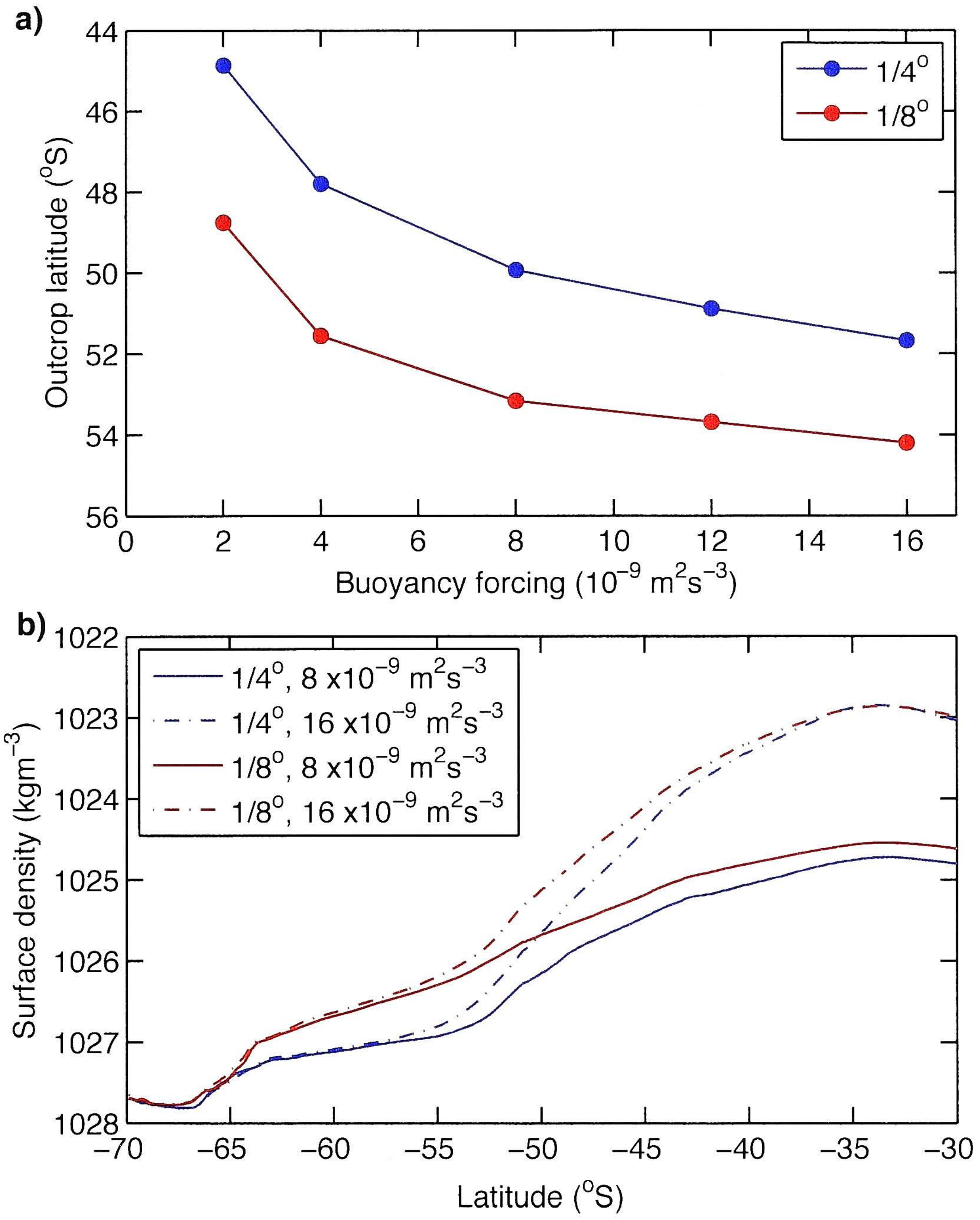

Figure 2.4: (a) The variation, with applied buoyancy forcing, of the latitude at which the 1 Sv overturning streamfunction outcrops into the upper isopycnal layer. (b) Mixed layer density for a range of simulations with varied resolution and buoyancy forcing. All values in this figure are zonal and temporal (25 year) averages.

2.4 Discussion

These idealised model results indicate that the overturning circulation is sensitive to mid-latitude buoyancy forcing. Increases in buoyancy forcing act to shift the location of upwelling southward, while enhancing the overturning circulation. The enhanced upwelling is qualitatively consistent with theoretical predictions (Marshall and Radko, 2003; Radko and Kamenkovich, 2011) which indicate the need for water mass transformation to occur if upwelled water masses are to travel northwards in the surface layers without being immediately subducted. The change in upwelling location helps to control the sensitivity of the overturning to buoyancy forcing.

The upwelling region in the model is determined by a number of factors, including bathymetry, the eddy field, wind and buoyancy forcing. The modelled upwelling therefore does not necessarily coincide with the location of the maximum potential Ekman-induced upwelling (profile shown in Figure 2.1b). As the upwelling location is forced southward by the mid-latitude buoyancy forcing perturbations, the modelled upwelling shifts from a region of low Ekman-induced upwelling, southward to a region of higher Ekman-induced upwelling. The Ekman-induced upwelling transport ($\nabla \times (\tau/(\rho_o f)) \Delta x \Delta y$) increases rapidly from zero at 45°S to a maximum at 56°S. The more northerly location of the upwelling in the $1/4^\circ$ runs with low buoyancy forcing (Figure 2.4a) results in a strong sensitivity of the overturning to buoyancy forcing perturbations, as the upwelling moves through a region with rapidly increasing Ekman-induced upwelling. The reduced sensitivity observed in the $1/8^\circ$ simulations may be traced to the increased stratification and the location of the upwelling region on the boundary of the applied mid-latitude buoyancy forcing. However, the profile of the Ekman-induced upwelling, which is nearly constant ($< 10\%$ variation) over the range 52° - 61°S, adds a further limit to the increase of the overturning circulation. Buoyancy forcing perturbations extending further south would not significantly alter the overturning sensitivity.

In our model, the sensitivity depends on the relative locations of the wind stress, buoyancy forcing and upwelling. The greatest sensitivity occurred for low buoyancy forcing at $1/4^\circ$ resolution, as the upwelling region was located furthest from the latitude of maximum Ekman-induced upwelling. The sensitivity for other models and the real ocean may vary widely from our results, depending on the stratification and the exact location and details of topography, wind stress and buoyancy forcing. However, we have highlighted that the Southern Ocean overturning may be strongly dependent on mid-latitude buoyancy forcing under certain conditions. Given the importance of the meridional overturning strength for the future of the oceanic CO_2 sink, our results indicate an urgent need to improve monitoring of Southern Ocean buoyancy forcing and overturning.

The sensitivity of the overturning to changes in buoyancy forcing presented here may play a role in solving the mystery of glacial-interglacial transitions. Radiocarbon evidence supports the hypothesis that the increased atmospheric CO_2 observed in Antarctic ice cores following the Last Glacial Maximum was released from deep water masses upwelling in the Southern Ocean (Skinner et al., 2010), though the trigger and mechanism for the increased upwelling remains unclear. Current theories rely predominantly on strengthening and southward shifting winds as the driving force for increased upwelling (Toggweiler et al., 2006). However, both observations and models have cast doubt on this wind driven theory. Paleoreconstructions of wind using pollen and dust sources are sparse and inconsistent (Fischer et al., 2010), while global coarse resolution modelling studies have shown that even a doubling in wind stress produces only $\sim$35 ppm increase in atmospheric CO_2 (D'Orgeville et al., 2010). Higher resolution models are likely to show even less sensitivity to wind stress changes as a result of eddy compensation. On the contrary, it is plausible that large changes in buoyancy forcing occurred at the end of glacial periods, due to sudden changes in air temperature and sea ice extent. The dependence we have found of the overturning on surface buoyancy forcing supports the hypothesis that buoyancy forcing (in addition to changes in wind stress) may have played a major role in the enhanced upwelling and subsequent outgassing of CO_2 from the Southern Ocean during glacial-interglacial transitions.

We have shown, using an idealised, but high resolution, model of the Southern Ocean, that surface buoyancy forcing, in addition to wind stress, may also be significant in setting the strength of the meridional overturning and that it may play an important role in past and future climate change. Increased mid-latitude buoyancy forcing may have led to enhanced Southern Ocean upwelling and therefore the rise in deglacial atmospheric CO_2 at glacial-interglacial transitions. Given the significance of the Southern Ocean CO_2 sink to future climate change, we have outlined the need for improved observations and an increased understanding of the dynamics of the meridional overturning circulation.

Acknowledgments

This work was supported by an ARC Discovery Project (DP0877824). Numerical computations were conducted using the National Facility of the Australian National Computational Infrastructure. We wish to thank Steve Rintoul for useful comments and Robert Hallberg, GFDL, for allowing access to GOLD.

Chapter 3

On the relationship between Southern Ocean overturning and ACC transport

Abstract

The eddy field in the Southern Ocean offsets the impact of strengthening winds on the meridional overturning circulation and Antarctic Circumpolar Current (ACC) transport. There is widespread belief that the sensitivities of the overturning and ACC transport are dynamically linked, with limitation of the ACC transport response implying limitation of the overturning response. Here, an idealised numerical model is employed to investigate the response of the large-scale circulation in the Southern Ocean to wind stress perturbations at eddy-permitting to eddy-resolving scales. Significant differences are observed between the sensitivities and the resolution dependence of the overturning and ACC transport, indicating that they are controlled by distinct dynamical mechanisms. The modelled overturning is significantly more sensitive to change than the ACC transport, with the possible implication that the Southern Ocean overturning may increase in response to future wind stress changes without measurable changes in the ACC transport. It is hypothesised that the dynamical distinction between the zonal and meridional transport sensitivities is derived from the depth dependence of the extent of cancellation between the Ekman and eddy-induced transports.

3.1 Introduction

The overturning of deep, carbon rich water masses in the Southern Ocean is closely linked to the outgassing rate of natural CO_2, and hence future changes in upwelling may significantly impact the present-day global oceanic sink of atmospheric CO_2. The strong link between outgassing and overturning (Toggweiler et al., 2006) has led to the suggestion that the Southern Ocean sink has weakened in response to increased westerly winds, due to an inferred enhancement of the overturning circulation (Le Quéré et al., 2007; Lovenduski et al., 2008). However, a number of recent eddy-permitting and eddy-resolving numerical studies (e.g. Meredith and Hogg, 2006; Hallberg and Gnanadesikan, 2006; Farneti et al., 2010) have shown that the sensitivity of the large-scale circulations in the Southern Ocean may be reduced by eddy effects. This has led to the suggestion that the overturning circulation may be less sensitive to changes in wind stress than previously thought. Despite the heightened focus on these questions, there remains significant uncertainty regarding the degree of sensitivity of the Southern Ocean circulation to wind stress and the potential interplay between the dynamical responses of the overturning and Antarctic Circumpolar Current (ACC) transport.

Numerical models and observations reveal the dominant role of the mesoscale eddy field in controlling the response of the ACC transport to changes in wind stress. Eddy-permitting and eddy-resolving models (Meredith and Hogg, 2006; Hallberg and Gnanadesikan, 2006; Farneti et al., 2010; Jones et al., 2011) show a decreased sensitivity of the zonal ACC transport relative to coarse resolution models that use a temporally invariant Gent and McWilliams (1990) eddy parameterisation. Limited response of the Southern Ocean isopycnal slopes over decadal timescales has also been observed, despite significant intensification of the westerlies (Böning et al., 2008). The limited sensitivity of the ACC transport is thought to be a result of the near linear response of the eddy kinetic energy to increasing wind stress; increased momentum input by surface wind stress is transferred to the bottom via enhanced interfacial form stress, rather than providing an acceleration of the zonal transport (Meredith and Hogg, 2006). This phenomenon is termed *eddy saturation.* Most eddy permitting models show a weak, non-zero ACC transport sensitivity (~10–20% ACC increase for doubled wind stress).

A similar phenomenon, termed *eddy compensation*, has been observed in eddy-permitting and eddy-resolving numerical models of the upper meridional overturning circulation (Hallberg and Gnanadesikan, 2006; Viebahn and Eden, 2010; Farneti et al., 2010; Abernathey et al., 2011). Increased wind stress over the Southern Ocean results in a one-to-one increase in the northward surface Ekman transport ($\overline{\psi} = \overline{v}\overline{h} = \tau/\rho f$), which is at least partially compensated by an opposing increase in the southward eddy-induced transport ($\psi^* = \overline{v'h'}$) (detailed in the theory of Marshall and Radko, 2003). Thus the residual overturning, which is the sum of the Ekman and eddy-induced transports ($\psi_{res} = \overline{\psi} + \psi^*$), increases substantially less than the Ekman transport. Perfect eddy compensation, whereby increases in the Ekman transport are exactly balanced by increases in the eddy-induced transport, has been hypothesised to occur at sufficiently high resolution and wind stress (Hallberg and Gnanadesikan, 2006; Farneti et al., 2010). However, two eddy-resolving numerical experiments (Viebahn and Eden, 2010; Abernathey et al., 2011), albeit with flat-bottom bathymetry, still show moderate increases in the residual overturning with wind stress.

The eddy compensation and saturation seen in these numerical studies has led to the development of a simplified conceptual framework portraying the response of the Southern Ocean to wind stress perturbations (e.g. Böning et al., 2008; Farneti et al., 2010; Hofmann and Morales Maqueda, 2011). As the westerlies increase in strength, increased northward Ekman transport is cancelled to some degree by increased southward eddy-induced transport. In the conceptual framework, this has the effect of limiting the increase in the net residual overturning, as well as limiting the increase in the tilt of the isopycnals (and therefore the ACC transport, through the thermal wind relation). Theories of the overturning circulation (e.g. Marshall and Radko, 2003), are based on this conceptual framework of a balance between the mean and eddy components of the overturning.

This simple conceptual picture of the Southern Ocean implies that if the ACC is eddy saturated, the overturning is therefore also eddy compensated (e.g. Böning et al., 2008; Farneti et al., 2010; Gent and Danabasoglu, 2011; Hofmann and Morales Maqueda, 2011). The assumption that there is a one-to-one relation between eddy saturation and compensation has perhaps been reinforced by the use of idealised numerical models suitable for investigating one, but not both, of the overturning or ACC transport. Eddy saturation at eddy-resolving scales has primarily been studied in quasigeostrophic channel models, with closed northern boundaries and by definition no diabatic transport or overturning (Meredith and Hogg, 2006), while eddy compensation at eddy-resolving scales has only been examined in flat-bottom models (Viebahn and Eden, 2010; Abernathey et al., 2011), in which the momentum input by surface wind stress is balanced by bottom friction rather than topographic form stress, thereby resulting in unrealistic ACC transports roughly ten times the observed value (Munk and Palmen, 1951).

However, there is growing evidence that eddy saturation and compensation are not as tightly linked as this simple conceptual framework might imply. The recent scaling theory of Meredith et al. (2012) demonstrated that under the assumption of complete eddy saturation, the expected response of the eddy-induced overturning spans a range resulting in moderate increases in overturning, rather than perfect eddy compensation. In addition, Downes et al. (2011) have analysed the effect of a single wind stress perturbation in a coupled eddy-permitting model and observed significant changes in the magnitude and spatial distribution of subduction rates, despite minimal increase in ACC transport.

In this paper we use an idealised numerical model to investigate the responses of both the ACC transport and residual overturning circulation under a wide range of wind stress perturbations and resolutions, from eddy-permitting to eddy-resolving scales.

3.2 Numerical model and experiments

We use GOLD (Generalized Ocean Layer Dynamics), a primitive equation, isopycnal layered ocean model (Hallberg and Gnanadesikan, 2006; Adcroft et al., 2008; Hallberg and Adcroft, 2009), with an experimental setup similar to that described in Morrison et al. (2011). The idealised domain is a zonally reentrant, 40° wide sector of the Southern Ocean with a simple Drake Passage-like sill, providing an unblocked circumpolar passage down to 2500 m below the surface, with a maximum ocean depth of 4000 m (Figure 3.1a). The latitudinal extent is 70°S to the equator at the northern boundary. The northern boundary is relaxed to a density stratification derived from observational data, using a sponge of width of 2° in latitude, with a decay timescale of 1 day. The sponge provides

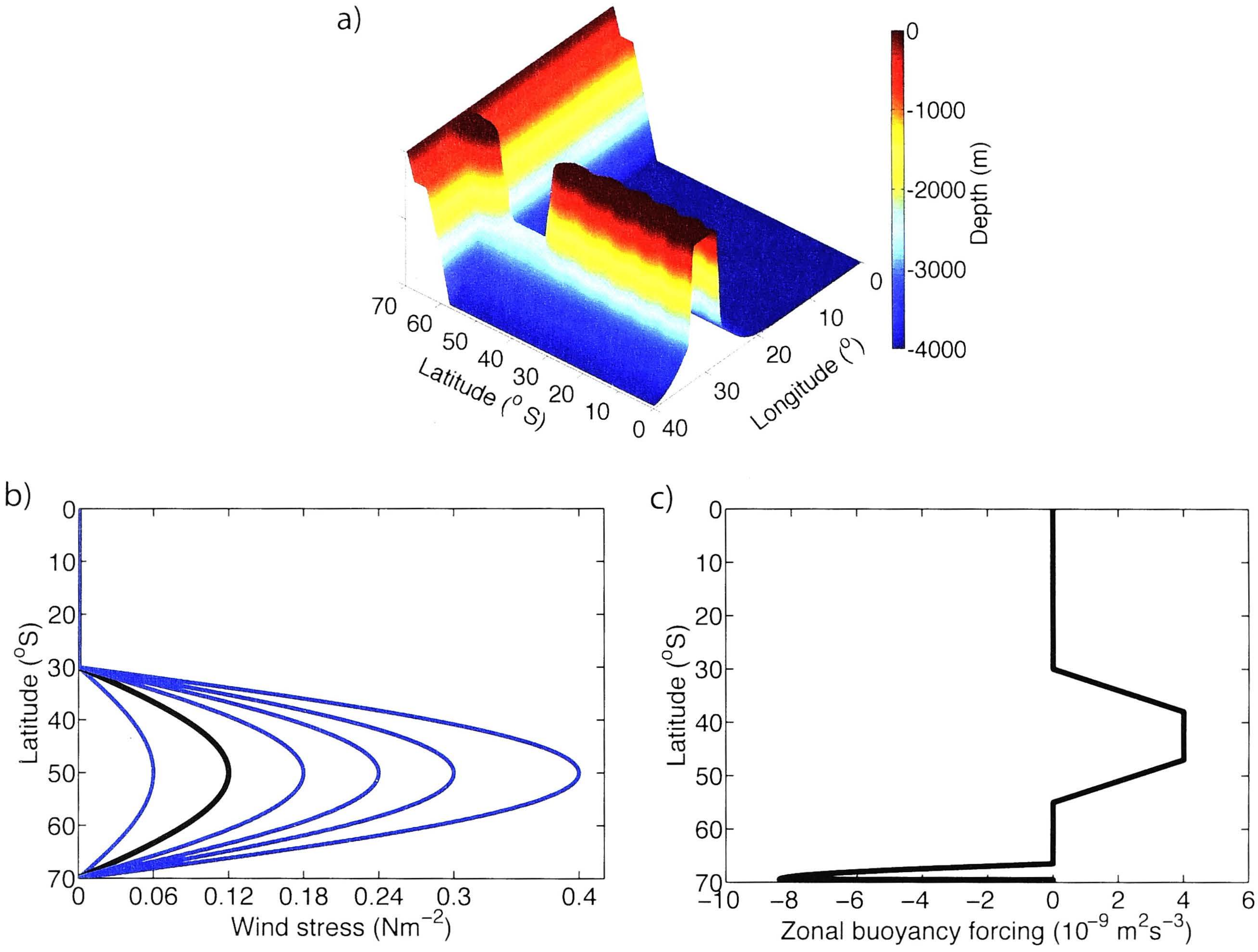

Figure 3.1: Model bathymetry and forcing. a) Bathymetry. b) Zonally averaged wind stress (control in black, perturbations in blue). c) Zonally averaged buoyancy forcing.

an effective parameterisation of North Atlantic Deep Water formation, without constraining incoming velocities. While the sponge places a non-ideal constraint on the model, reducing the freedom of the isopycnals to adjust over long timescales, it reduces the spin-up timescale from $O(1000$ yr$)$ to $O(100$ yr$)$, thereby allowing the exploration of a large parameter space at eddy-resolving scales. The caveat is that the results are applicable to relatively fast (decadal) responses of the Southern Ocean, rather than the millennial timescale adjustment of the deep stratification (Jones et al., 2011).

A Mercator grid, with grid size decreasing towards the southern boundary, is employed at four horizontal resolutions ($^1/_4$°, $^1/_8$°, $^1/_{12}$°, $^1/_{16}$°), resulting in square grid cells of size 13.9 km, 7.0 km, 4.6 km and 3.5 km at 60°S respectively, compared with a Rossby radius ~13 km at 60°S. Eddy parameterisations are not used in any of the simulations. A three layer bulk mixed layer is used, in addition to nine interior constant density layers. Biharmonic viscosity with an additional Smagorinsky component provides numerical closure, with biharmonic coefficients set to 2×10^{11} m^4 s^{-1} ($^1/_4$°), 2×10^{10} m^4 s^{-1} ($^1/_8$°), 8×10^{9} m^4 s^{-1} ($^1/_{12}$°) and 5×10^{9} m^4 s^{-1} ($^1/_{16}$°). A weak diapycnal diffusivity of 10^{-6} m^2 s^{-1} in the interior ensures a largely adiabatic circulation.

The model is forced by idealised, temporally invariant wind stress and surface buoyancy forcing (Figure 3.1b,c). The wind stress is sinusoidal and zonally uniform, while the buoyancy forcing is fixed and non-interactive, with a positive (i.e. acting to decrease the density of surface waters), zonally uniform forcing in the mid-latitudes and a region of spatially localised, negative buoyancy forcing near the southern boundary. The control cases have a maximum wind stress of 0.12 N m^{-2} and a spin-up period of ~120 years. Wind stress perturbations applied at the end of the control spin-up are allowed to reach equilibrium (~30 years) and 25 year averages after these spin-up times are used in the analysis.

3.3 Results

3.3.1 Mean state and eddy kinetic energy

The surface forcing generates a Southern Ocean-like state with isopycnals tilted towards the surface in the south, an energetic eddy field with associated fronts and jets, and an upper and lower meridional overturning cell. The spin-up timeseries, mean stratification, surface density snapshot and mean overturning for the $1/8^\circ$ control simulation are illustrated in Figure 2 of Morrison et al. (2011). The ACC transport in the control runs ranges from 85–110 Sv, decreasing in magnitude with increasing resolution. The lower overturning cell (analogous to Antarctic Bottom Water) is driven principally by the negative buoyancy forcing near the southern boundary. The upper meridional overturning cell simulates the upwelling of North Atlantic Deep Water in the latitudes unblocked by bathymetry. Scaled up to the full width of the Southern Ocean, the transports of the upper and lower cells in the $1/8^\circ$ control run are 23 Sv and 9 Sv respectively. The meridional overturning in the model is largely adiabatic in the interior, with diapycnal transport occurring predominantly in the mixed layers, as allowed by the surface buoyancy forcing and lateral diabatic eddy buoyancy fluxes.

We first illustrate the sensitivity of the eddy kinetic energy (EKE $= (\overline{u'^2 + v'^2})/2$) in the model to changes in resolution and wind stress (Figure 3.2), as the response of the eddy field is expected to have a significant impact on the dynamics of both the overturning and ACC transport. Consistent with previous observational (Meredith and Hogg, 2006) and eddy-permitting numerical (Hallberg and Gnanadesikan, 2006; Abernathey et al., 2011; Meredith et al., 2012) studies we find an approximately linear relationship between wind stress and EKE. The eddy field in the 'eddy-permitting' $1/4^\circ$ simulation is both weaker and less sensitive to change than that in the higher resolution simulations. The magnitude of the EKE continues to increase with resolution from $1/8^\circ \rightarrow 1/12^\circ \rightarrow 1/16^\circ$. However, the response of the EKE to wind stress (as indicated by the gradient of the lines in Figure 3.2) is similar between these resolutions, particularly at high values of wind stress. We therefore may expect to see some convergence in the response of the Southern Ocean circulation at large values of wind stress and high resolution.

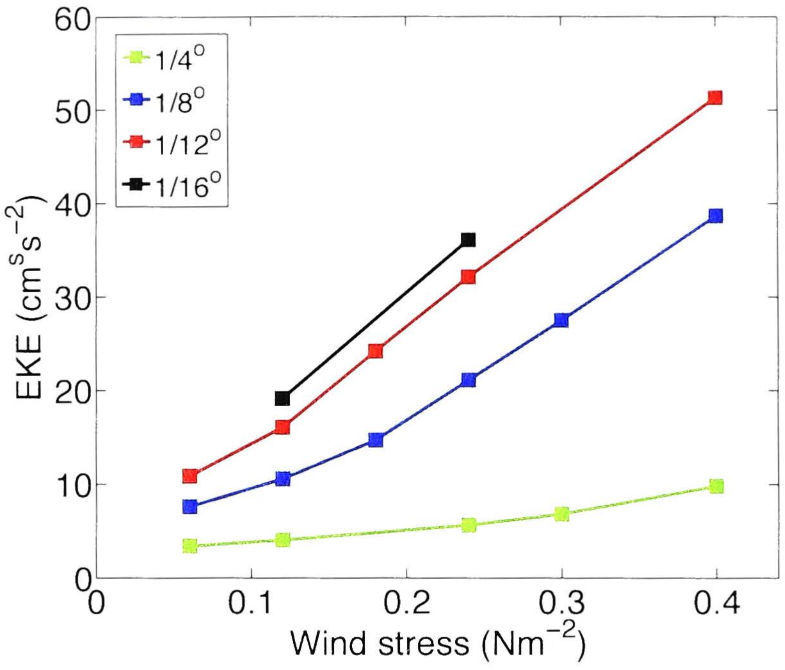

Figure 3.2: Variation of eddy kinetic energy with wind stress and resolution, averaged over 40–65°S and full depth.

3.3.2 Overturning response

The modelled residual overturning in the upper cell is partially eddy compensated, as shown by the divergence of the Ekman and residual overturning in Figure 3.3a. We define the residual overturning as the maximum of the zonally averaged overturning streamfunction at 30°S. Due to the adiabatic nature of the overturning, the results are largely unaffected by the choice of latitude used in the analysis. The mean component of the overturning (dashed black line in Figure 3.3a) is taken as the maximum of the theoretically calculated Ekman transport ($\overline{\psi} = \tau/\rho f$). The 1/8° residual overturning increases moderately with wind stress, though the sensitivity is substantially reduced in comparison with the changes in Ekman transport. There is a significant increase in the amount of compensation between 1/8° resolution and 1/12°, both nominally 'eddy resolving' models.

The zonally averaged, eddy-induced overturning, ψ^*, in the higher resolution simulations scales in accordance with the high EKE limit of Meredith et al. (2012) (Figure 3.3b). The scaling theory predicts that the isopycnal eddy diffusivity response should lie between $K \sim \tau^{1/2}$ (high EKE) and $K \sim \tau^{3/2}$ (low EKE). In order to extend the scaling to a prediction for the eddy-induced overturning (i.e. $\psi^* = K\overline{s} \sim K \sim \tau^{1/2}$), it is necessary to make the assumption that the dependence of the isopycnal slope, $\overline{s}$, on wind stress is negligible (i.e. the ACC transport is close to eddy saturation). Evidence for this is provided by previous numerical studies (Viebahn and Eden, 2010; Abernathey et al., 2011) as well as the simulations under discussion (e.g. Figs. 3.4b, 3.5b and 3.7a). The 1/4° eddy-induced overturning has a much weaker sensitivity to wind stress in comparison with the higher resolution simulations, reflecting the weak magnitude and limited response of the EKE at this resolution.

As may be expected from the variation of EKE and eddy-induced overturning with resolution, the extent of eddy compensation in the residual overturning circulation is also resolution dependent (Figure 3.4a). In order to compare the different resolutions, we

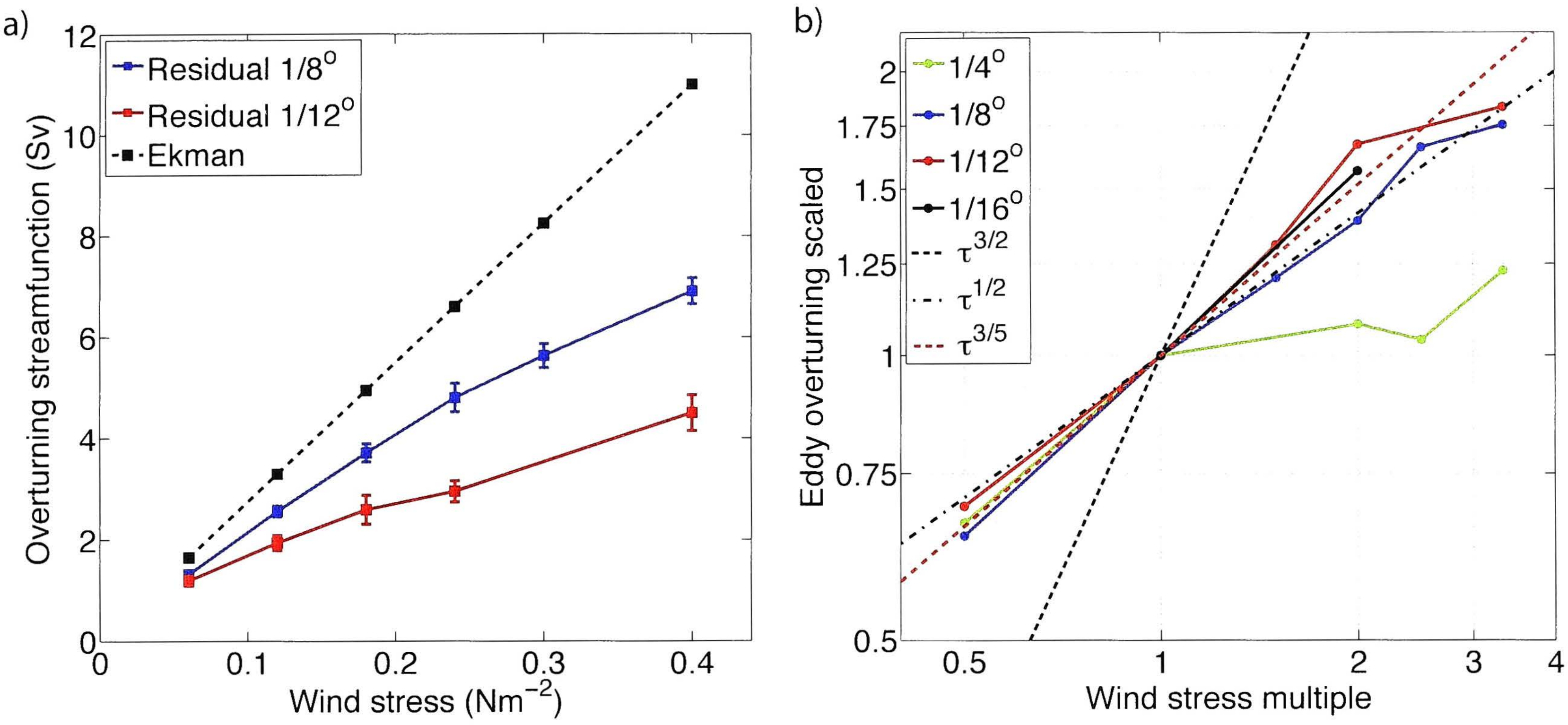

Figure 3.3: Partial eddy compensation. a) The maximum of the residual overturning streamfunction, ψ_{res}, at 30°S in the $^1/_8$° simulation (solid blue) and $^1/_{12}$° simulation (solid red), compared with the theoretically calculated maximum Ekman transport (dashed black). The error bars show the standard deviation of 1 year overturning averages from the 25 year mean. b) Sensitivity of the zonally averaged, eddy-induced overturning streamfunction, ψ^*, on isopycnal layer 1027.5, averaged between 40 – 60°S (solid lines), compared with the scaling arguments of Meredith et al. (2012): $\psi^* \sim \tau^{3/2}$ (black dashed) and $\psi^* \sim \tau^{1/2}$ (black dot dashed). The red dashed line shows the diffusivity scaling ($\psi^* \sim \tau^{3/5}$) used for the ACC transport prediction in Figure 3.5.

have scaled the overturning relative to the magnitude of the overturning in the control case for each resolution. The dotted line in Figure 3.4a represents a one-to-one increase in the residual overturning with wind stress. However, if the magnitude of the residual overturning transport is less than the Ekman transport (i.e. $\psi^* \neq 0$), this dotted line does not necessarily imply zero eddy compensation; a linearly increasing eddy overturning could produce a residual overturning scaling of one-to-one or even greater. Weak eddy compensation is seen in the $^1/_4$° simulation, corresponding to the weak sensitivity of the EKE at lower resolution. Enhanced eddy compensation is seen in the higher resolution runs, yet all of the simulations show at least a moderate increase of the overturning with wind stress. We note that the sensitivities of the $^1/_{12}$° and $^1/_{16}$° simulations are similar to previous high resolution idealised model studies (Viebahn and Eden, 2010; Abernathey et al., 2011). The overturning response appears to converge at $^1/_{12}$°, as was also the case for the EKE anomalies. The implication of this convergence is that, even at resolutions above $^1/_{16}$°, perfect eddy compensation would not occur in this model.

3.3.3 ACC response

In contrast to the overturning circulation response, the modelled ACC transport sensitivity shows a surprising independence of resolution (Figure 3.4b). Partial eddy saturation is observed at all resolutions, from eddy-permitting to eddy-resolving. A doubling of wind stress results in a weak increase in ACC transport of ~25%. The weak, but non-zero

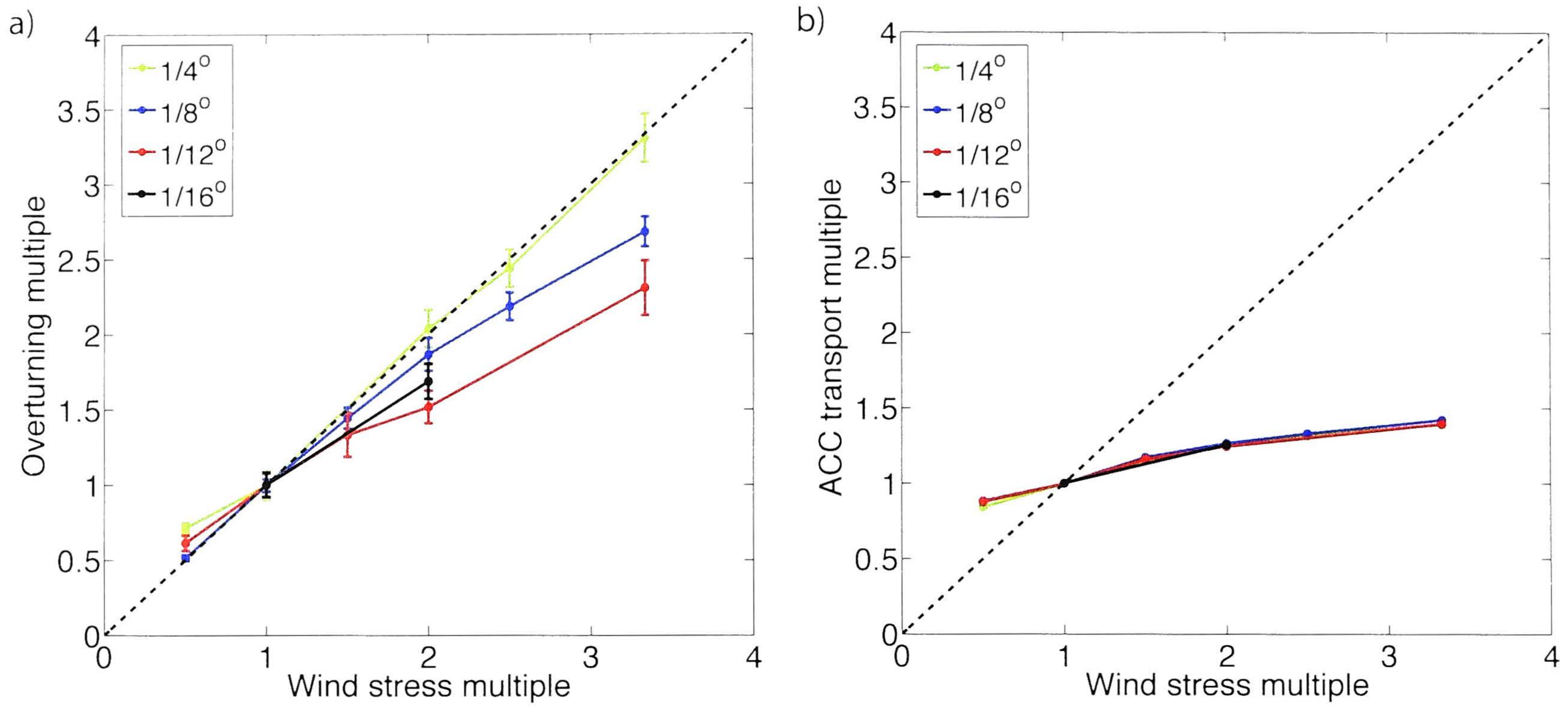

Figure 3.4: a) Maximum residual overturning streamfunction at 30°S, scaled relative to the magnitude of the overturning in the control wind stress case ($\tau = 0.12$ N m^{-2}). The dashed black line corresponds to a one-to-one increase in overturning with wind stress (but not necessarily zero eddy compensation). Perfect eddy compensation would be represented by a horizontal line. The error bars show the standard deviation of 1 year overturning averages from the 25 year mean. b) ACC transport sensitivity. The dashed black line corresponds to a one-to-one increase in transport with wind stress. Perfect eddy saturation would be represented by a horizontal line. Error bars as for Figure 3.4a have been excluded, due to the minimal variability of ACC transport.

response of the ACC transport is similar to other primitive equation, eddy-permitting studies of the ACC (Hallberg and Gnanadesikan, 2006; Farneti et al., 2010; Jones et al., 2011).

Theories predicting the response of the ACC transport to changing wind stress vary from complete eddy saturation (Straub, 1993) to a linear dependence on applied wind stress (Gnanadesikan and Hallberg, 2000; Marshall and Radko, 2003). We compare the modelled ACC sensitivity to the scaling theory of Olbers and Visbeck (2005), which is a modification of Marshall and Radko (2003), updated to include the effect of a non-zero residual overturning circulation on the prediction of ACC transport. Assuming an adiabatic interior and a vertically constant eddy diffusivity, K, Olbers and Visbeck (2005) write the transport as

$$T_{ACC} \sim \frac{-g\Delta B h_m}{K f^2}(\tau + \psi_{res}), \tag{3.1}$$

where ΔB is the meridional density difference across the ACC and h_m is a representative mean isopycnal depth. Consistent with the limited sensitivity of the ACC transport, we find that h_m responds only weakly to wind stress perturbations (Figure 3.5b) and for the purposes of reducing the complexity of the scaling, we assume h_m is constant. The meridional density difference, ΔB, depends strongly on wind stress (Figure 3.5c) and therefore cannot be ignored. Incorporating a power law scaling for the eddy diffusivity, $K \sim \tau^n$ (to be determined from the model data in Figure 3.3b), reduces the ACC transport scaling to

$$T_{ACC} \sim -\Delta B \left(\tau^{(1-n)} + \psi_{res} \tau^{-n} \right). \tag{3.2}$$

For the 1/12° simulation, we find that a diffusivity scaling of $K \sim \tau^{3/5}$ (as shown by the dashed red line in Figure 3.3b) provides a surprisingly good fit between the theory and modelled ACC transport (Figure 3.5a). The slope of the theoretical prediction is very sensitive to the choice of diffusivity scaling. We also find a good fit for the 1/8° simulation using $K \sim \tau^{1/2}$.

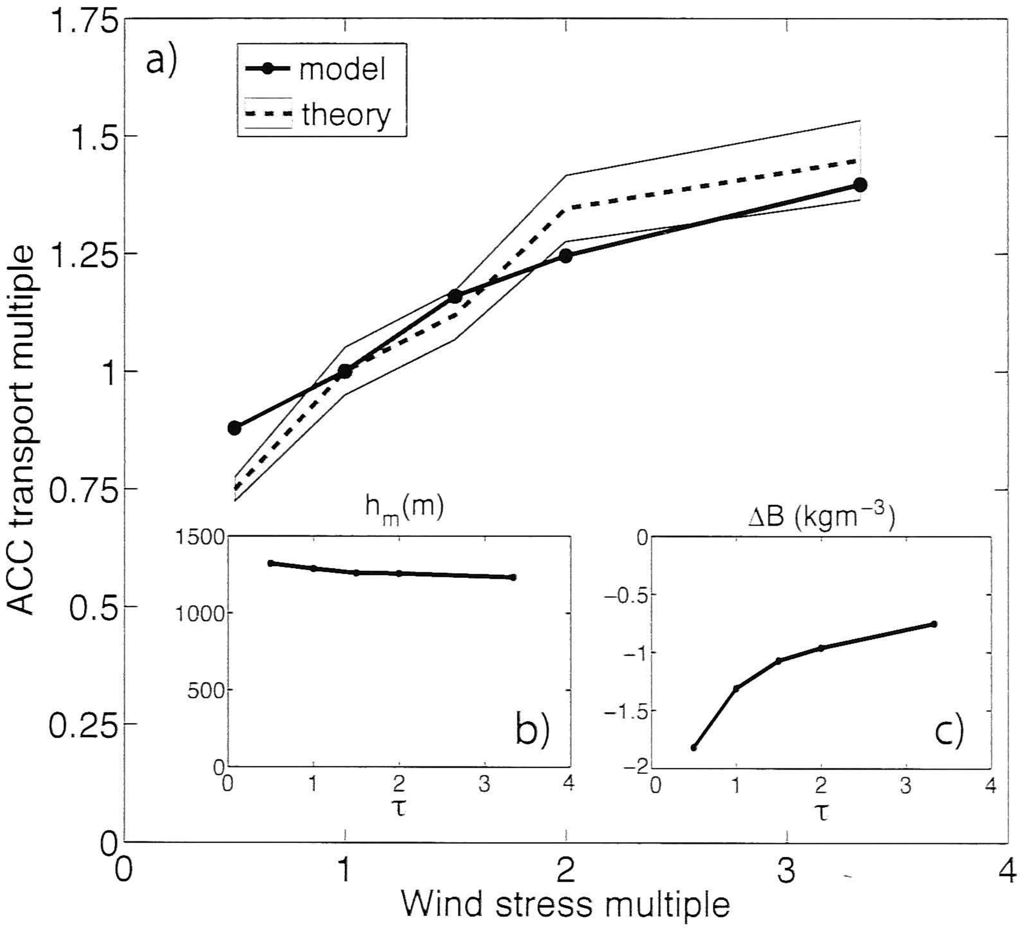

Figure 3.5: a) Comparison of the 1/12° modelled ACC transport sensitivity (solid) with the theoretical prediction of Olbers and Visbeck (2005) (dashed). The shaded region accounts for the variability in the residual overturning (using the uncertainty values shown in Figure 3.4a). b) Representative mean isopycnal depth. c) Surface density difference between 40 and 60°S.

3.4 Discussion and conclusions

Comparison of Figs. 3.4a and 3.4b reveals that the model is substantially closer to the eddy saturation limit than it is to the eddy compensation limit, consistent with the scaling predictions of Meredith et al. (2012). At the highest resolution (1/16°), a doubling of wind stress results in a 70% increase in the overturning, but only a 25% increase in the ACC transport. This difference in sensitivities holds significance for observational studies attempting to measure changes in the Southern Ocean overturning by indirect methods, such as via stratification changes. For example, Böning et al. (2008) concluded that the overturning has not responded to recent changes in wind stress, because there has been no discernible variation in the zonally averaged isopycnal slopes. However, our results indicate that it is possible to have a Southern Ocean-like state where large changes in the overturning may occur, despite minimal changes in the isopycnal slopes and ACC transport. We would expect the sensitivities of the overturning and ACC transport to diverge even further with the use of a surface buoyancy relaxation condition, instead of the fixed flux condition we have presented here. Surface relaxation allows for the buoyancy flux to also increase with wind stress, thereby resulting in larger increases in the overturning when compared with fixed flux experiments (Abernathey et al., 2011).

The discrepancy between the obvious resolution dependence of the EKE and overturning sensitivity and the resolution independence of the ACC transport sensitivity conflicts with the simple conceptual picture of the Southern Ocean presented in Section 1. In the simple model, increased wind stress acts to increase the surface southward eddy-induced transport, which partially opposes the increase in the northward Ekman transport. The net result of the changes in the Ekman and eddy-induced transports is often considered to have the effect of limiting both the increase in residual overturning (eddy compensation) and the increase in isopycnal slopes (eddy saturation). However, our numerical model results conflict with this simple conceptual model. As the resolution in the numerical model is increased from eddy-permitting to eddy-resolving, we observe an enhanced response of the southward eddy-induced transport, which increases the extent of eddy compensation. Yet as the eddy field increases with resolution, we observe no change in the degree of eddy saturation. Given that the numerical model contains the essential dynamics of the Southern Ocean, it is likely that eddy saturation and eddy compensation in the real ocean are controlled by different factors, and that the simple conceptual framework is deficient.

One plausible explanation for the increase in eddy compensation with resolution, but constant eddy saturation, is the different depth profiles of the changing Ekman and eddy-induced transports, as also hypothesised by Meredith et al. (2012). The depth structure of the different components of the overturning in the mean state has been investigated in several previous studies (e.g. Speer et al., 2000b,a; Olbers et al., 2004). However, here we focus on the vertical structure of the meridional transport anomalies, in response to changing wind stress. The increase in the northward Ekman transport is surface intensified and confined to the mixed layer (Figure 3.6b), while the increase in the southward eddy-induced transport is spread across all layers (Figure 3.6c). Therefore the degree of cancellation between the two components will vary with depth.

Figure 3.7 shows the variation of zonal and meridional transports for different density layers in the $^{1}/_{12}°$ model. Over the full depth of the water column, the meridional transports consistently increase in such a way as to enhance the overturning. However, the changes in zonal transport are more spatially variable (both in depth and latitude) and regions exist where the isopycnals flatten and the zonal transport decreases, despite increasing wind stress. Careful consideration of the stratification changes in Figure 7d of Farneti et al. (2010) reveals a similar response of the isopycnal slopes in a coupled eddy-permitting model, with a flattening of isopycnals in the northern part of the ACC region and steepening limited to the south.

In summary, we have shown that there is not a one-to-one relationship between the

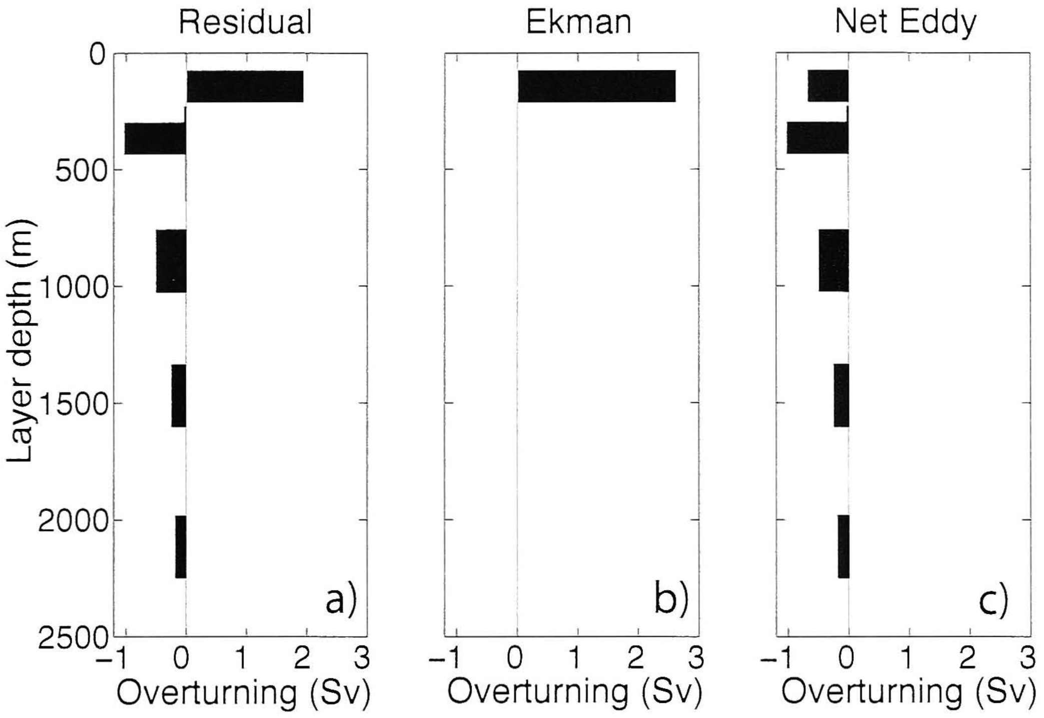

Figure 3.6: Depth structure of the changes in meridional transport at 53°S in the 1/12° simulation as a result of wind stress doubling from $\tau = 0.12 \rightarrow 0.24\,\mathrm{Nm}^{-2}$. Only the portion of the overturning above the depth of topography is shown. The top bar in each figure shows transport in the bulk mixed layer, while lower bars show transport in interior isopycnal layers. Positive values reflect northward transport. a) The zonally averaged, residual meridional transport ($\overline{vh}$). b) Theoretically calculated Ekman transport at 53°S ($\tau/\rho f$). c) Net eddy-induced overturning ($\overline{vh} - \tau/\rho f$).

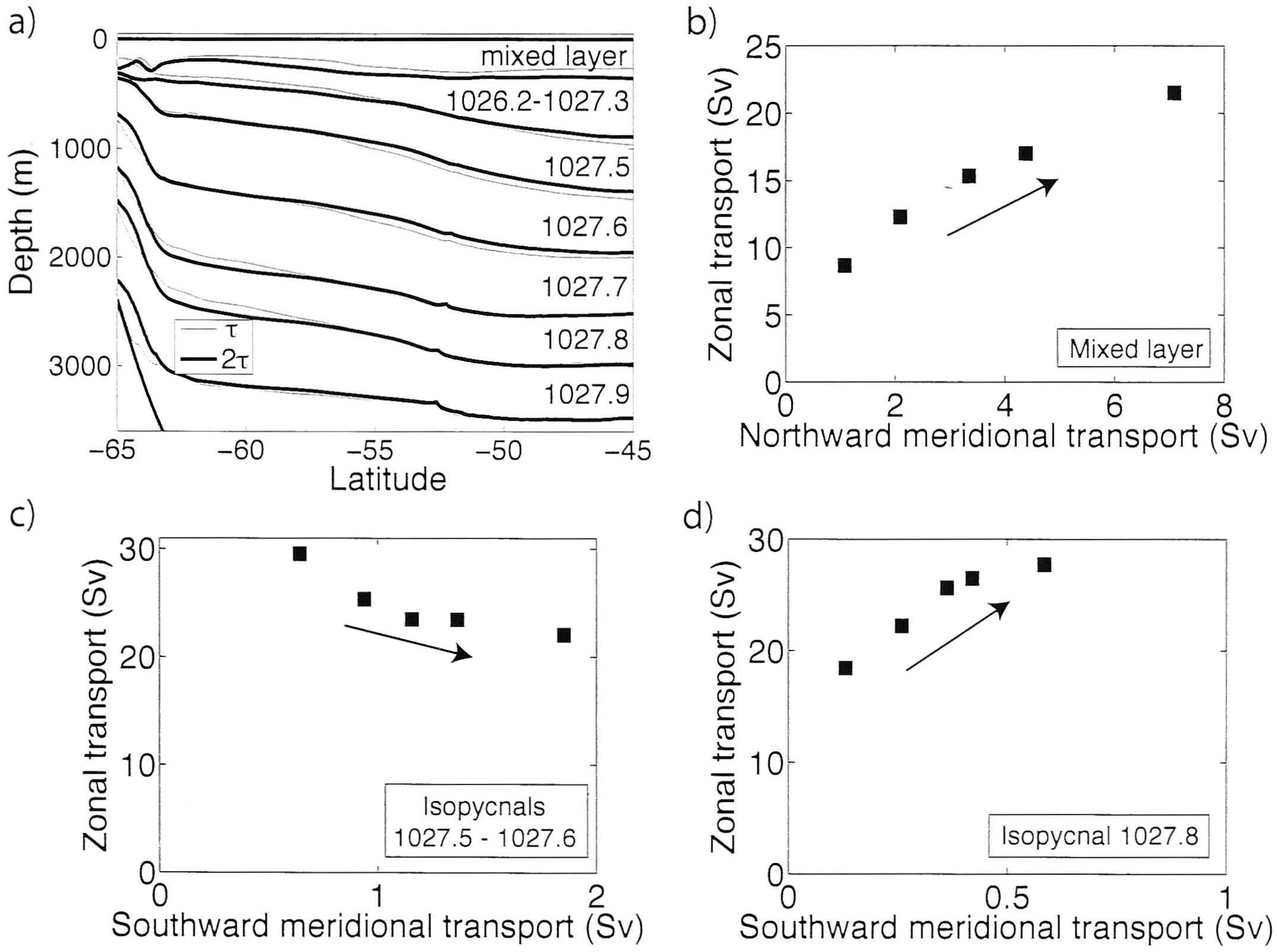

Figure 3.7: a) Zonally averaged isopycnals in the 1/12° simulation for the control (thin grey) and doubled (thick black) wind stress runs. b-d) The meridional vs zonal transport summed across (b) the mixed layers, (c) isopycnal layers 1027.5–1027.6, as labelled in a), and (d) isopycnal layer 1027.8. The arrows indicate the direction of wind stress increase.

responses of the Southern Ocean overturning and ACC transport to increasing wind stress. The modelled overturning is significantly more sensitive to change than the ACC transport, even at $^1/_{16}°$ resolution. The implication of these results is that future increases in overturning may occur without noticeable changes in stratification or ACC transport. As the model resolution is refined from eddy-permitting to eddy-resolving, the eddy kinetic energy and the degree of eddy compensation increase. However, the eddy saturation is surprisingly resolution independent. We hypothesise that the lack of a dynamical link between eddy compensation and eddy saturation is a result of the depth dependence of the cancellation between the Ekman and eddy-induced transports. The overturning response is particularly sensitive to the balance between Ekman and eddy-induced transports near the surface, while the ACC transport is a depth-integrated measure and will depend on stratification changes throughout the water column. However, it remains unclear as to what sets the degree of eddy saturation in different models and why, above eddy-permitting scales, this should not be affected by resolution and the associated large changes in eddy kinetic energy.

Acknowledgments

This work was supported by an ARC Discovery Project (DP0877824). Numerical computations were conducted using the National Facility of the Australian National Computational Infrastructure. We wish to thank Marshall Ward for useful advice, as well as the editor and two anonymous reviewers for their assistance in evaluating this paper. We also thank Robert Hallberg, GFDL, for allowing access to GOLD.

Chapter 4

The role of vertical eddy flux in Southern Ocean heat uptake

Abstract

The role of changing vertical eddy heat flux on Southern Ocean heat uptake is investigated in an idealised eddy-permitting ocean model. Enhanced air-sea heat flux drives deep-reaching southern warming, due to a reduction in the isopycnal meridional temperature gradient and therefore decreased upward eddy heat flux. This mechanism is qualitatively similar in models with either permitted or parameterised eddies, due to its dependence on the isopycnal temperature gradient rather than the dynamical response of the eddy field. In contrast, increased wind stress drives mid-depth Southern Ocean cooling through an enhancement of the eddy field and resultant eddy heat divergence. The transient cooling extends over multiple decades while the mean flow adjusts to balance the faster eddy response. This wind-driven cooling mechanism has not been captured by coarse resolution models with fixed eddy parameterisations and is a possible candidate for the recent cooling observed in the Southern Ocean.

4.1 Introduction

The oceans account for an overwhelming proportion (~93%) of the warming of the earth system over the past fifty years (Levitus et al., 2012), and a large fraction of that ocean heat uptake has occurred in the upper 2000 m of the midlatitude Southern Ocean (Gille, 2008). The intensified Southern Ocean warming has likely been driven by some component of the changing local surface forcing; a positive trend in the Southern Annular Mode has enhanced and shifted the westerly winds southward (Thompson and Solomon, 2002), surface air temperatures have increased (Chapman and Walsh, 2007) and evidence points towards increased precipitation over far southern latitudes due to an amplified hydrological cycle (Durack et al., 2012). Yet the relative importance of the different forcing components and the mechanisms by which they may cause deep-reaching southern warming are unclear, due to a combination of limited observations, uncertain atmospheric forcing and insufficient modelling resolution.

Meijers et al. (2011) divided the Southern Ocean temperature trend into an adiabatic component due to a wind-driven poleward migration of the Antarctic Circumpolar Current (as suggested by Gille, 2008) and a diabatic component due to changes in the vertical flux of heat from the surface and between ocean layers. The adiabatic component contributes a large warming trend, while the diabatic component contributes an opposing cooling trend, which acts to reduce the adiabatic trend by approximately half to produce the net observed deep warming. Meijers et al. (2011) do not attribute the cause of the diabatic cooling. Our aim in this paper is to investigate the dynamics of heat uptake processes which may be contributing to the diabatic trend in the Southern Ocean and in particular the role of eddies in modifying ocean temperature trends.

The ocean heat content trend arising from diabatic processes will be reflected in changes in the time mean vertical heat flux budget. Numerical modelling studies have found that below the surface mixed layer, the globally averaged vertical flux of heat is primarily a balance between the wind-driven mean circulation pumping heat downwards and eddies (permitted or parameterised) transporting heat upwards along isopycnals (Gregory, 2000; Wolfe et al., 2008). It is reasonable to expect that eddies transport buoyancy (i.e. heat) upwards in the global integral, because the baroclinic instability process acts to reduce available potential energy. Both the mean and eddy terms in the vertical heat flux budget are dominated by contributions from the Southern Ocean. Downward flux of heat by vertical diffusion in the tropics is only significant in the global budget in the upper few hundred metres of the ocean.

Two main mechanisms for Southern Ocean heat uptake have been proposed - one driven by increased atmospheric surface temperature and the other by enhanced westerly winds. In the first mechanism, warming is amplified at mid-depths due to a reduced along-isopycnal meridional temperature gradient in a warmer climate and therefore decreased upward eddy heat flux, as shown in a coarse resolution model with parameterised isopycnal diffusion by Gregory (2000). Huang et al. (2003) looked at the sensitivity of deep ocean heat uptake to a range of surface forcing and diffusivity perturbations and concluded that the large variation in deep ocean heat uptake between models arises primarily due to the high sensitivity to parameterised isopycnal diffusivity in the Southern Ocean and diapycnal diffusivity in the tropics. Brierley et al. (2008), in another coarse resolution coupled model study, found that reduced isopycnal diffusion was the largest contributor to the global imbalance leading to the warming trend between 350-1500 m.

Despite the dependence of this Southern Ocean warming mechanism on the eddy field, it has been largely untested in eddy-permitting or eddy-resolving models. Wolfe and Cessi (2009) investigated ocean heat uptake in an idealised eddy-resolving simulation with a northern hemisphere surface warming perturbation. In agreement with the coarse resolution study of Gregory (2000), the northern surface temperature gradient decreased in the warmer climate, reducing the vertical eddy heat flux and resulting in deep ocean heat uptake. However in their model, density was a linear function of temperature only. With no isopycnal temperature gradient, the only mechanism available for eddies to alter the vertical heat budget is through a change in the potential energy that maintains the eddy activity. Whether the Southern Ocean vertical eddy heat flux decreases in response to surface warming due to a change in baroclinicity or due to a change in the isopycnal temperature gradient remains to be tested in an eddy-permitting or eddy-resolving model.

The second proposed mechanism for Southern Ocean heat uptake acts through a wind-driven enhancement of the downward mean heat flux and is the primary cause of Southern Ocean warming in the Third Coupled Model Intercomparison Project (CMIP3) twentieth-century experiments (Cai et al., 2010). However, none of the CMIP3 models resolve eddies and are therefore missing the response of the eddy heat flux to changing wind stress (Hogg et al., 2008), which may significantly offset the wind-driven heat uptake. In this paper, we use a suite of wind stress and surface warming perturbations in an idealised eddy-permitting model to explore the role of the Southern Ocean eddy field on these two mechanisms of deep ocean heat uptake.

4.2 Numerical Model

We use an idealised, $1/4°$ eddy-permitting ocean sector configuration of the MITgcm (Marshall et al., 1997), with an experimental setup identical to that described in Hogg et al. (2013). We refer the reader to Figure 1 of that paper for an illustration of the model bathymetry and surface forcing for the reference case. The model domain is a 40° wide sector, extending from 70°S to 70°N, with a southern reentrant channel containing a simple Drake Passage-like sill of depth 1800 m. Vertical resolution increases towards the surface over 36 vertical levels. The model is run in hydrostatic, Boussinesq mode, and no explicit eddy parameterisation scheme is used. Horizontal viscosity/diffusion are minimised with a biharmonic lateral viscosity/diffusivity of 10^{11} m^4 s^{-1}. Background vertical diffusion is set to 10^{-5} m^2 s^{-1}, with a surface enhancement in the upper 300 m to generate appropriate mixed layer depths. The convective adjustment scheme also amplifies the background vertical diffusivity to remove unstable density profiles. A linear equation of state is employed, with both temperature and salinity dependence. The surface forcing is temporally invariant and zonally uniform, with prescribed wind stress, surface temperature relaxation and a fixed freshwater flux (see Hogg et al. (2013)). The model is close to equilibrium after a spinup period of 2500 years, after which point perturbations are split off from the reference case and run for a further 100 years. The forcing undergoes a step change and is then kept steady in the new perturbed configuration for the entire 100 years. In the warming perturbations, the surface relaxation temperature is increased uniformly across the domain by 0.5°C, 1°C, 2°C or 4°C as specified in the analysis. For the wind stress perturbations, the prescribed wind stress south of 30°S is scaled by factors of 0.7, 1.2, 1.3 and 2, as specified in the analysis. There is only minimal feedback between wind stress changes and local surface heat fluxes, meaning that we can easily separate the wind- and warming-induced changes.

4.3 Mean Vertical Heat Transport

Vertical heat fluxes are calculated following Wolfe et al. (2008). The time-mean heat budget is separated into the sum of the heat content tendency ($\mathcal{T}$), advective heat fluxes due to the mean flow ($\mathcal{M}$) and eddies ($\mathcal{E}$), and heat fluxes arising from parameterised sub-gridscale processes ($\mathcal{P}$; including turbulent diffusion and convective adjustment), as follows:

$$\mathcal{T} + \mathcal{M} + \mathcal{E} + \mathcal{P} = 0. \tag{4.1}$$

If we integrate from the bottom $-H$ to a reference level z_o and over a horizontal subdomain $\mathcal{A}$ (with boundary $\partial\mathcal{A}$), the first three terms are calculated as

$$\mathcal{T} = \rho_o c_p \int_{-H}^{z_o} \int_{\mathcal{A}} \frac{\Delta\theta}{\Delta t} \, dA \, dz \tag{4.2}$$

$$\mathcal{M} = \rho_o c_p \left(\int_{\mathcal{A}} \overline{w}\overline{\theta}(z_o) \, dA + \int_{-H}^{z_o} \oint_{\partial\mathcal{A}} \overline{u}_H \overline{\theta} \, d\sigma \, dz \right) \tag{4.3}$$

$$\mathcal{E} = \rho_o c_p \left(\int_{\mathcal{A}} \overline{w'\theta'}(z_o) \, dA + \int_{-H}^{z_o} \oint_{\partial\mathcal{A}} \overline{u'_H \theta'} \, d\sigma \, dz \right) \tag{4.4}$$

where c_p is the specific heat content, θ is potential temperature, u_H is the horizontal component of velocity normal to the boundary, $\bar{\cdot}$ is the temporal average over the time period Δt and primed quantities indicate deviations from the temporal mean. dA is the differential area of the subdomain $\mathcal{A}$, while $d\sigma$ is the differential length along its boundary $\partial\mathcal{A}$. The second term in Equations 4.3 and 4.4 represents the heat flux through the lateral boundary of the subdomain. The sub-gridscale term, $\mathcal{P}$, is not calculated explicitly, but rather as the residual of the first three terms in Equation 4.1. The sign of $\mathcal{P}$ indicates whether convective or diffusive fluxes are dominating the sub-gridscale term; in the polar regions, convection dominates and $\mathcal{P}$ is positive, indicating upward heat flux, while in the tropics, vertical diffusion dominates and $\mathcal{P}$ is negative, indicating downward heat flux.

The vertical heat flux components for the reference case simulation, averaged over the entire domain, are shown in Figure 4.1a. Figures 4.1b-d show the 'vertical' heat flux (actually the net divergence, including the lateral terms in Equations 4.3 and 4.4) for three subdomains, divided according to the sign of the mean heat flux, following Wolfe and Cessi (2009). At mid-depth (~300–2000 m) and averaged over the entire domain, the primary balance is between downward heat flux by the mean flow and upward heat flux by eddies, both dominated by contributions from the Southern Ocean (Figure 4.1b) and consistent with the previous studies of Gregory (2000) and Wolfe et al. (2008). The magnitude of the eddy heat flux is close to that in the eddy-resolving MITgcm model analysed in Wolfe et al. (2008): the area-averaged mid-depth eddy flux in our eddy-permitting model is 20% less than in their higher resolution model. In the upper ocean, where the model has increased vertical diffusivity (above 300 m), the primary global balance is between downward diffusive heat flux from the tropics and upward heat flux by Southern Ocean eddies. Since we are primarily interested in the response of the vertical heat fluxes to forcing changes, we refer the reader to Wolfe et al. (2008) for a more in-depth explanation and regional analysis of the time mean vertical heat flux.

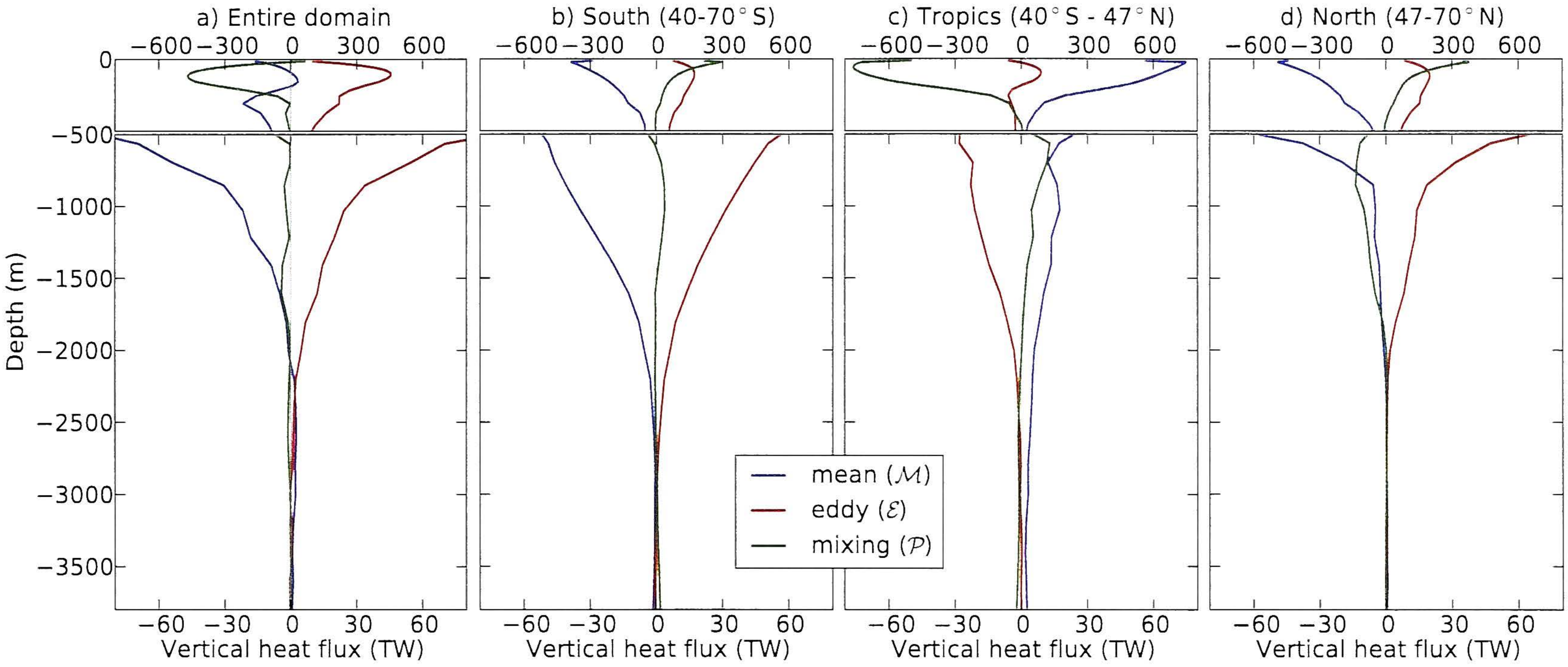

Figure 4.1: Vertical heat fluxes for the reference case, averaged over 10 years and different subdomains as follows: a) the entire model domain, b) the southern region (40-70°S), c) the tropics (40°S-47°N), and d) the northern region (47-70°N). Note that the 'vertical' mean and eddy fluxes, as defined in Equations 4.3 and 4.4, represent the net divergence, including horizontal fluxes across the subdomain boundaries. Positive values indicate upward heat flux. Colours show the heat flux components as defined in Section 4.3, with 'mixing' being the sum of sub-gridscale fluxes including parameterised convection and turbulent diffusion. The heat content tendency ($\mathcal{T}$; not shown) is negligible. The horizontal scale has been increased below 500 m to show detail at depth.

4.4 Response to Idealised Climate Change Scenarios

4.4.1 Surface Warming

We first consider the response to a uniform +2°C surface warming perturbation. The ocean warms (i.e. $\mathcal{T} > 0$) due to changes in each of the mean, eddy and sub-gridscale vertical heat fluxes (solid lines in Figure 4.2a). The large warming in the upper 300 m is concentrated in the tropics (not shown) and arises from both increased downward diffusive heat flux and decreased upward mean heat flux. At mid-depths (~300-2000 m), a significant fraction of the heat uptake occurs in the southern region (dashed lines in Figure 4.2a) and is predominantly due to a decrease in the upward eddy heat flux, consistent with the atmospheric warming driven mechanism identified in previous coarse resolution studies with parameterised eddies (Gregory, 2000; Huang et al., 2003; Brierley et al., 2008). As time progresses over the 100 years of the warming perturbation, the anomalous vertical eddy heat flux remains the dominant cause of heat uptake in the global integral in the depth range 300-1000 m, and the dominant cause of heat uptake in the southern region down to 2000 m. Below 1000 m in the global integral, the change in the mean vertical heat flux becomes increasingly significant in the heat uptake over the first century. The response is qualitatively similar for warming perturbations of different magnitudes.

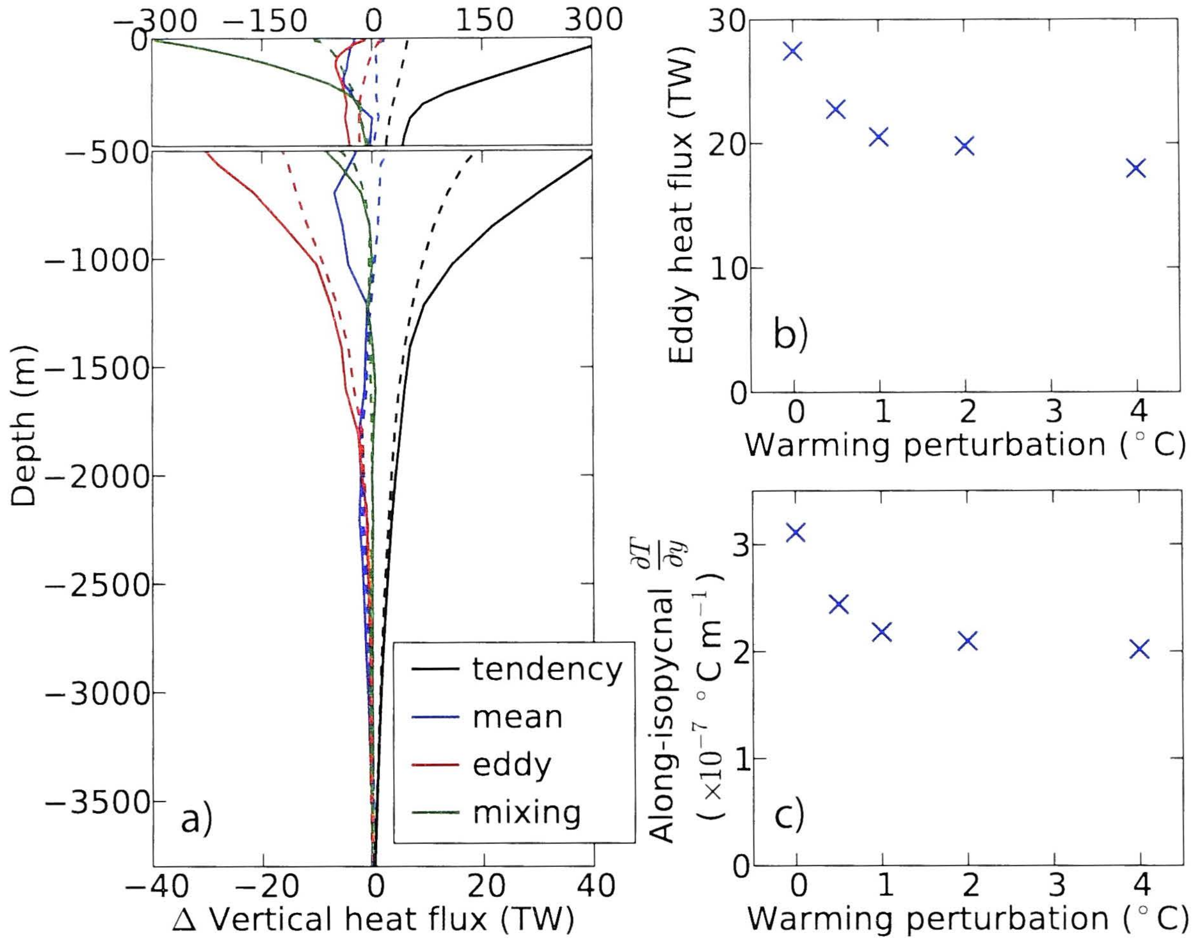

Figure 4.2: Vertical heat flux response to a uniform +2°C warming perturbation. a) Change from the equilibrium vertical heat fluxes, averaged over the first ten years of the perturbation, integrated over the entire domain (solid lines) and the contribution from the southern region (dashed lines). Heat flux components (colours) are defined as in Figure 4.1, with the additional heat content tendency, $\mathcal{T}$ (black). b) Scaling of the vertical eddy heat flux in the southern region (i.e. the blue line in Figure 4.1b), averaged over the depth range 700-1600 m. c) Scaling of the along-isopycnal, meridional temperature gradient on a mid-depth isopycnal (1500 m depth at 42°S, 700 m depth at 62°S).

The upward eddy heat flux in the mid-depth southern region scales inversely with the magnitude of the surface warming perturbation (Figure 4.2b). In the Southern Ocean, eddies flux heat along tilted isopycnals and the vertical eddy heat flux shown in Figure 4.2a is actually the vertical component of the along-isopycnal heat flux. Strong precipitation over the Southern Ocean leads to surface waters that are fresher than deep waters. Considered on an isopycnal, this salinity gradient necessitates a negative along-isopycnal temperature gradient (i.e. colder surface waters), since these quantities must compensate, to first order, on an isopycnal. Assuming downgradient, along-isopycnal tracer diffusion (e.g. Redi, 1982) of the form $\overline{v'\theta'}^{\rho} = -\kappa\overline{\theta}_y^{\rho}$ (where $(\cdot)^{\rho}$ indicates we are using an isopycnal framework), it is possible to trace the cause of the reduced upward eddy heat flux and hence the mid-depth warming in the southern region to the change in the along-isopycnal meridional temperature gradient (Figure 4.2c). In agreement with the coarse resolution study of Gregory (2000), the upward eddy heat flux in the southern region decreases due to faster warming in the surface region than at depth and a consequent reduction in the rate of along-isopycnal eddy mixing of temperature. The isopycnal temperature gradient across southern latitudes decreases as the surface relaxation temperature is increased, scaling similarly to the vertical eddy heat flux (Figure 4.2b).

4.4.2 Enhanced Southern Wind Stress

Previous Southern Ocean observational and modelling studies have found a fast (2-3 year) and approximately linear response of the eddy kinetic energy to increasing wind stress (e.g. Meredith and Hogg, 2006; Hogg et al., 2008). The enhancement of the eddy field with wind stress is a release of available potential energy, leading to an increase in the upward vertical eddy heat flux in the southern region (Figure 4.3a). This is the opposite response compared with the surface warming perturbation described in Section 4.4.1 (Figure 4.2a). The mean vertical downward heat flux associated with the upper overturning cell acts to deepen isopycnals on the northern side of the circumpolar current and thereby to warm at mid-depth; the timescale for this process is advective and therefore slower than the eddy response. Although we refer to the 'vertical' mean and eddy heat fluxes in the southern region, these include significant contributions from lateral fluxes across the subdomain boundary at 40°S. Figure 4.3b shows the separation of the net heat divergence into the true vertical and lateral components.

The net result of the mean and eddy responses is a small transient cooling trend in the mid-depth levels of the southern region. The cooling continues for around 60 years, until the mean flow increases sufficiently to balance the change in the eddy flux. Despite

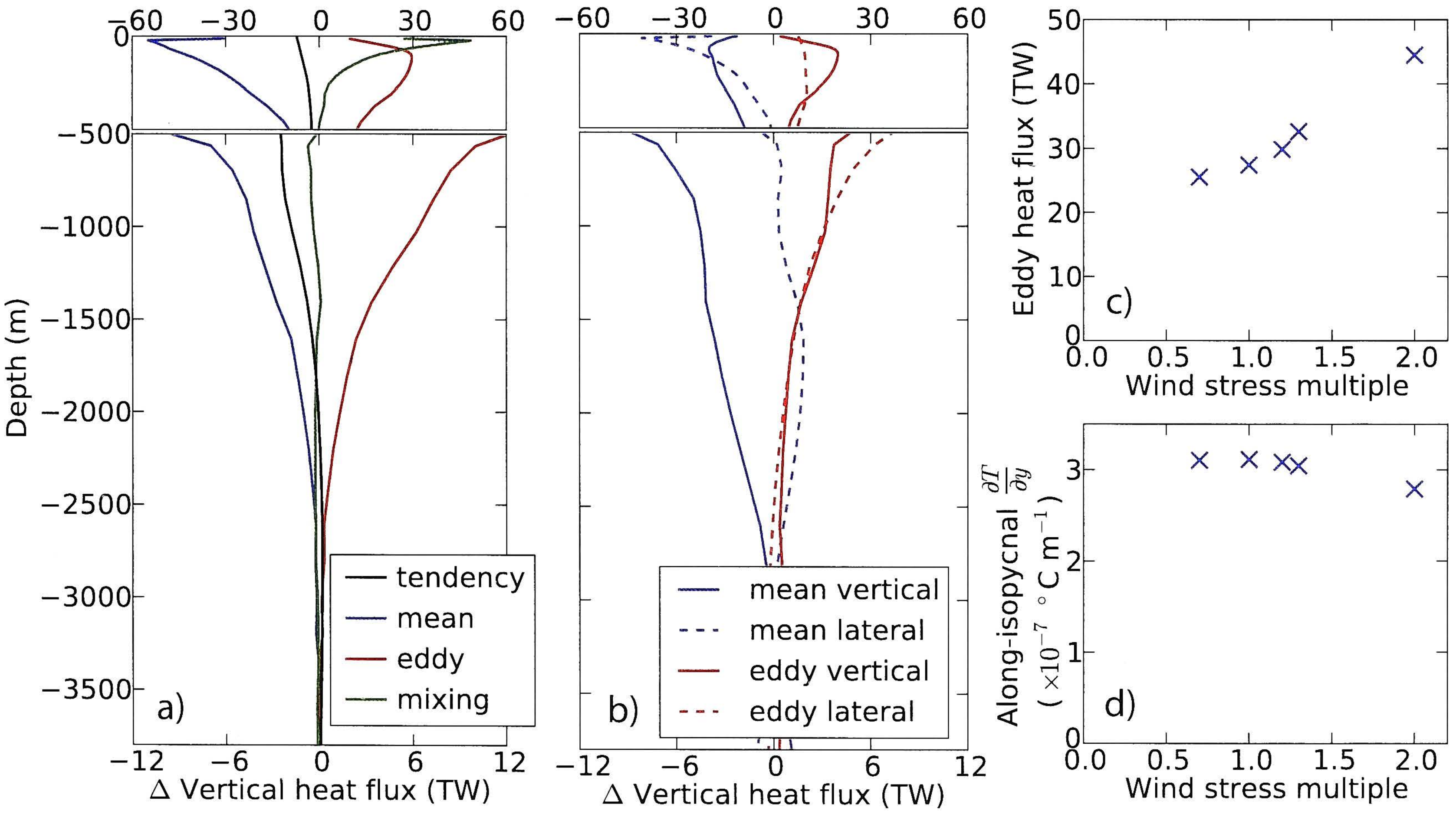

Figure 4.3: Heat flux response in the southern region (40-70°S only) to a 30% increase in Southern Ocean wind stress. a) Change from the equilibrium vertical heat fluxes (net heat divergence) in the southern region, averaged over the first ten years of the perturbation. Heat flux components (colours) are defined as in Figure 4.1, with the additional heat content tendency, $\mathcal{T}$ (black). b) Separation of the net mean and eddy heat fluxes shown in a) into true vertical (solid lines) and lateral (dashed lines) components. c) Scaling of the net eddy heat flux in the southern region, averaged over the depth range 700-1600 m. d) Scaling of the along-isopycnal, meridional temperature gradient on a mid-depth isopycnal (1500 m depth at 42°S, 700 m depth at 62°S).

minimal change in the local surface heat flux, cooling is able to extend throughout the water column due to changes in the lateral components of the mean and eddy heat fluxes (shown in Figure 4.3b). Analysis of a range of wind stress perturbations indicates a near one-to-one relationship between the mid-depth eddy heat flux and the prescribed wind stress (Figure 4.3c). In contrast to the surface warming perturbations, the along-isopycnal temperature gradient remains approximately constant for small ($\sim \pm 30\%$) wind stress perturbations (Figure 4.3d). The change in eddy heat flux is instead driven by increased baroclinicity (i.e. the eddy heat flux scales with the eddy kinetic energy). Although the mid-depth southern region cools following the change in wind forcing, the net heat uptake integrated over the entire domain is positive (not shown), due to a reduction in the mean upward heat flux in the tropics.

4.4.3 Combined Warming and Enhanced Wind Stress

The response of the vertical eddy heat flux to a wind stress perturbation (Figure 4.3c) has the opposite sign compared with the response to a warming perturbation (Figure 4.2b). If the two perturbation responses were to combine in an approximately linear way, the increase in westerly winds could partially reduce surface heat flux-driven warming in the mid-depth Southern Ocean. To explore this possibility, we have run a combined surface warming (uniform +2°C) and enhanced southern wind stress ($1.3 \times \tau_o$) perturbation experiment. As would be expected from the linear sum of the separate warming and wind stress experiments, the net heat uptake integrated over the entire domain is larger in the combined perturbation than in either of the independent perturbations. However, in the southern region, the addition of the enhanced wind stress to the warming perturbation results in a small decrease in the heat uptake, compared with the surface warming only perturbation (not shown); this mechanism may account for the observed recent cooling in the mid-depth Southern Ocean that was inferred to be due to diabatic processes (Meijers et al., 2011). The southern region heat uptake is reduced for a period of ~60 years, while the mean flow adjusts to the increased wind stress. After the mean heat flux has adjusted to balance the change in the eddy heat flux, the rate of heat uptake matches that in the warming only perturbation. The cumulative heat uptake in the southern region, integrated over full depth, is reduced by 5% over the 100 years of simulation.

4.5 Discussion and Conclusions

We have used an eddy-permitting numerical model to investigate two mechanisms of mid-depth Southern Ocean temperature change, both of which rely on changes in the vertical eddy heat flux. The first mechanism, driven by increased surface heat flux and identified in a coarse resolution model by Gregory (2000), causes mid-depth warming through a reduction in the upward eddy heat flux. In a warmer climate, the along-isopycnal meridional temperature gradient decreases, leading to reduced isopycnal diffusion of temperature. Since the mechanism does not depend on a change in the eddy field, the response of the vertical eddy heat flux in our eddy-permitting model is qualitatively similar to that found in coarse resolution simulations with parameterised isopycnal diffusion.

The second mechanism involves a response to increased wind stress forcing, which causes a transient cooling in the mid-depth southern region due to the faster response of the vertical eddy heat flux compared with the vertical mean heat flux. The upward eddy heat flux scales with the eddy kinetic energy and therefore responds on a timescale of 2-3 years, while the downward mean heat flux changes on the timescale for the adjustment of the upper overturning circulation, which in our model is $\sim$60 years. During this adjustment, a transient cooling occurs in the mid-depth southern region. Note that the relation between the mean and eddy components in the Southern Ocean vertical heat budget is quite different to that in the overturning circulation; at equilibrium, the vertical eddy heat flux nearly exactly opposes the vertical mean heat flux (Figure 4.1b), while the mean component of the overturning is significantly larger than the eddy component of the overturning (Morrison and Hogg, 2013). Unlike in the surface warming mechanism, the response of the vertical eddy heat flux to enhanced wind stress may differ greatly between coarse resolution and eddy-permitting or eddy-resolving models. Indeed, in the CMIP3 models, enhanced wind stress drives Southern Ocean warming, rather than cooling, due to the unresponsive eddy parameterisations in these coarse resolution models (Cai et al., 2010).

Acknowledgments

AMH was supported by Australian Research Council Future Fellowship FT120100842. The numerical model was run on the NCI National Facility in Canberra, Australia, which is supported by the Australian Commonwealth Government.

Chapter 5

Southern Ocean surface cooling in response to a warming perturbation in an eddy permitting ocean model

Abstract

This study explores how modulations in Antarctic dense water formation affect Southern Ocean temperatures in an eddy permitting ocean model. Consistent with previous studies, the modelled upper ocean south of 50°S cools and freshens in response to enhanced surface freshwater fluxes. Paradoxically, upper ocean cooling also occurs for small increases (up to a threshold) in the surface relaxation temperature. In both cases, the surface cooling and freshening trends are linked to the shutdown process of the abyssal overturning circulation and the associated changes in oceanic transport of heat and salt. The surface cooling occurs in two distinct phases – the first is dominated by decreasing advective fluxes of heat and salt to the surface, and the latter by a delayed collapse of convection, triggered at the point when the salinity change overwhelms the temperature change. During the advection dominated phase, the deep ocean freshens in response to a surface freshwater perturbation or warms in response to an increase in surface relaxation temperature. For both types of buoyancy forcing perturbation, the deep ocean warms and becomes more saline during and following the collapse of convection. The overturning shutdown and surface cooling trend progress at a faster rate for more extreme forcing perturbations, yet smaller perturbations result in a larger maximum surface cooling anomaly, due to the extended timescale of the advection dominated phase.

5.1 Introduction

Broadscale patterns in high-latitude Southern Ocean temperature and salinity trends have emerged in the observations over recent decades. Despite warming atmospheric temperature and enhanced heat flux entering the upper ocean, sea surface temperature (SST) south of 50°S has cooled (Bintanja et al., 2013; Latif et al., 2013). Durack and Wijffels (2010) have shown freshening of the sea surface salinity (SSS) extending across the same region. In contrast, in the deep Southern Ocean a warming trend is evident across nearly all ocean basins (Purkey and Johnson, 2010; Kouketsu et al., 2011), accompanied by a widespread freshening (Purkey and Johnson, 2013). The extent to which these changes have been caused directly by altered surface fluxes or through a feedback of ocean circulation changes is unclear.

One obvious possible mechanism for driving surface cooling simultaneously with deep ocean warming is through a modulation of the abyssal overturning circulation and the associated vertical ocean heat flux. The lower oceanic overturning cell is fed by the production of Antarctic Bottom Water (AABW) on the continental shelves around Antarctica, through a process which entrains fresher, ambient waters into the dense shelf waters cascading down from sea ice formation regions. AABW spreads northward to fill the bottom of the world's oceans, gradually mixing into the lighter overlying waters, and completing the meridional overturning loop by upwelling in the Southern Ocean as warmer and saltier Circumpolar Deep Water. A decrease in the abyssal overturning circulation would therefore change the net transport of heat and salt to the surface region where the lower cell outcrops around Antarctica. By analogy with the more familiar case of North Atlantic Deep Water shutdown (e.g. Manabe and Stouffer, 1995), a slower rate of AABW formation would result in a cooling of the sea surface temperature south of around 50°S in the Southern Ocean, due to the reduced upward heat flux. In the Southern Hemisphere case, the cooling would be accompanied by a freshening of the sea surface salinity, due to the higher salinity of the upwelling water masses compared with the relatively fresher AABW.

Present observational uncertainties are too large to conclude if the AABW transport or formation rate have changed in line with the recent abyssal temperature and salinity trends. However, several observation-based studies have suggested that AABW transport may be decreasing. Kouketsu et al. (2011) hypothesised a reduction in transport in the lower overturning cell, based on the correlation in their ocean reanalysis data between the abyssal warming and AABW transport. Observations from the Ross Sea, a bottom water formation region, indicate that a reduced volume transport of $(21 \pm 23)\%$ is contributing to the warming of Ross Sea Bottom Water (Shimada et al., 2012). Sloyan et al. (2013) also report an 18% decrease in the northward geostrophic transport of AABW below 3700 m in the southwest Pacific Ocean between 1996 and 2009. Both changing atmospheric forcing and internal natural variability are plausible drivers for reduced AABW transport. Atmospheric forcing changes are consistent with reduced dense water formation, through increased surface buoyancy: Antarctic ice sheet melt is accelerating (Rignot et al., 2011), surface air temperatures are increasing (Chapman and Walsh, 2007) and it is likely that precipitation over far southern latitudes is increasing due to an amplified hydrological cycle (Durack et al., 2012) and increasing Southern Annular Mode trend (Karoly, 2003). Meanwhile, Latif et al. (2013) have suggested that recent decadal changes in AABW properties and southern surface cooling may be a signature of the long-term rebound response from the occurrence of the 1974-76 Weddell Polynya. However, given the scarcity of transport observations, it is also possible that the remote changes in AABW properties may be caused by temperature and salinity changes at the formation regions, or enhanced deep mixing, rather than reduced volume fluxes. Furthermore, we note from the outset that although we motivate the study with the recent trends in Southern Ocean temperature and salinity, we do not implicate a definite or exclusive causal link between the abyssal overturning shutdown mechanism and the recent observed trends. Indeed, there are other plausible explanations for the observed surface cooling; for example, it has been suggested that an increase in the Southern Annular Mode may result in surface cooling through an enhancement of the upper overturning cell in combination with reduced atmospheric heat fluxes (Hall and Visbeck, 2002; Sen Gupta and England, 2006; Thompson et al., 2011).

A number of coarse resolution, coupled GCM experiments have previously shown surface cooling and deep warming linked to a reduction in the rate of Southern Ocean bottom water formation, driven either by increased freshwater or atmospheric CO_2 perturbations (e.g. Stouffer et al., 2007; Aiken and England, 2008; Swingedouw et al., 2008; Menviel et al., 2010; Kirkman and Bitz, 2011; Bintanja et al., 2013) or natural centennial variability (Galbraith et al., 2011; Martin et al., 2013; Latif et al., 2013). In response to a slowdown of southern convection, these models show surface cooling and freshening, an increase in sea ice extent and deep warming. However, there is disagreement in these studies regarding what controls the magnitude of the surface cooling: Swingedouw et al. (2008) found that the magnitude of cooling increases with the rate of freshwater input, while Menviel et al. (2010) have shown that a smaller freshwater perturbation results in a larger surface cooling. The disagreement is likely a result of the large variation in the location, rate and length of freshwater release applied in the different models, as well as the model dependent mean AABW formation rate and the difficulty of disentangling the response in coupled models.

Here we present a process study investigating the ocean dynamics and resultant temperature and salinity anomalies associated with decreasing Southern Ocean bottom water formation in an eddy permitting, idealised ocean model. Through the analysis of a wide range of surface freshwater and heat flux perturbations, we explore the dynamical ocean control on the timescale and magnitude of the modelled changes in temperature and salinity.

5.2 Numerical model

We investigate the surface response of an imposed change in Southern Ocean forcing in a series of perturbation experiments using the MITgcm (Marshall et al., 1997) in an idealised, pole-to-pole, ocean sector configuration with an eddy permitting resolution of $1/4°$. The reference case is the same as that described in Hogg et al. (2013), but with a longer spinup period of 2500 years. The domain is a 40° longitudinal sector of ocean, extending from 70°S to 70°N, with a simple Drake Passage-like sill of depth 1800 m (Figure 5.1a). There are 36 vertical levels with resolution increasing towards the surface. We use the model in hydrostatic, Boussinesq mode, and with no explicit eddy parameterisation scheme.

Horizontal and vertical viscosity/diffusion are minimised with a biharmonic lateral viscosity/diffusivity of 10^{11} m^4 s^{-1} and a vertical viscosity/diffusivity of 10^{-5} m^2 s^{-1}. The vertical diffusivity is amplified by a factor of 200 near the surface to generate mixed layers of an appropriate depth (parameterised by a Gaussian vertical diffusivity profile with a decay depth of 150 m and surface diffusivity of 2×10^{-3} m^2 s^{-1}), and is also enhanced to enable convective adjustment of unstable density profiles. The model uses a linear equation of state with density depending upon both temperature and salinity. The reference case is forced by prescribed wind stress (Figure 5.1b), temperature relaxation at the surface with a restoring timescale of 60 days applied over the top grid cell of thickness 10 m (Figure 5.1c), and a fixed freshwater flux (Figure 5.1d). All forcing is temporally invariant and zonally uniform, although variations in the model SST fields imply that atmosphere-ocean heat fluxes vary zonally and in time, even though the relaxation temperature does not. The model is run in ocean-only configuration, with no sea ice formulation. The uncoupled configuration has the advantage of higher resolution, better control over forcing perturbations and ease of isolating the dynamical processes involved in the transient responses. The possible influence of sea ice feedbacks on the results are discussed further in Section 5.7.

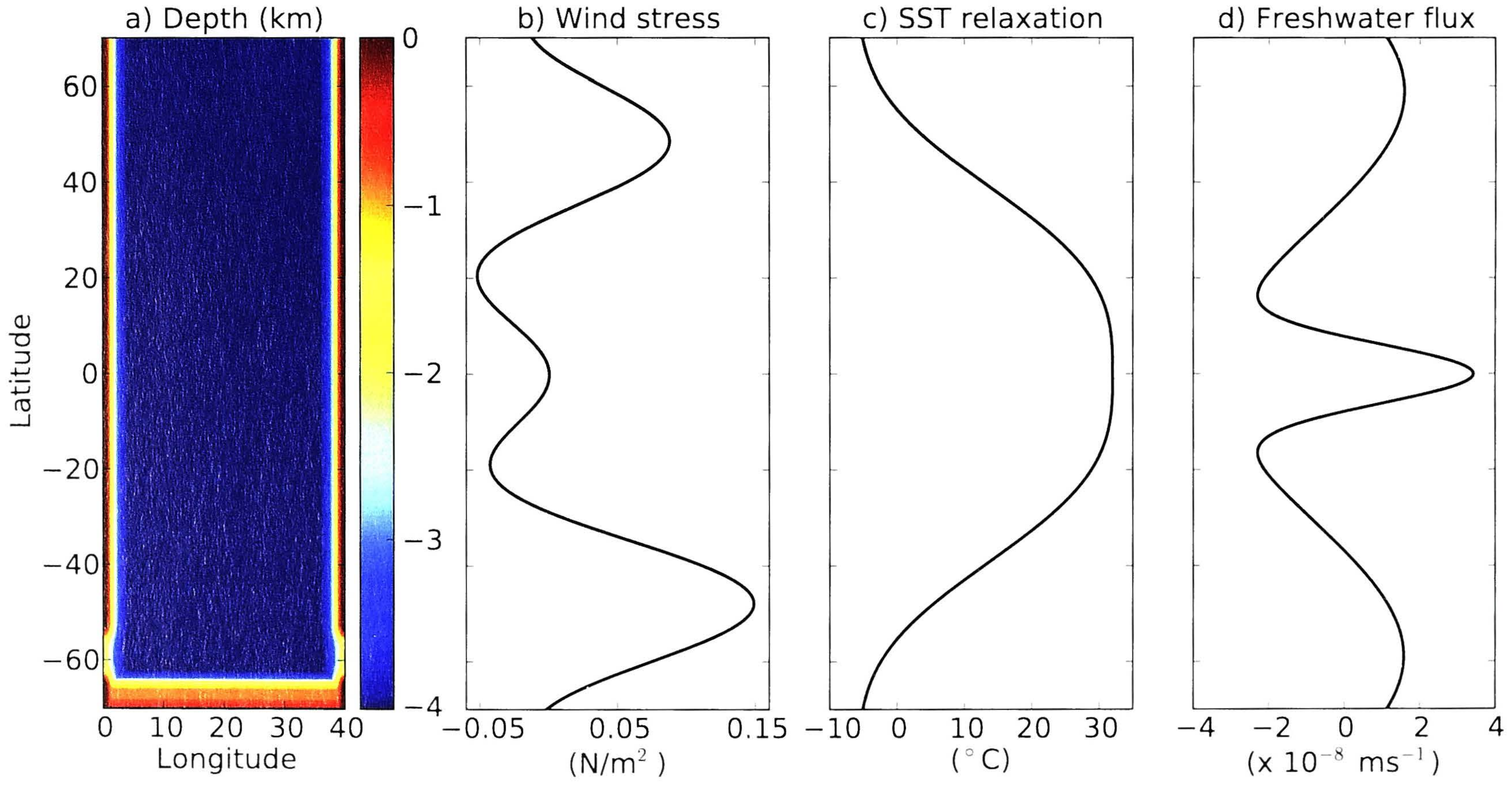

Figure 5.1: a) Model bathymetry. b) Zonal wind stress. c) Sea surface temperature relaxation. d) Freshwater flux.

Following the 2500 years of spinup, a number of independent surface warming and freshwater flux perturbations are run for a duration of 100 years. The change in Southern Ocean forcing used in the warming perturbations is shown in Figure 5.2a. Except for experiment SST0.5S, we have uniformly increased the surface temperature relaxation profile by a constant amount over all latitudes (including northern latitudes, not shown). SST0.5S has enhanced warming only south of 55°S. All of the perturbations are step changes in forcing switched on at year 0, except for SST0.5RAMP, which has the same uniformly

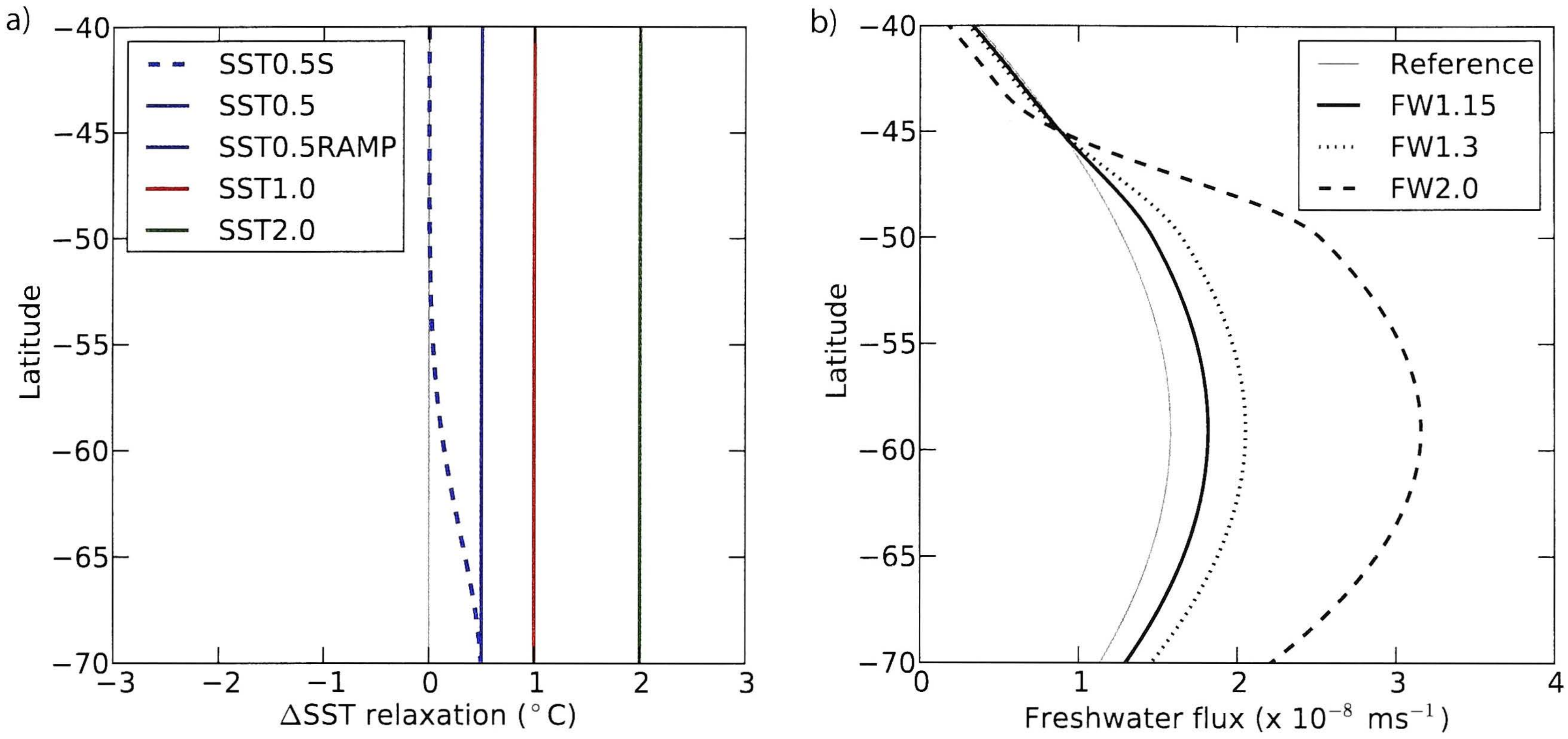

Figure 5.2: Buoyancy forcing perturbations applied in the respective numerical model experiments: a) Change in SST relaxation profile for the surface warming perturbations, and b) freshwater flux perturbations (precipitation minus evaporation).

increased SST relaxation profile as SST0.5, but is ramped linearly from +0°C to +0.5°C over 50 years starting from year 0. For the freshwater perturbations (Figure 5.2b), we scale the freshwater flux by a constant factor between 50-70°S, decreasing to no change at 43°S. The global freshwater flux is then recalibrated to eliminate any imbalance in the meridional integral, which has the effect of slightly reducing the freshwater input relative to the reference case north of 43°S. After the recalibration, the freshwater flux between 50-70°S has been increased by 1.15×, 1.3× and 2.0× in the perturbations labelled FW1.15, FW1.3 and FW2.0 respectively.

The state of the Southern Ocean portion of the reference case is shown in Figure 5.3. The surface imprint of the stratification and the eddying nature of the model is highlighted in the snapshot of SST (Figure 5.3a). The overturning circulation, shown in Figure 5.3b, has been calculated on density surfaces and remapped back to depth space using the zonal and temporal mean stratification. The model reproduces three overturning cells, analogous to the observed Southern Ocean overturning cells: the surface subtropical cell, confined to the upper 300 m north of 50°S, the upper, 'North Atlantic Deep Water' cell and the lower 'AABW' cell, which fills the deep and abyssal layers. To compare the modelled overturning with observations of the global overturning, the transports should be scaled up from the limited zonal domain by a factor (of approximately 9) to account for the width of the model domain compared to the real ocean.

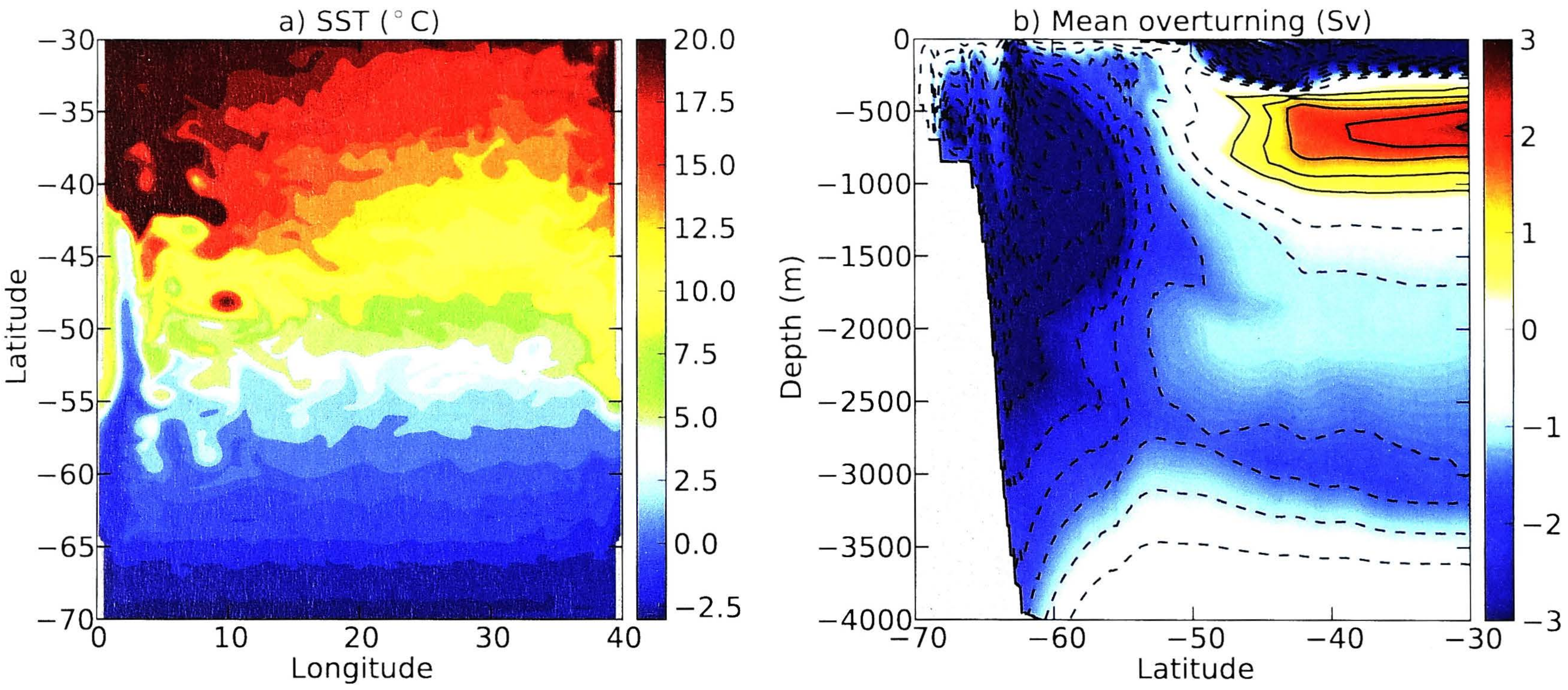

Figure 5.3: Equilibrium state of the reference case. a) Snapshot of sea surface temperature. b) Zonal and time averaged overturning circulation, evaluated on density surfaces and mapped back to depth space (black lines are 0.5 Sv contours). Red colours and solid black lines denote clockwise circulation, while blue colours and dashed black lines indicate anti-clockwise circulation. Note that to compare with observations, the overturning should be scaled by a factor that accounts for the width of the model domain relative to the width of the real ocean.

5.3 Surface response to buoyancy forcing perturbations

5.3.1 Freshwater perturbations

Consistent with previous coupled model studies (e.g. Stouffer et al., 2007; Aiken and England, 2008; Swingedouw et al., 2008; Menviel et al., 2010; Kirkman and Bitz, 2011; Bintanja et al., 2013), the modelled upper ocean cools and freshens over the latitudes of the Antarctic Circumpolar Current in response to enhanced freshwater perturbations (Figure 5.4). The region 45-70°S cools nearly uniformly and the freshening anomaly peaks over the same latitude range. Although the region of surface cooling and freshening coincides with the spatial extent of the applied freshwater perturbation (south of 45°S; Figure 5.2b), we show in Section 5.4 that the pattern of surface salinity and temperature anomalies are primarily determined by changes in ocean circulation, rather than the applied forcing perturbation.

As expected, the surface salinity anomaly scales with the size of the freshwater perturbation (Figure 5.5b): more freshwater input results in a fresher surface layer. Interestingly, the surface cooling (Figure 5.5a) scales inversely: smaller freshwater perturbations lead to larger maximum cooling anomalies. The time taken to reach the maximum cooling / freshening and a pseudo-equilibrium state also scales inversely with the magnitude of the freshwater perturbation. The dynamics setting the magnitude of the temperature and salinity anomalies, as well as the timescale of adjustment, are investigated in greater detail in Section 5.4.

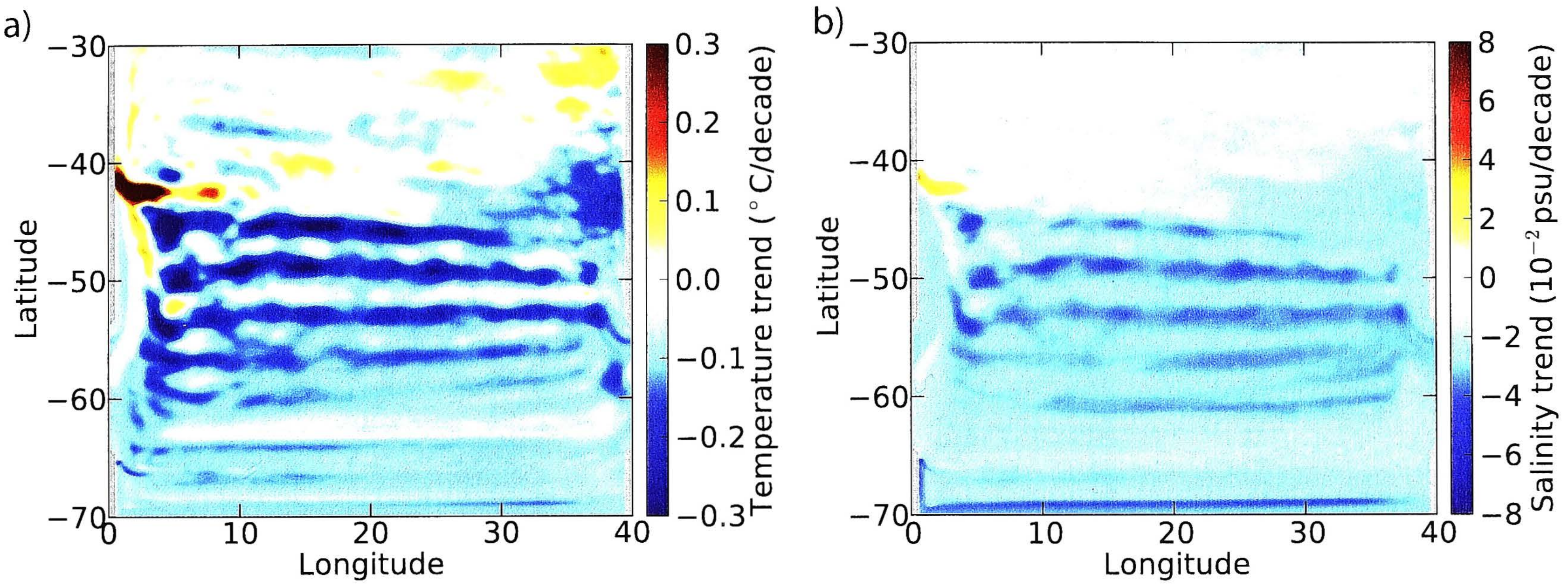

Figure 5.4: Linear decadal trends in a) sea surface temperature and b) sea surface salinity, calculated over years 0-50 of the freshwater perturbation FW1.15.

5.3.2 Warming perturbations

Despite a uniform increase in the imposed atmospheric temperature, significant surface cooling over the latitudes of the Antarctic Circumpolar Current also occurs in response to moderate warming perturbations (Figure 5.5c). Similar to the freshwater perturbations, the region 45-70°S cools nearly uniformly. As expected, SST increases north of 40°S and into the Northern Hemisphere. There is a small region of cooling in the western half of the simulated North Atlantic basin. However, the spatial extent and magnitude of the northern cooling trend are minimal compared with the Southern Ocean. The inter-hemispheric asymmetry arises due to the difference in the net meridional salt transport between the upper and lower overturning cells. The salinity difference between the poleward and equatorward limbs of the lower cell is much larger than for the upper overturning cell, resulting in a significant salinity feedback process in the Southern Ocean (discussed further in Section 5.4), which is not present in the northern hemisphere. As a result of this salinity feedback, the surface south of 45°S also freshens in response to the warming perturbations (Figure 5.5d). Apart from the most extreme warming perturbation (SST2.0), the spatial pattern of surface cooling and freshening is similar for all of the warming experiments, independent of whether the forcing was altered locally or globally. For example, SST0.5S, which has no change in the relaxation temperature north of 55°S, shows significant cooling trends extending to 45°S (though less warming north of this latitude compared with SST0.5).

As for the freshwater perturbations, the magnitude of the cooling and the timescale of both the cooling and freshening are strongly dependent on the size of the warming perturbation. The greatest cooling occurs for the smallest change in relaxation temperature, with the most extreme perturbation (SST2.0) causing surface warming rather than cooling (Figure 5.5c). Variation in the location (SST0.5S) or timescale (SST0.5RAMP) of the anomalous forcing does not significantly affect the magnitude of the surface cooling or freshening, relative to a perturbation with a uniform, step change in forcing (SST0.5), pro-

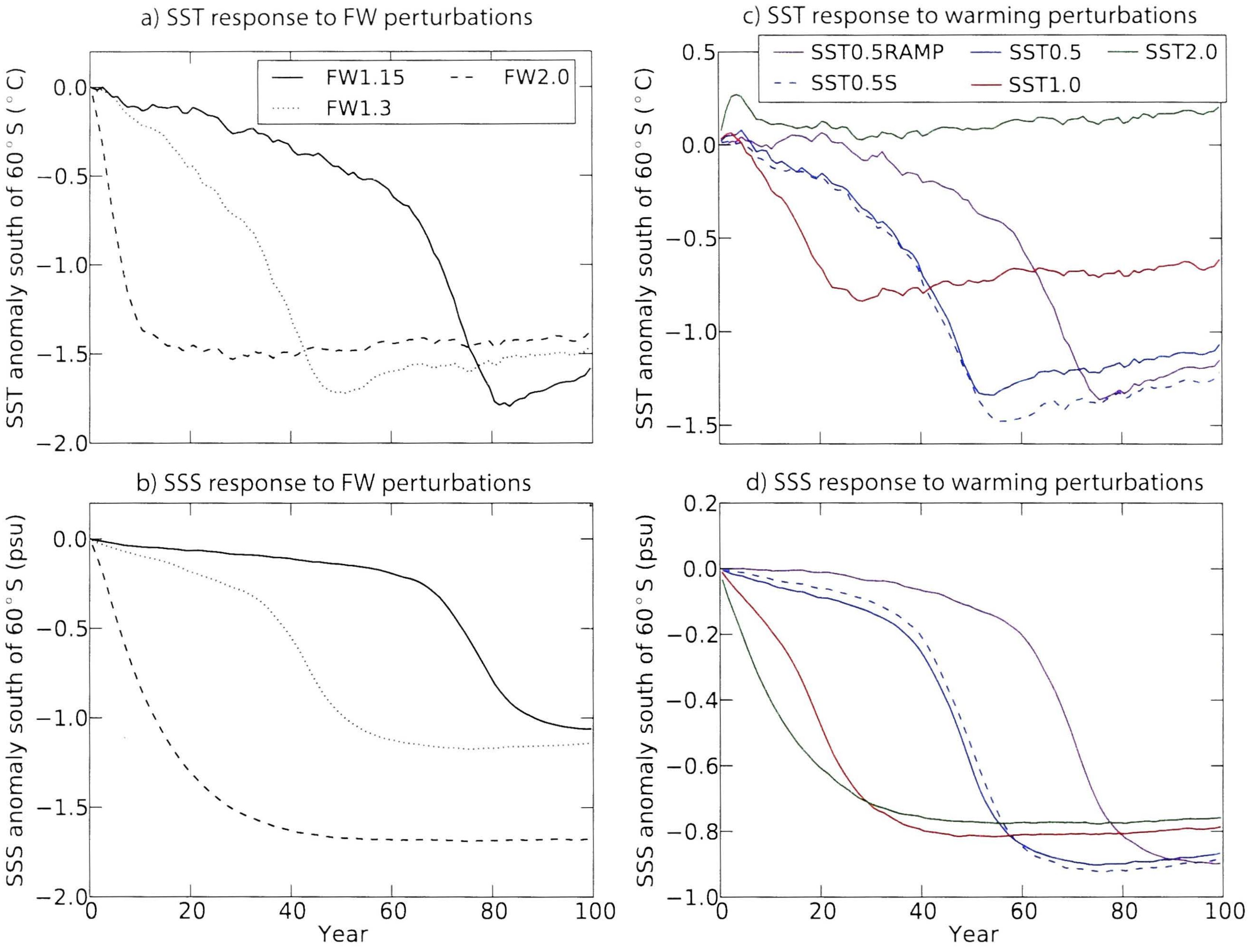

Figure 5.5: Time series of SST (upper) and SSS (lower) anomalies, relative to the reference case, for the different freshwater (left) and warming (right) perturbations and averaged over the region south of 60°S.

vided that the forcing is sufficiently far from the threshold where SST warms rather than cools, i.e. the threshold between SST1.0 and SST2.0. The magnitude of the freshening (Figure 5.5d) varies much less than the cooling between the different warming perturbations. As for the freshwater perturbations, the timescale to reach a quasi-equilbrium decreases for larger forcing changes.

5.4 Heat and salt budgets

5.4.1 Methods

The modelled cooling and freshening described in the previous section is surface enhanced and limited to the upper ocean (Figure 5.6). Below the cooling region, there is a widespread warming trend to full depth, in both the warming and freshwater perturbations. In this paper, our primary goal is to explore the transient surface cooling and freshening in the model, and for this reason, we have chosen to analyse the heat and salt budgets for the upper 12 model levels (~(0-180) m depth) between 60-70°S, as shown by the white box in Figure 5.6.

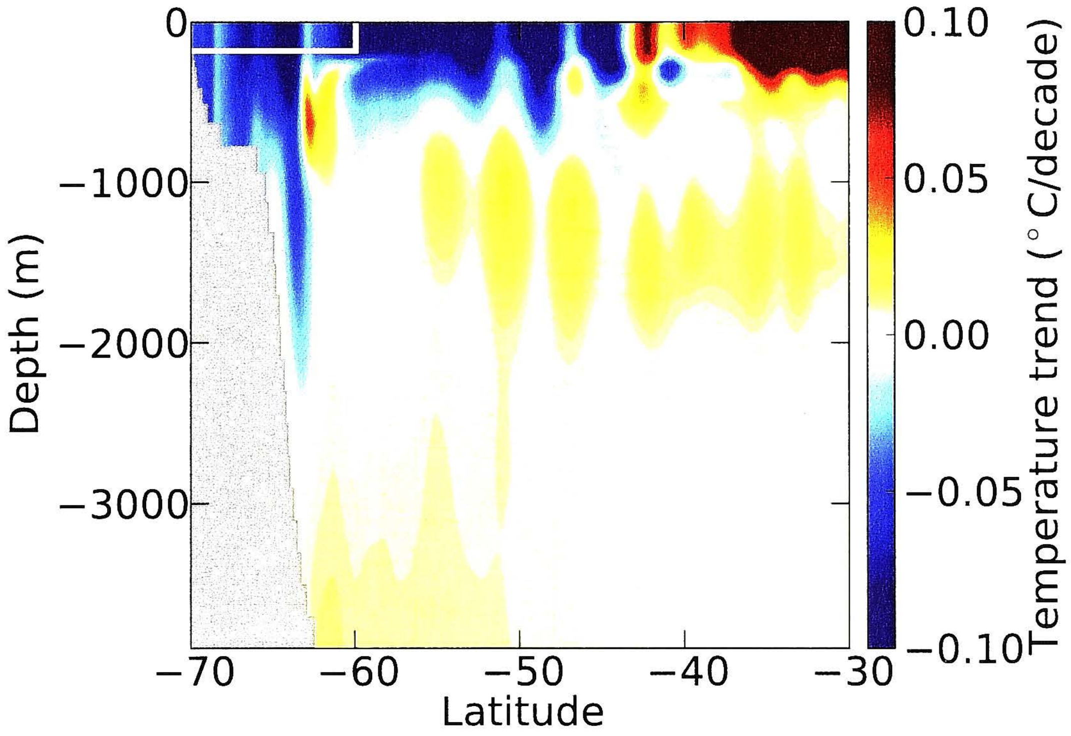

Figure 5.6: The zonally averaged, linear decadal temperature trend, calculated over years 0-50 of the warming perturbation SST0.5RAMP, relative to the reference case. The white box in the upper left shows the region used for the heat and salt budgets in Section 5.4.

The heat budget, integrated over the subdomain, is given by

$$\mathcal{T} = \mathcal{S} + \mathcal{A} + \mathcal{D} + \mathcal{C}, \tag{5.1}$$

where $\mathcal{T}$ is the heat content tendency, $\mathcal{S}$ is the flux through the ocean surface, $\mathcal{A}$ is the advective flux through the lateral and lower boundaries, $\mathcal{D}$ is the parameterised turbulent diffusive flux through the lower boundary and $\mathcal{C}$ is the parameterised convective flux through the lower boundary. The tendency term is calculated as

$$\mathcal{T} = \rho_o c_p \int_{-180m}^{0m} \int_{70^\circ S}^{60^\circ S} \int_{0^\circ}^{40^\circ} \frac{\Delta\theta}{\Delta t} \, dx \, dy \, dz, \tag{5.2}$$

where $\Delta\theta$ is the change in temperature calculated over the time period $\Delta t = 1$ year, ρ_o is a reference density and c_p is the specific heat capacity. The surface heat flux, $\mathcal{S}$, varies in time, dependent on the temperature difference between the relaxation temperature profile and SST. The advective flux is the difference between the time mean fluxes through the northern and lower boundaries:

$$\mathcal{A} = \rho_o c_p \int_{70^\circ S}^{60^\circ S} \int_{0^\circ}^{40^\circ} \overline{w_L \theta_L} \, dx \, dy - \rho_o c_p \int_{-180m}^{0m} \int_{0^\circ}^{40^\circ} \overline{v_N \theta_N} \, dx \, dz, \tag{5.3}$$

where v and w are the meridional and vertical components of the velocity, the subscripts L and N denote evaluation at the lower and northern boundaries of the subdomain respectively, and the overbar represents a 1 year time average. The diffusive flux is given by

$$\mathcal{D} = -\rho_o c_p \int_{70^\circ S}^{60^\circ S} \int_{0^\circ}^{40^\circ} \kappa_v \overline{\frac{\partial \theta}{\partial z}} \, dx \, dy, \tag{5.4}$$

evaluated at the lower surface of the subdomain and where κ_v is the vertical diffusivity.

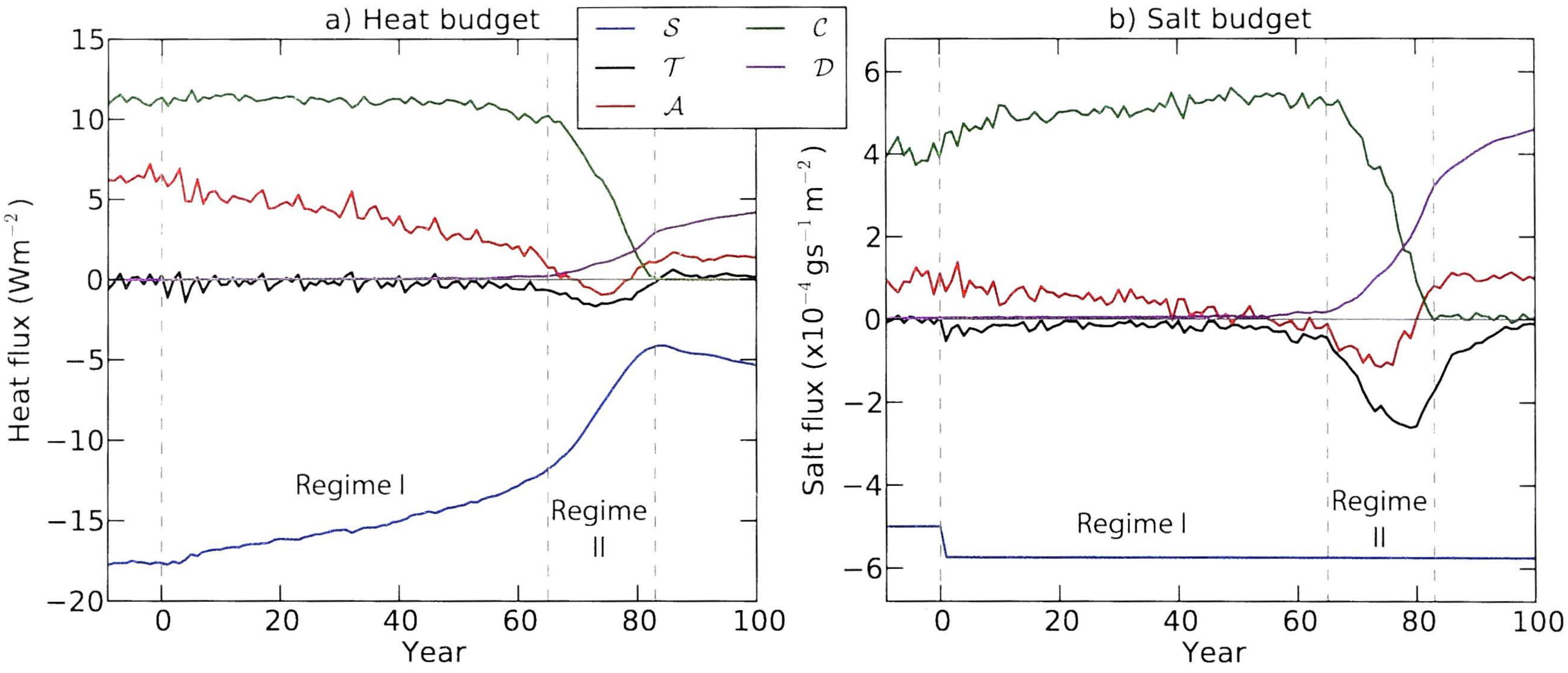

Figure 5.7: Temporal evolution of the a) heat and b) salt budgets for the freshwater perturbation FW1.15, calculated over the subdomain of the white box in Figure 5.6 and annually averaged. The terms are the surface flux, $\mathcal{S}$, heat or salt content tendency, $\mathcal{T}$, advective flux, $\mathcal{A}$, convective flux, $\mathcal{C}$, and the diffusive flux, $\mathcal{D}$. The years −10→0 are the reference case and years 0→100 are the perturbation. Positive heat fluxes warm the region, while positive salt fluxes increase the salinity.

The meridional diffusion through the northern boundary is negligible.

The salinity budget is identical to the heat budget with specific heat content, $\rho_o c_p \theta$, replaced by salt content, $\rho_o S$, where S is the salinity. Unlike the surface heat flux, the surface salt flux is temporally invariant.

The heat and salt fluxes for the reference simulation, normalised by the surface area of the subdomain, are shown in years −10 to 0 of Figure 5.7. As the system is in a long-term equilibrium, the heat and salt content tendencies (black lines) are negligible. In the reference case, the cooling and freshening inputs from the surface forcing (blue lines) are largely ($\sim$60% for the heat flux and $\sim$80% for the salt flux) balanced by the parameterised convective fluxes (green lines), which mix the cool, fresh surface waters with the lower relatively warm, salty water masses. Although the lower cell is fed by convection in the model, this does not imply a linear relationship between the convective fluxes of heat and salt and the lower cell transport, as changes in temperature and salinity may compensate for changes in volume transport. The remainder of the surface fluxes are balanced by the advective fluxes (red lines), through the lower and northern boundaries. Although the location of the overturning cells when averaged in density space (Figure 5.3b) suggests that the advective fluxes south of 60°S should be entirely due to the lower overturning cell, the picture is very different in the depth space framework we have used for the heat and salt budget analysis. Figure 5.8 compares the location and strength of the overturning cells, in the region surrounding the subdomain of interest, calculated using density layer and depth level frameworks. In depth space, the magnitude and extent of the lower overturning cell is greatly diminished and the Deacon cell is the dominant feature (Döös and Webb, 1994). In this study, we are primarily interested in determining the cause

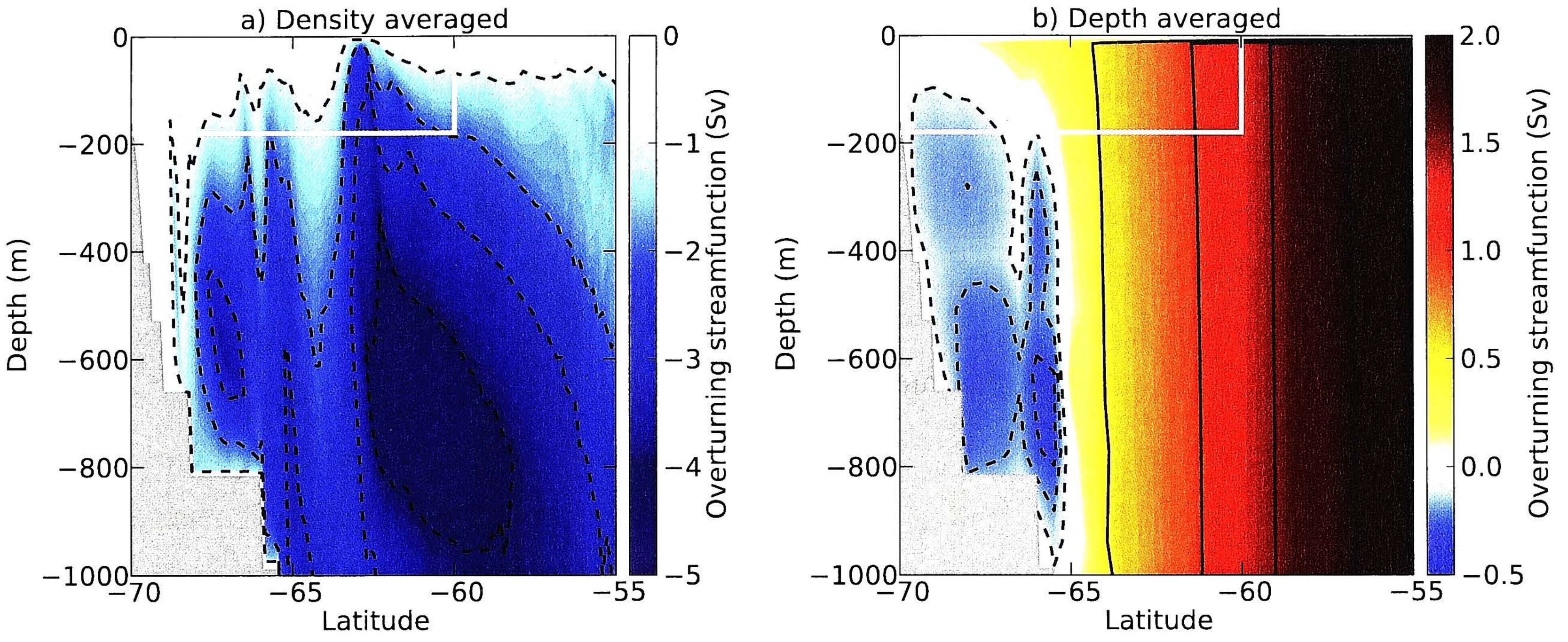

Figure 5.8: The zonally averaged overturning streamfunction near the analysis region (subdomain shown by white box), for a 10 year mean of the reference case. a) Averaged on density surfaces (then mapped back into depth coordinates), with 1 Sv contour intervals. b) Averaged on depth levels, with 0.1 Sv contour intervals for negative streamfunction values, and 0.5 Sv contours for positive streamfunction values. Red colours and solid black lines denote clockwise circulation, while blue colours and dashed black lines indicate anti-clockwise circulation.

of the surface cooling and freshening, and therefore it is logical to use a depth space framework for the problem. However, the use of a depth space framework means that there is a more complicated relationship between the advective volume flux through the subdomain and the magnitude of the density-averaged overturning, than would be the case in an isopycnal framework. We explicitly examine the changes in the lower overturning cell transport in Section 5.5. The advective flux for the reference case, analysed in the depth space framework, contributes a positive flux (i.e. warming and increasing salinity) to the subdomain, due to upwelling of relatively warmer and saltier water masses, which are modified by cooling and freshening inputs at the surface, before exiting the domain through the northern boundary or the southern part of the lower boundary (Figure 5.8b).

5.4.2 Freshwater perturbations

In this section, we describe the evolution of the heat and salt fluxes for the perturbation FW1.15, as shown in Figure 5.7, which leads to the changes in SST and SSS shown in Figure 5.5 (solid lines). The shutdown of convection does not begin immediately following the perturbation, but is instead dependent on a slow preceding adjustment of temperature and salinity by the advective fluxes. The transient surface cooling occurs in two distinct dynamical regimes, as shown by the dashed vertical lines labelled in Figure 5.7.

The first dynamical regime spans years 0-65 and is dominated by decreasing advective fluxes. The sudden increase in applied surface freshwater flux induces an immediate freshening response at the surface and a subsequent small increase in the convective salt flux over the first decade, due to the enhanced salinity difference between the surface and deep waters. However, the dominant effect of the surface freshening over years 0-65 is

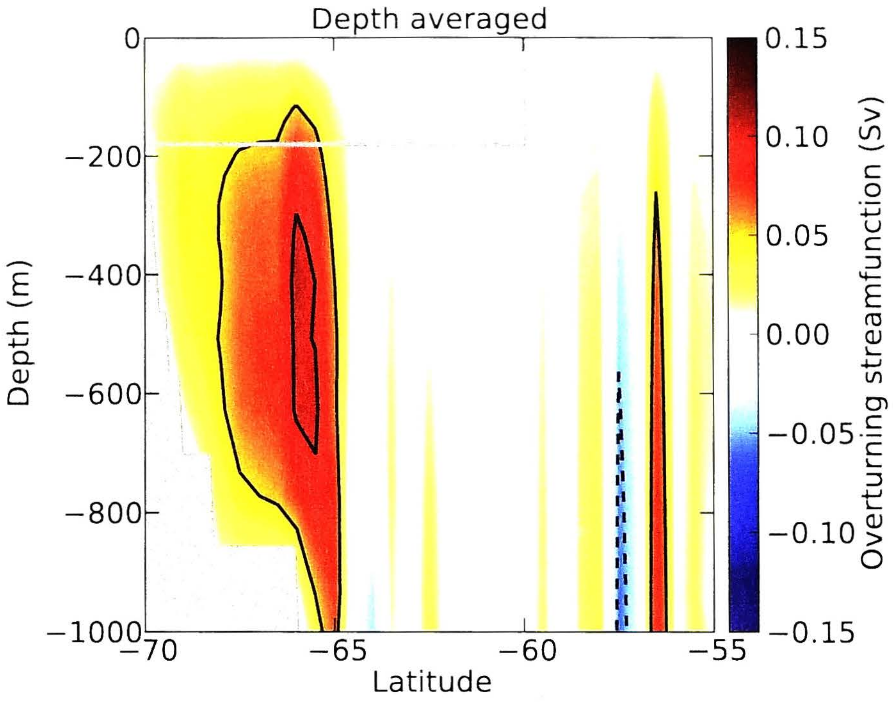

Figure 5.9: The change in the zonally averaged overturning streamfunction averaged over years 20-30 of the freshwater perturbation FW1.15 (relative to the reference case shown in Figure 5.8b). Black contours show 0.05 Sv intervals and red colours indicates clockwise circulation.

a reduction in the overturning circulation and the advective volume fluxes through the subdomain. Figure 5.9 shows that the lower cell overturning, averaged over years 20-30 of perturbation FW1.15 and in a depth space framework, is significantly diminished compared with the reference case overturning shown in Figure 5.8b. The depth averaged 'lower cell' decreases while the Deacon cell remains unchanged. The decreased volume flux slows the advective heat and salt transports to the surface, resulting in sustained cooling and freshening trends during years 0-65. Lower SST increases the surface heat flux (i.e. there is less surface cooling; Figure 5.7a), due to the interactive surface boundary condition. This SST response results in a positive feedback, whereby the increased surface heat flux further reduces advection, causing more surface cooling and thereby further increased surface heat flux. The convective heat and salt fluxes remain approximately constant during this period, due to the opposing effects of cooling and freshening on the surface density. Roughly half of the net cooling in the shutdown process occurs during this advection dominated regime (years 0-65; Figure 5.5a).

Convection shuts down during the second regime, 65-83 years after the start of the freshwater forcing perturbation. As found in other simulations of AABW slowdown (e.g. Kirkman and Bitz, 2011; Martin et al., 2013), at some point salinity changes have a greater effect on surface density than temperature changes, causing surface density to decrease and convection to slow. In our model, the nature of the surface boundary conditions contribute to the dominance of salinity changes over temperature changes: the surface heat flux increases as convection shuts down, while the surface salt flux remains constant, resulting in a greater imbalance in the salinity budget. Decreasing convection has the same effect on SST and SSS as the advection changes in Regime I, but at a much faster rate. The upper ocean becomes isolated from the deep ocean, and the vertical gradients of temperature and salinity increase, which allows diffusion to increase and provide an upward flux of heat and salt.

After convection has shut down, from year 83 onwards, the system is in a quasi-equilibrium, in which diffusion approximately balances the surface fluxes.

Similar transient responses of the heat and salt fluxes occur for different freshwater perturbations. The timescale of Regime I (the period of advection-induced surface cooling) scales inversely with the magnitude of the freshwater perturbation. That is, smaller increases in surface freshwater flux result in slower rates of advective overturning decrease. The timescale of the convection shutdown in Regime II is similar for all perturbations. The increased timescale of Regime I for small perturbations explains the larger magnitude of cooling seen in these experiments (Figure 5.5a). For extreme freshwater perturbations, such as experiment FW2.0, the initial change in surface salinity is sufficient to begin shutdown of convection without the prior advective feedback process, and Regime II begins immediately following the perturbation. The magnitude of the surface salinity anomaly increases with the size of the freshwater forcing perturbation, due to the direct effect of the change in surface salt flux.

5.4.3 Warming perturbations

Figure 5.10 shows the response of the heat and salt fluxes to the warming perturbation SST0.5. The same two distinct surface cooling regimes, as described for the freshwater perturbation in Figure 5.7, are easily identifiable - the first dominated by changes in the advective fluxes and the second by the shutdown of convection.

The one notable difference for the warming perturbation is an initial period of surface warming during years 0-5 before the cooling begins (seen in Figure 5.5c). The sudden

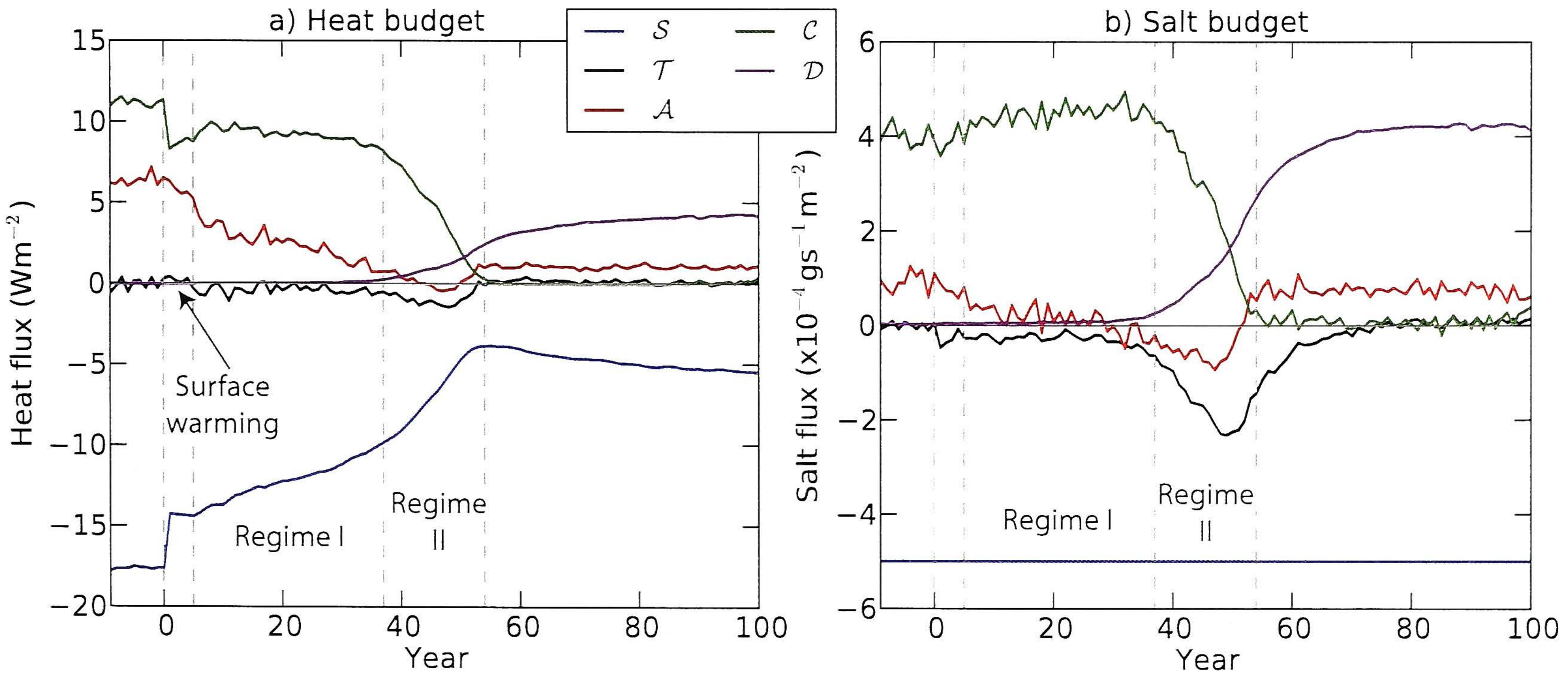

Figure 5.10: Temporal evolution of the a) heat and b) salt budgets for the warming perturbation SST0.5, calculated over the subdomain of the white box in Figure 5.6 and annually averaged. The terms are the surface flux, $\mathcal{S}$, heat or salt content tendency, $\mathcal{T}$, advective flux, $\mathcal{A}$, convective flux, $\mathcal{C}$, and the diffusive flux, $\mathcal{D}$. The years −10→0 are the reference case and years 0→100 are the perturbation. Positive heat fluxes warm the region, while positive salt fluxes increase the salinity.

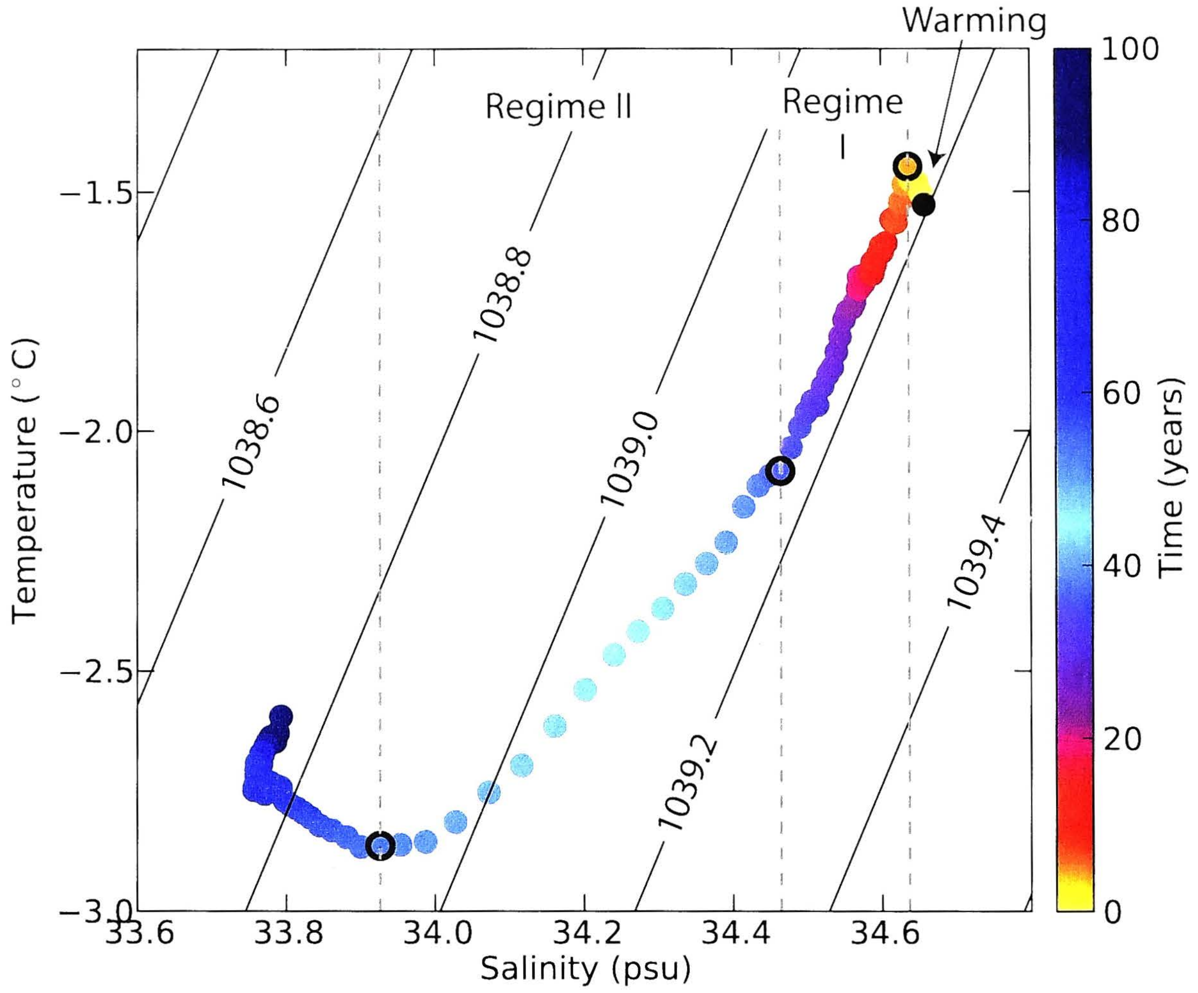

Figure 5.11: Temporal evolution of SST and SSS, averaged over the region 60-70°S, for the warming perturbation SST0.5. Each dot represents a one year time average and colours show the temporal evolution. The black dot is the time mean of the reference case and dots with black outlines highlight the duration of the different cooling regimes. Density contours (in kg m^{-3}) are shown by the diagonal black lines.

increase of the relaxation temperature by 0.5°C at year 0 increases the surface heat flux. Within the first five years, the advective and convective heat fluxes do not adjust quickly enough to balance the change in surface input, which results in a warming at the surface, shown more clearly in Figure 5.11. The increase in SST reduces the surface density and hence the convective fluxes during the first 5 years. The surface freshwater input remains fixed, and therefore the reduced convective salt flux results in a freshening trend during the first five years.

From year 5 onwards in the warming perturbation, the response of the heat and salt fluxes follows a similar sequence to that described for the freshwater perturbation. The reduction in surface heat flux and subsequent surface freshening reduces the overturning circulation and advective volume fluxes through the subdomain. As for the freshwater perturbation, the temperature and salinity changes during the advection dominated regime largely compensate. It is shown more clearly in Figure 5.11 that the surface properties evolve parallel to a density contour in temperature and salinity space during Regime I (years 5-37). Once convection begins to shutdown around year 37, the surface freshening dominates over the cooling signal and the surface density rapidly reduces.

As for the freshwater perturbations, the timescale of the advection dominated Regime I scales inversely with the size of the perturbation, and the magnitude of surface cooling scales with the length of the advective-induced cooling period. That is, smaller changes in surface relaxation temperature result in larger maximum surface cooling anomalies. Moderate increases in surface flux, such as perturbation SST1.0, have a sufficiently large initial change in surface heat flux to begin the shutdown of convection without the prior advective feedback process, and Regime II begins immediately following the initial surface warming. The final surface temperature change in SST1.0 is around half that of SST0.5, due to the missing advective cooling process. In large warming perturbations (e.g. SST2.0), the surface heat flux switches from negative to postive, and thus no surface cooling occurs. The salinity anomaly at 100 years is similar for all warming perturbations, as the majority of the salinity change occurs during the convection shutdown (Regime II), rather than during the advective dominated period (Regime I).

5.5 Response of the lower overturning cell

5.5.1 Overturning transport

The lower overturning cell shuts down in all of the warming (Figure 5.12a) and freshwater perturbations. The transport at 60°S, close to the formation region, decreases approximately linearly throughout the period when surface temperatures are cooling (Figure 5.5c). The timescale for the shutdown is the same as the cooling timescale, i.e. the lower overturning cell persists longer for smaller warming and freshening perturbations. Figure 5.13 shows the link between the lower cell transport and the sum of the advective and convective heat fluxes, for the warming perturbation SST0.5. Within the initial surface warming period, there is a significant decrease in the convective heat flux by the end of the first year. The lower cell transport at 60°S responds with a small delay, decreasing by roughly

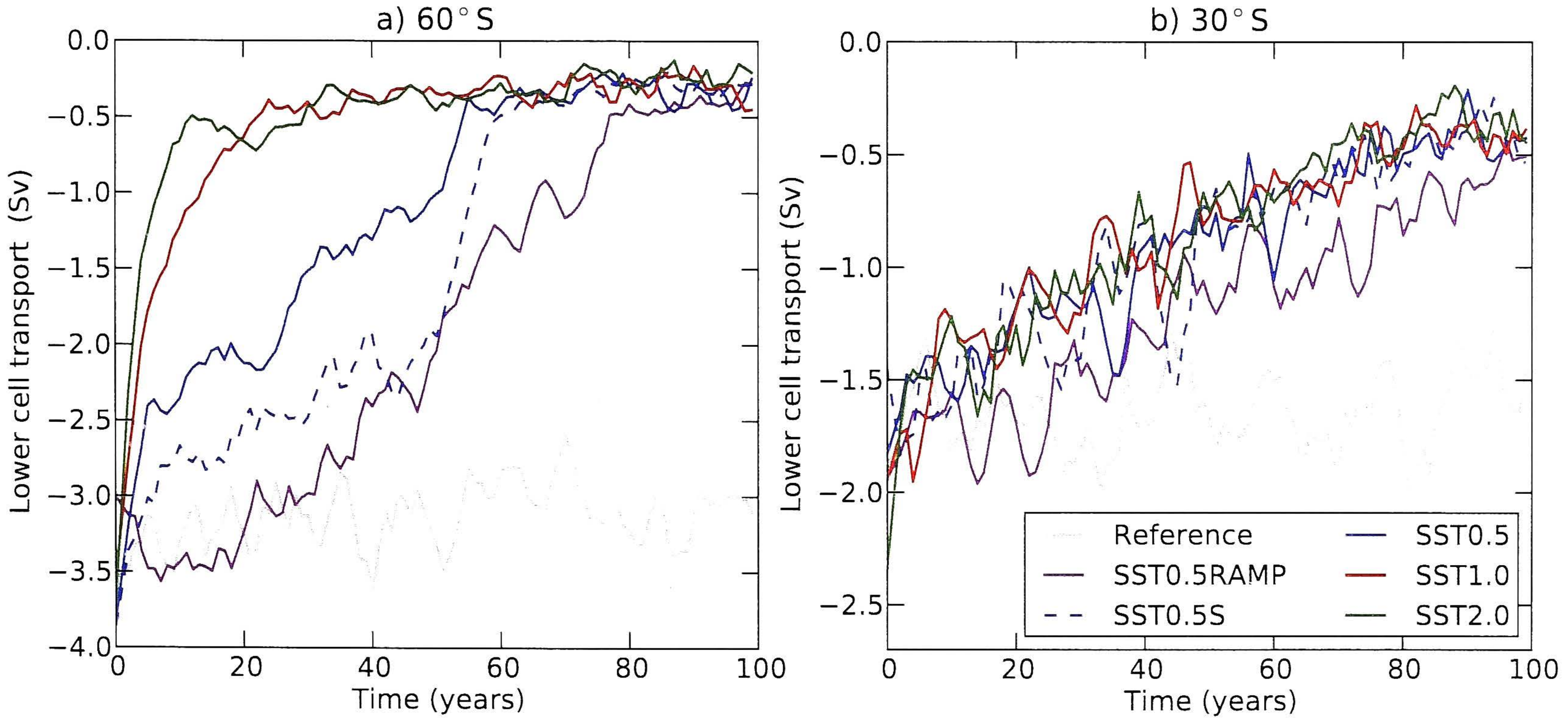

Figure 5.12: Time series of the lower cell streamfunction minimum at a) 60°S and b) 30°S for the reference case and warming perturbations. The data has been smoothed using a 4 year window, so that the underlying trends are clear.

one third over years 1-5. During the first cooling regime, when the heat budget is dominated by advective changes, the lower cell transport scales linearly with the advective heat flux, indicating that the advective heat flux is primarily controlled by the volume flux in the lower cell, rather than the upper overturning cell or temperature changes. The sudden change in the convective heat flux beginning at year 37 of the perturbation SST0.5 occurs too rapidly for the lower overturning cell transport to respond within the same time frame. There is a delay of around 10 years before the overturning transport adjusts to the decrease in the convective fluxes. The other warming and freshening perturbations have similar dynamics to SST0.5.

Despite the variation between perturbations in formation rates and the lower cell shutdown timescale at 60°S (Figure 5.12a), the sensitivity of the lower cell transport response at 30°S is surprisingly independent of the perturbation magnitude (Figure 5.12b). With the exception of experiment SST0.5RAMP, in all of the warming perturbations, the transport in the lower cell reaches 50% of the reference value at 30°S during years 45-55, despite vastly different formation rates further south. The slower rate of decrease in SST0.5RAMP occurs due to the extended length of the initial surface warming regime in this perturbation. Surface temperatures in SST0.5RAMP do not begin to cool (Figure 5.5c) and the lower cell transport at 60°S is not distinguishable from the reference case (Figure 5.12a) until around year 25. However, once the lower cell transport at 30°S begins to respond to the changing surface conditions, the rate of decrease in SST0.5RAMP is similar to that of

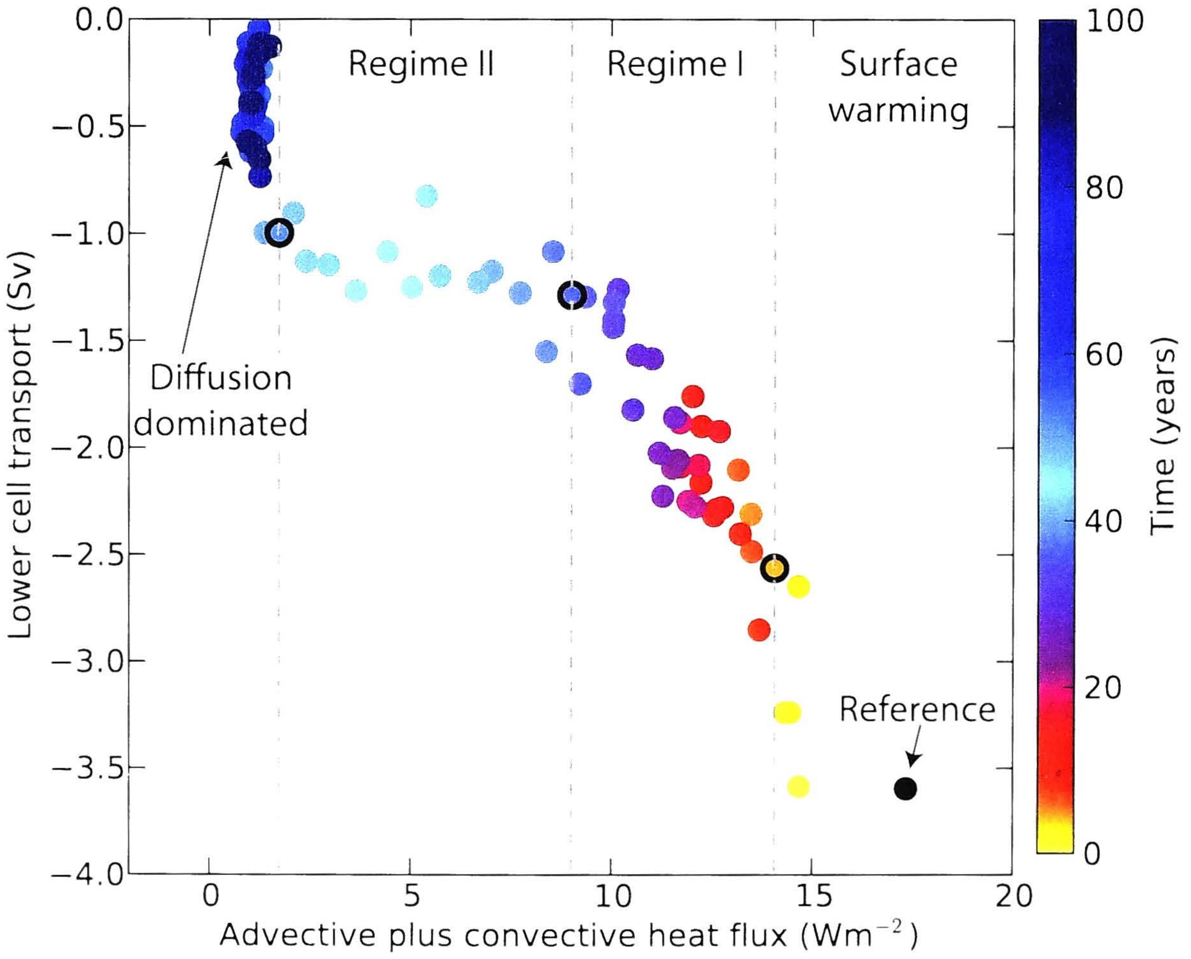

Figure 5.13: Relationship between lower cell transport at 60°S and the sum of the advective and convective heat flux into the subdomain for the warming perturbation SST0.5. Each dot represents a one year time average and colours show the temporal evolution. The black dot is the time mean of the reference case and dots with black outlines show years 5, 37 and 54 (i.e. dividing the different regimes).

the larger warming perturbations. The same insensitivity of the rate of lower cell transport decrease at 30°S to the perturbation magnitude is observed in the freshwater experiments.

5.5.2 Abyssal temperature and salinity

Figure 5.14 compares the evolution of abyssal temperature and salinity between a warming and a freshwater perturbation, averaged below 3000 m and over the region 50-70°S. The magnitude and direction of the trends during the advective dominated Regime I are strongly dependent on the type of buoyancy forcing perturbation. Initially, the abyssal water mass freshens in the freshwater perturbation FW1.15, with minimal temperature change until Regime II (marked by the black circle in Figure 5.14). In the warming perturbation SST0.5, the abyssal water mass warms and becomes saltier. From the beginning of Regime II, when the convective fluxes shut down, the response is similar for both the warming and freshwater perturbations, with significant warming and increasing salinity.

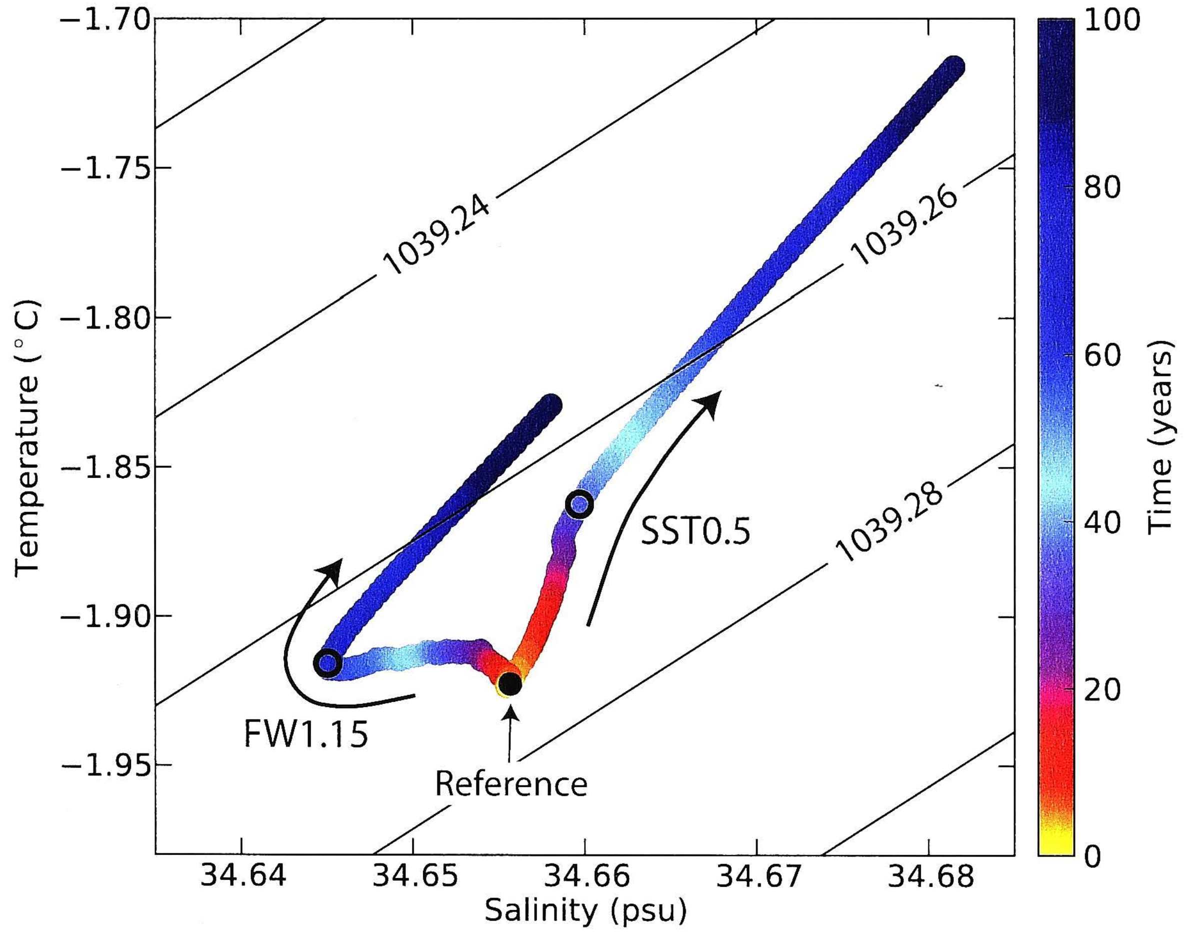

Figure 5.14: Temporal evolution of abyssal temperature and salinity relative to the reference case, averaged below 3000 m and over the region 50-70°S, for the warming perturbation SST0.5 (right) and freshwater perturbation FW1.15 (left). The colours show the temporal evolution and the black dot is the time mean of the reference case. The black circles show the division between the advective and convective dominated phases, corresponding to year 37 for the perturbation SST0.5 and year 65 for FW1.15. Density contours (in kg m^{-3}) are shown by the diagonal black lines.

Unlike the nearly identical surface response for both the warming and freshwater perturbations, the temperature and salinity changes in the abyssal ocean are qualitatively different during the first part of the overturning shutdown process.

5.6 Comparison to observations

Observations of Southern Ocean temperature and salinity at the surface (Durack and Wijffels, 2010; Bintanja et al., 2013) and in the deepest ocean layers (Purkey and Johnson, 2010; Kouketsu et al., 2011; Purkey and Johnson, 2013) show significant decadal trends, which so far remain unexplained. The changes include freshening and cooling at the ocean surface (despite ongoing global warming), and significant warming and freshening in the abyssal ocean. In this section we expand on the hypothesis put forward by Latif et al. (2013) and Bintanja et al. (2013) - that observed Southern Ocean surface cooling may be linked to a slowdown of the bottom water formation rate - and show that both surface and abyssal observations are broadly consistent with the mechanism examined in this study.

The magnitude and spatial coverage of observed surface temperature and salinity trends (Figure 5.15) are comparable to the modeled surface trends that occur in response to an overturning shutdown (e.g. Figure 5.4). The SST data in Figure 5.15a is sourced from the Hadley Centre Sea Ice and Sea Surface Temperature data set (HadISST; Rayner et al., 2003), which incorporates satellite data, float and ship measurements. The SST trend is calculated over the period 1982 - 2012, in order to align with the satellite period. The observed Southern Ocean surface freshening shown in Figure 5.15b is reproduced from the analysis of Durack and Wijffels (2010), which utilised salinity measurements from in situ historical archives and Argo floats over the period 1950 - 2008.

Averaged over far southern latitudes, other SST data sets show similar cooling trends to HadISST (compared in Figure 5.16 and Table 5.1). In addition to HadISST, we have analysed four other SST data sets - NOAA Extended Reconstructed Sea Surface Temperature (ERSST.v3b; Smith et al., 2008), NOAA Optimum Interpolation Sea Surface Temperature (OI.v2; Reynolds et al., 2002) and the Japan Meteorological Agency Centennial in situ Observation-Based Estimates (COBE; Ishii et al., 2005). Of these, only HadISST and OI.v2 incorporate satellite data in addition to in situ data derived from float and ship measurements. Other than HadSST3, all of the data sets are interpolated and use sea ice concentration to calculate SST near sea ice using statistical relationships. HadSST3 is uninterpolated, but contains bias adjustment to reduce the effect of spurious trends due to changes in measurement practices. For the time series of SST shown in Figure 5.16, each data point represents a 1 year time mean and spatial average over all available data in the region south of 50°S. The large offset in mean temperature between the data sets arises from variation in interpolation methods, bias-adjustment and treatment of sea ice, as well as spatial and temporal gaps in the data. The HadSST3 dataset consists of SST anomalies from a climatological mean, so we have adjusted the HadSST3 time series by a constant offset, so that it has the same mean SST as HadISST over the period 1982-2012. However, this adjustment does not affect the HadSST3 trend. All five SST data sets show a cooling trend over this period (Table 5.1), and the trends are robust when calculated over the region south of 50°S or the smaller region south of 60°S, suggesting that the presence and treatment of sea ice, which extends to ~60°S in winter, is not adversely affecting the data.

The SST trends in the model simulations are comparable to the observations (Table 5.1), with a cooling of -0.08 °C/decade in both the smallest warming (SST0.5RAMP) and freshening (FW1.15) experiments, averaged south of 60°S and over years 0-50. The modeled SST cooling rate of -0.08 °C/decade is relatively constant throughout the advection dominated period (Regime I). The cooling rate during Regime II, when convection shuts down, is considerably larger, around -0.5 °C/decade in both the SST0.5RAMP and FW1.15 experiments.

The observational estimates of abyssal warming are much more uncertain than the surface trends, but have been estimated as +0.03°C/decade, using data from the last two decades below 4000 m in the Southern Ocean and south of the Subantarctic Front (Purkey and Johnson, 2010). The modeled abyssal warming rate in the experiment SST0.5RAMP, is smaller, but of the same order of magnitude as the observed trend, at around +0.01 °C/decade, calculated as a linear trend over years 0-50 of the perturbation, and below 3000 m in the region south of 50°S.

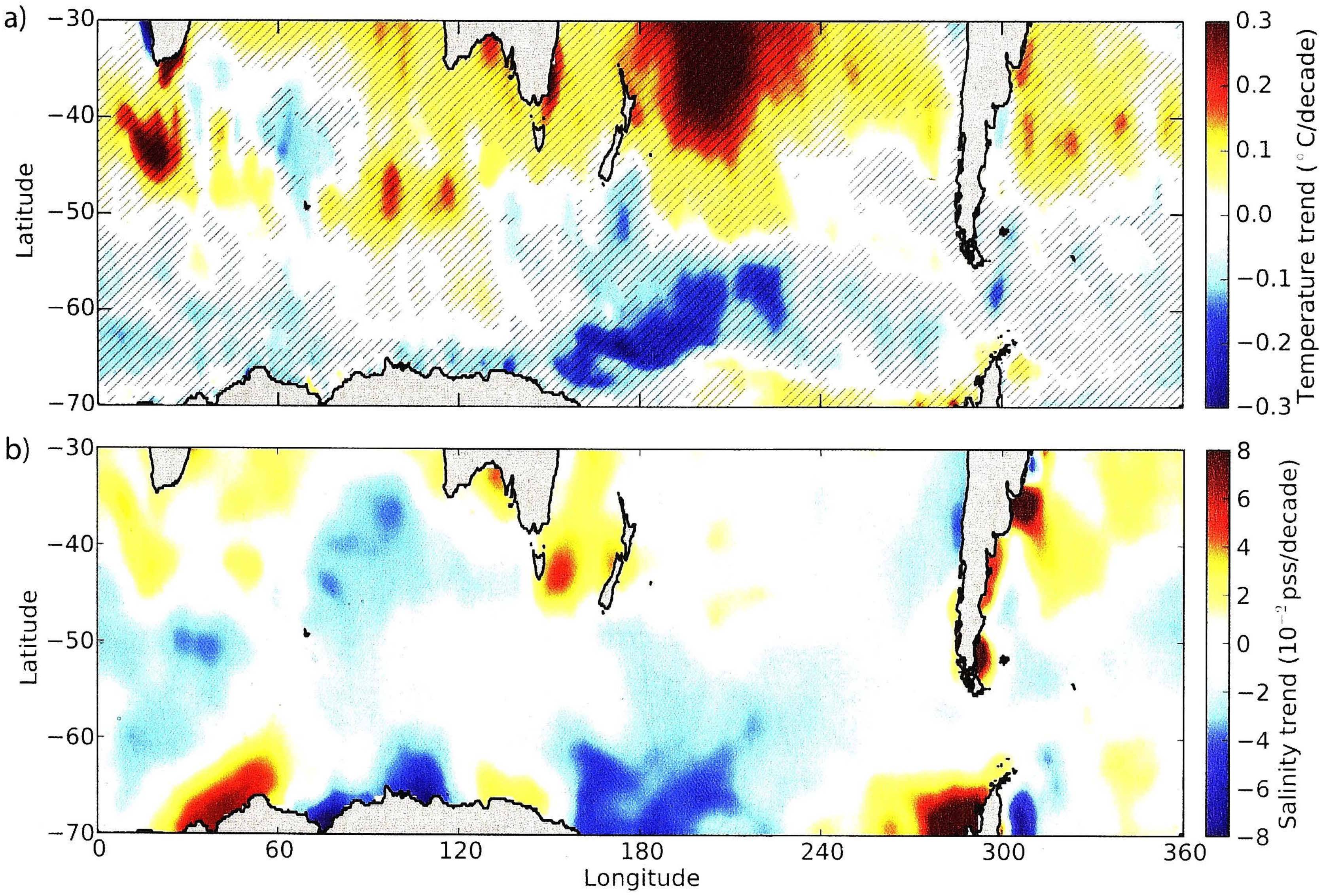

Figure 5.15: Observed linear trends in Southern Ocean surface properties. a) SST trend from the HadISST data set, calculated over the period 1982 - 2012 (°C/decade). Hatching shows where three of the four other SST data sets (HadSST3, ERSST, OISST and COBE), analysed over the same time period, agree with the sign of the HadISST temperature trend. b) Salinity trend from Durack and Wijffels (2010), calculated over the period 1950 - 2008 (pss/decade).

Table 5.1: Linear, decadal SST trends calculated over the period 1982 - 2012. Trends that are significantly different from zero at the 99% confidence level are shown in bold font.

Data set	SST trend 60-90°S (°C/dec)	SST trend 50-90°S (°C/dec)
COBE	**-0.02**	**-0.03**
HadISST	**-0.04**	**-0.03**
OI.v2	-0.05	-0.04
ERSST	**-0.06**	**-0.06**
HadSST3	-0.06	**-0.07**

5.7 Discussion and summary

We have investigated the dynamics of the Southern Ocean surface cooling and freshening that occurs in response to reduced abyssal overturning circulation transport, using an eddy permitting, idealised ocean model. The ocean-driven mechanism relies on surface buoyancy forcing perturbations (enhanced freshwater flux or paradoxically, atmospheric warming) inducing changes in the overturning circulation. We find that a transient SST trend, of similar magnitude and spatial extent to the observations, occurs in the model on a timescale of order 100 years, in response to a range of such perturbations. The surface cooling and freshening are linked to the shutdown process of the lower overturning circulation, due to the changing oceanic transport of heat and salt to the surface region.

The modelled overturning shutdown process follows a sequence of distinct stages, dominated by different heat and salt fluxes. Surface cooling occurs in two distinct regimes: the

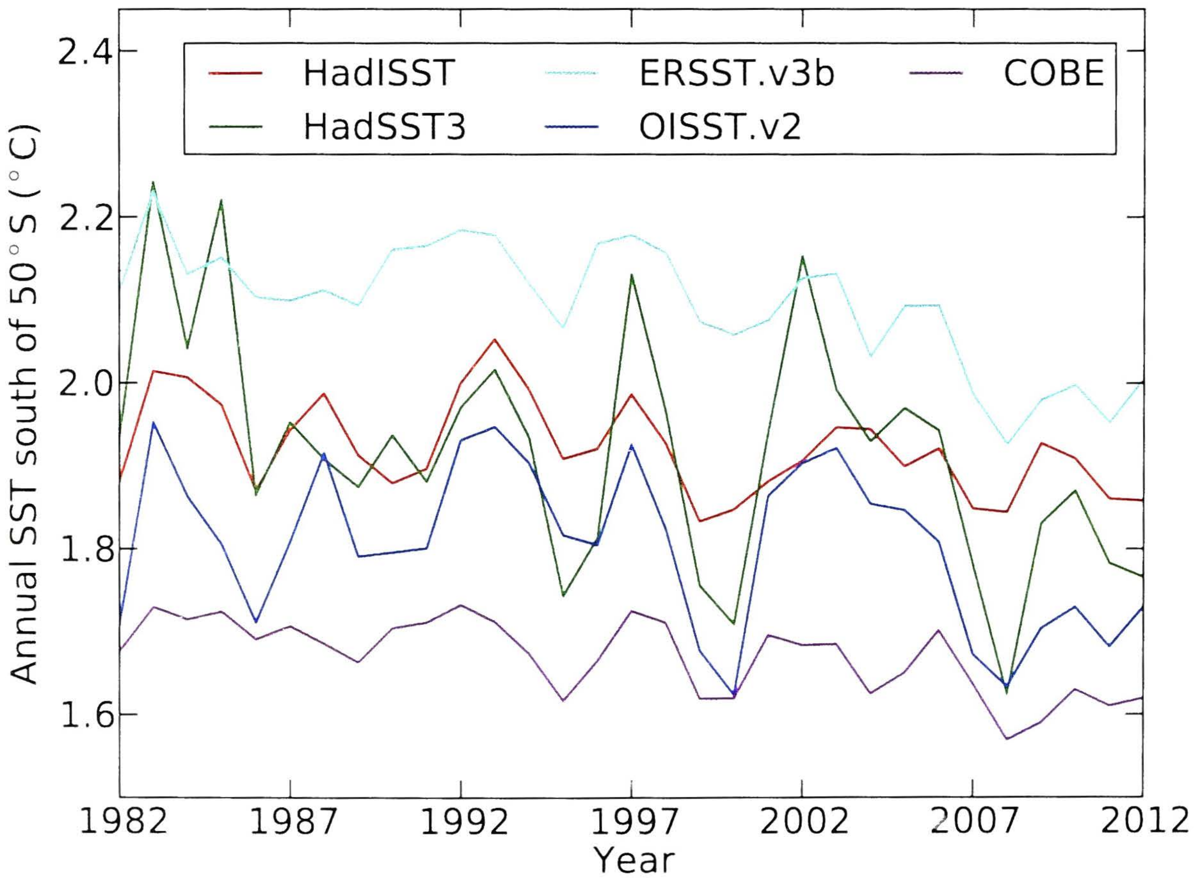

Figure 5.16: Time series of annual SST for five different observational data sets, averaged over all available data south of 50°S. The linear trends for each of the data sets are given in Table 5.1.

first is characterised by decreasing advective heat flux to the surface, linked to a simultaneous reduction in the volume transport of the lower overturning cell, and the second is characterised by a sudden drop in convective heat flux, resulting from a surface freshwater cap and driving a delayed decrease in the lower cell transport. The cooling and freshening is a transient effect; all of the perturbations reach a quasi-equilibrium within 100 years, in which enhanced stratification allows diffusion to balance the surface fluxes. The shutdown process and associated cooling occurs at a faster rate for larger perturbations, since the threshold for shutdown of convection is reached sooner. However, since the cooling occurs during both the advective and convective dominated regimes, smaller perturbations (in which the advective dominated regime persists for an extended period) have a significantly stronger net cooling anomaly compared with larger perturbations (in which the convective flux shutdown begins nearly immediately). The surface heat flux in the largest warming perturbation is indeed sufficient to warm, rather than cool, SST south of 50°S, as may be expected from a simple, non-dynamical view of the system.

The idealised numerical model used in this paper incorporates many simplifications in terms of topography, forcing, dense water formation processes and lack of coupling to atmosphere and sea ice, which leads to the obvious question: to what extent are the results applicable to the real climate system? In this section we address possible impacts of the idealised nature of the model and discuss some of the missing feedbacks. However, we also argue that, despite the simplifications, this model captures the most relevant ocean dynamics and the ocean overturning feedback process.

One of the most obvious and perhaps consequential simplifications is the method of dense water formation in the model. In the real ocean, dense shelf waters are formed as a result of atmospheric cooling and brine rejection in localised polynyas, which subsequently entrain fresher surrounding waters to form AABW. We combine the net buoyancy effect of these separate dense water production and entrainment processes into the zonally averaged surface freshwater flux and temperature relaxation, which results in an abyssal water mass with similar properties to AABW, but likely different sensitivity to forcing changes. The idealised buoyancy fluxes are also temporally invariant with no seasonal cycle. In the real ocean, the intense buoyancy fluxes that lead to convective onset are intermittent in both space and time, leading to a density profile that appears stable in a long time average, but which has transient unstable events. In our model, the lack of seasonally varying surface forcing means that our density profile is, in some regions, always marginally unstable. However, the results of a high resolution polynya modelling study by Marsland et al. (2007) found that dense water production responds at least qualitatively similarly to that in our idealised model. Using a coupled ocean and sea ice model with realistic topography and forcing, Marsland et al. (2007) found a 40% decrease in dense shelf water production in response to a +2°C atmospheric warming, and a 33% reduction following a 20 cm/year increase in precipitation.

The other major simplification commonly used for modelling the lower overturning cell is the use of parameterised convection, which enables the transport of dense waters from the upper ocean formation regions to the lower layers. In our model this is achieved by enhancing vertical mixing of temperature and salinity. Parameterised convection results in an artificial separation of the advective and convective fluxes; in the real ocean, these are both parts of the same overturning circulation cell and are unquestionably dependent on each other. However, given that a resolution of order $3 - 5$ km is needed to resolve the downslope AABW pathways in z-coordinate models (Winton et al., 1998), which is approximately one to two orders of magnitude higher than the resolution of present climate models, it remains a worthwhile exercise to improve understanding of the dynamical processes associated with parameterised convection.

The formation of dense water and its sensitivity to forcing perturbations is also likely to be greatly affected by the use of a linear equation of state in the model. Along with missing water mass formation due to cabbeling and thermobaric processes (Klocker and McDougall, 2010), salinity is of relatively greater importance for determining density at cold temperatures. This could have consequences for the timing of the convection shutdown at the start of Regime II. In particular, as convection begins to shutdown at the point where the impact of the salinity anomaly on density dominates over the impact of the temperature anomaly, it is possible that in a setup using a full equation of state, the convection may be more sensitive to forcing changes.

With no sea ice model, it is possible that we may be neglecting an important feedback process in the formation of dense water. Aiken and England (2008), in a coupled ocean-atmosphere-sea ice model, investigated a negative feedback process, whereby a decrease in convection reduced the upward heat flux and cooled SST in the dense water formation region, resulting in a higher rate of sea ice formation and therefore an increase in brine rejection and at least a partial offset in the original convective decrease. This negative sea ice feedback implies that there may be a forcing perturbation threshold, below which the lower overturning cell is stable to small perturbations. Observations are currently showing an increase in Southern Ocean sea ice coverage (Zhang, 2007), as predicted by the negative feedback process of Aiken and England (2008). However, the coupled ocean-sea ice modelling study of Zhang (2007) suggests that the sea ice increase is not due to an enhanced formation rate, but rather to the subsurface melt rate decreasing faster (due to reduced upward heat flux) than the decrease in formation rate. The recent modelling study of Bintanja et al. (2013) is in agreement with Zhang (2007), showing that the cool, fresh surface layer has isolated sea ice from warm upwelling waters and therefore decreased the rate of basal melt. The similarity of the lower overturning cell shutdown and surface response in our idealised model compared with previous studies using models coupled to sea ice (e.g. Stouffer et al., 2007; Aiken and England, 2008; Swingedouw et al., 2008; Menviel et al., 2010; Kirkman and Bitz, 2011; Bintanja et al., 2013) leads us to argue that we are capturing the most relevant dynamics of the ocean overturning system.

Furthermore, despite the possible influences of the simplified dense water formation, it is worth noting that the modelled SST cooling is also strongly dependent on the larger scale dynamical ocean feedback and in particular the dynamics of the advective fluxes. In the Southern Ocean, the mesoscale eddy field has a significant effect on the circulation and advection of tracers, which means we are most likely modelling this part of the system more accurately than previous studies.

In conclusion, we have shown that small atmospheric warming perturbations, in addition to freshwater perturbations, can induce Southern Ocean surface cooling, linked to the shutdown process of the abyssal overturning cell. We hypothesise that a significant component of such processes may be responsible for the recent observed surface cooling and freshening trends south of 50°S in the Southern Ocean.

Acknowledgments

AMH was supported by an Australian Research Council Future Fellowship FT120100842 and MHE by Australian Research Council Laureate Fellowship FL100100214. The analysis in Section 5.6 is based on data made freely available by the International Argo Program and the national programs that contribute to it (http://www.argo.ucsd.edu). The Argo Program is part of the Global Ocean Observing System. The numerical model was run on the NCI National Facility in Canberra, Australia, which is supported by the Australian Commonwealth Government. We wish to thank Anand Gnanadesikan, Bob Hallberg and three anonymous reviewers for providing useful feedback on the original manuscript, and Nicola Maher for valuable discussions regarding the observational data sets and trends.

Chapter 6

Conclusions

6.1 Summary

This research presented in this thesis has deepened our understanding of the role of the Southern Ocean circulation in the global climate system.

The major research findings are:

1. Buoyancy forcing plays a dominant role in setting the strength of the upper overturning circulation in the Southern Ocean.

   The implication of this result is that the increase in Southern Ocean upwelling following glacial periods may have been driven by enhanced surface temperatures or freshwater fluxes, rather than enhanced wind stress. Predicted changes in future heat and freshwater fluxes over the Southern Ocean may also contribute to enhanced upwelling.

2. Eddy saturation is more complete than eddy compensation. The upper overturning cell responds significantly more to wind stress perturbations compared with the ACC transport.

   The upper overturning cell is therefore likely to increase in response to present and future changes in wind stress.

3. Eddies play a critical role in present-day mid-depth Southern Ocean heat uptake. Enhanced air-sea heat flux drives ocean warming through a decrease in the isopycnal temperature gradient and hence in the upward eddy heat transport. Enhanced wind stress drives a transient ocean cooling, due to a faster response of the upward eddy heat transport compared with the mean downward heat transport.

4. The recent sea surface temperature cooling trend south of 50°S in the Southern Ocean is consistent with a slowdown of the lower overturning cell, driven by a combination of increased heat and freshwater fluxes south of the ACC.

6.2 Future directions

While this research has improved our dynamical understanding of the Southern Ocean circulation response, there remain many questions yet to be answered.

6.2.1 Ocean-atmosphere coupling

This thesis has exclusively made use of idealised ocean-only numerical models. Idealised models have the advantage of permitting precise control over atmospheric forcing and allowing dynamical processes to be disentangled with relative ease. However, these models are not able to simulate the exact quantitative response of the Southern Ocean to changing forcing. The results of Chapters 2 and 3 indicate that the upper overturning cell is sensitive to both wind stress and buoyancy forcing perturbations, and also highlight the need for resolving the eddy field.

The next step in refining our understanding of the sensitivity of the Southern Ocean overturning is to investigate the effects of atmosphere-ocean feedbacks. Chapters 2 and 3 applied independent prescribed changes in the surface buoyancy and wind forcing. However, the atmosphere-ocean interaction is not a one-way mechanism, and changes in the overturning will alter the local atmospheric state and may lead to potentially significant feedbacks on the ocean circulation. Some of these feedbacks have been investigated in coarse resolution coupled models (Sen Gupta and England, 2006; Delworth and Zeng, 2008), but not yet in eddy resolving coupled models.

Southern Hemisphere buoyancy forcing and wind stress are also not independent of one another and changes in different components of the forcing may be correlated with one another. For example, Downes and Hogg (2013) found that the simulated effects of future wind stress and buoyancy forcing changes on the ACC transport in the CMIP5 coupled models largely compensate each other, resulting in a net weak sensitivity. It is unclear how interactions between buoyancy and wind stress forcing will influence the overturning circulation. However, it is possible that the modelled sensitivity of the Southern Ocean circulation to wind stress shifts may be traceable to associated changes in buoyancy forcing (Hirabara et al., 2007). For example, changes in wind stress directly influence evaporation and upper ocean mixing rates and indirectly influence the heat flux into the ocean through induced changes in sea surface temperature. Further research is required using eddy resolving coupled models.

6.2.2 Detecting change in the Southern Ocean overturning

One pressing requirement for improved interpretation and prediction of anthropogenic climate change is an accurate method of measuring changes in the Southern Ocean overturning circulation. The Southern Ocean carbon sink and global abyssal ocean heat uptake are closely tied to the strength of the upper and lower overturning cells respectively. However we currently have no accurate method for detecting overturning change in the Southern Ocean.

As outlined in Chapter 1, several studies have suggested that the upper overturning circulation may have increased in response to enhanced westerly winds over the last several decades (Le Quéré et al., 2007; Takahashi et al., 2012; Waugh et al., 2013). These studies used indirect methods based on changes in CO_2 and chlorofluorocarbon concentrations. However the tracer concentration data is spatially and temporally limited to a few Southern Ocean hydrographic sections, leading to large uncertainties in the inferred overturning changes. As a result, these present methods are too imprecise to conclusively demonstrate whether or not the upper overturning circulation has changed over recent decades.

A more precise method may be possible based on analysis of temperature and salinity data, which is far more comprehensive than tracer data due to additional observations from remote sensing floats, as well as ship-based data. Changes in the strength of the overturning circulation should result in distinct spatial patterns of change in temperature and salinity in the Southern Ocean. In an idealised modelling study, Xie and Vallis (2012) have shown that at least half of the spatial pattern of ocean temperature anomaly may be explained by ocean circulation changes, as opposed to passive heat uptake by a fixed ocean circulation. It is possible that numerical modelling studies could be used to identify the particular spatial patterns of temperature and salinity anomalies associated with a change in the overturning circulation. Mapping these patterns onto the observational data would then allow separation of the temperature and salinity trends into a component arising directly from surface buoyancy forcing changes and a component giving a quantitative estimate of overturning change. The cooling trend linked to the eddy response identified in Chapter 4 implies that an eddy resolving model would be needed for such a study.

6.2.3 How eddy saturated is the ocean?

Eddy permitting and eddy resolving modelling studies agree that the response of the upper overturning circulation to increased wind stress far exceeds the response of the ACC transport (Chapter 3; Dufour et al., 2012; Munday et al., 2013). However the range of modelled sensitivities for the ACC transport is large; varying from no transport change (Meredith and Hogg, 2006; Munday et al., 2013) to a 25-30% increase in ACC transport (Chapter 3; Jones et al., 2011) for a doubling of wind stress. Other eddy permitting modelling studies include a latitudinal wind stress shift and hence are not directly comparable, but predict a 5-10% increase in ACC transport for similar wind stress perturbations (Farneti et al., 2010; Dufour et al., 2012). The majority of research on the ACC transport sensitivity to wind stress has focused on the effect of changing model resolution. However, the results of Chapter 3 and Munday et al. (2013) indicate that an eddy permitting resolution may be sufficient and that further increases in resolution have limited effect on the transport response to increasing wind stress. Instead, the wide range of ACC transport sensitivities may be linked to other factors in the setup of these model experiments, such as topography (flat bottom or Drake Passage sill; straight southern boundary or Antarctic peninsula), quasigeostrophic or primitive equation model formulation, atmospheric coupling, northern overturning closure method, etc. Future advancements in our understanding of the ACC will require a comprehensive exploration of the effect of a wide range of experimental parameters on the ACC transport sensitivity.

6.2.4 Improved observations

The research presented in this thesis is useful largely because the observational record in the Southern Ocean is so short and sparse; numerical modelling studies are the predominant way to estimate and interpret changes in the ocean circulation. Even if observations can not be expanded sufficiently to directly measure change in the Southern Ocean circulation, improvements would greatly help to constrain modelling estimates.

Knowledge of the time mean surface buoyancy forcing over the Southern Ocean is particularly lacking (Bourassa et al., 2013). Water mass formation rates are strongly dependent on surface buoyancy forcing, yet different reanalyses and flux products do not even agree on the sign of the buoyancy fluxes over large regions of the Southern Ocean (Cerovečki et al., 2011). Accurate predictions of future changes in the overturning circulation driven by changes in buoyancy forcing are therefore near impossible.

Chapter 5 highlights the urgent need for improved transport measurements in the AABW overturning cell pathways and formation regions. The lower overturning cell may have decreased in strength over recent decades and the modelling study in Chapter 5 indicates that temperature and salinity observations are consistent with this hypothesis. A slowdown of the lower overturning may have significant consequences on abyssal ocean heat uptake and the melt rate of Antarctic ice sheets. Improved observations of the lower overturning cell transport are therefore critical for reducing uncertainty in future sea level rise.

One final observational domain that could be improved is the spatial and temporal coverage of ocean chemical tracer concentrations. Ship-based tracer measurements are currently the most reliable method of estimating changes in the upper overturning cell and Southern Ocean carbon sink. However, a remote observing system of biogeochemical profiling floats (Juranek et al., 2011) has been proposed and would greatly reduce the uncertainty on overturning and air-sea carbon flux trends.

Bibliography

Abernathey, R., J. Marshall, and D. Ferreira, 2011: The dependence of Southern Ocean meridional overturning on wind stress. *J. Phys. Oceanogr.*, **41**, 2261–2278.

Adcroft, A., R. Hallberg, and M. Harrison, 2008: A finite volume discretization of the pressure gradient force using analytic integration. *Ocean Modell.*, **22**, 106–113.

Aiken, C. M. and M. H. England, 2008: Sensitivity of the present-day climate to freshwater forcing associated with Antarctic sea ice loss. *J. Clim.*, **21**, 3936–3946.

Barker, S., G. Knorr, M. J. Vautravers, P. Diz, and L. C. Skinner, 2010: Extreme deepening of the Atlantic overturning circulation during deglaciation. *Nat. Geosci.*, **3**, 567–571.

Bintanja, R., G. J. van Oldenborgh, S. S. Drijfhout, B. Wouters, and C. A. Katsman, 2013: Important role for ocean warming and increased ice-shelf melt in Antarctic sea-ice expansion. *Nat. Geosci.*, **6**, 1–4.

Böning, C. W., A. Dispert, M. Visbeck, S. R. Rintoul, and F. U. Schwarzkopf, 2008: The response of the Antarctic Circumpolar Current to recent climate change. *Nat. Geosci.*, **1**, 864–869.

Bourassa, M. A., et al., 2013: High-latitude ocean and sea ice surface fluxes: Challenges for climate research. *B. Am. Meterol. Soc.*, **94**, 403–423.

Bracegirdle, T. J., W. M. Connolley, and J. Turner, 2008: Antarctic climate change over the twenty first century. *J. Geophys. Res.*, **113**, D03 103.

Bracegirdle, T. J., E. Shuckburgh, J.-B. Sallee, Z. Wang, A. J. S. Meijers, N. Bruneau, T. Phillips, and L. J. Wilcox, 2013: Assessment of surface winds over the Atlantic, Indian, and Pacific Ocean sectors of the Southern Ocean in CMIP5 models: Historical bias, forcing response, and state dependence. *J. Geophys. Res.*, **118**, 547–562.

Brierley, C. M., M. Collins, and A. J. Thorpe, 2008: The impact of perturbations to ocean-model parameters on climate and climate change in a coupled model. *Clim. Dyn.*, **34**, 325–343.

Broecker, W., 2009: The mysterious ^{14}C decline. *Radiocarbon*, **51**, 109–119.

Cai, W., T. Cowan, S. Godfrey, and S. Wijffels, 2010: Simulations of processes associated with the fast warming rate of the southern midlatitude ocean. *J. Clim.*, **23**, 197–206.

Cerovečki, I., L. D. Talley, M. R. Mazloff, and I. Cerovecki, 2011: A comparison of Southern Ocean air-sea buoyancy flux from an ocean state estimate with five other products. *J. Clim.*, **24**, 6283–6306.

Chapman, W. L. and J. E. Walsh, 2007: A synthesis of Antarctic temperatures. *J. Clim.*, **20**, 4096–4117.

Cunningham, S. A., S. G. Alderson, and B. A. King, 2003: Transport and variability of the Antarctic Circumpolar Current in Drake Passage. *J. Geophys. Res.*, **108**, C58 084.

Delworth, T. L. and F. Zeng, 2008: Simulated impact of altered Southern Hemisphere winds on the Atlantic Meridional Overturning Circulation. *Geophys. Res. Lett.*, **35**, L20 708.

Döös, K. and D. J. Webb, 1994: The Deacon cell and the other meridional cells of the Southern Ocean. *J. Phys. Oceanogr.*, **24**, 429–442.

D'Orgeville, M., W. P. Sijp, M. H. England, and K. J. Meissner, 2010: On the control of glacial-interglacial atmospheric CO_2 variations by the Southern Hemisphere westerlies. *Geophys. Res. Lett.*, **37**, L21 703.

Downes, S. M., A. S. Budnick, J. L. Sarmiento, and R. Farneti, 2011: Impacts of wind stress on the Antarctic Circumpolar Current fronts and associated subduction. *Geophys. Res. Lett.*, **38**, L11 605.

Downes, S. M. and A. M. Hogg, 2013: Southern Ocean circulation and eddy compensation in CMIP5 models. *J. Clim.*, **26**, 7198–7220.

Dufour, C. O., J. Le Sommer, J. D. Zika, M. Gehlen, J. C. Orr, P. Mathiot, and B. Barnier, 2012: Standing and transient eddies in the response of the Southern Ocean meridional overturning to the Southern Annular Mode. *J. Clim.*, **25**, 6958–6974.

Durack, P. J. and S. E. Wijffels, 2010: Fifty-year trends in global ocean salinities and their relationship to broad-scale warming. *J. Clim.*, **23**, 4342–4362.

Durack, P. J., S. E. Wijffels, and R. J. Matear, 2012: Ocean salinities reveal strong global water cycle intensification during 1950 to 2000. *Science*, **336**, 455–458.

Farneti, R., T. L. Delworth, A. J. Rosati, S. M. Griffies, and F. Zeng, 2010: The role of mesoscale eddies in the rectification of the Southern Ocean response to climate change. *J. Phys. Oceanogr.*, **40**, 1539–1557.

Fischer, H., et al., 2010: The role of Southern Ocean processes in orbital and millennial CO_2 variations - A synthesis. *Quaternary Sci. Rev.*, **29**, 193–205.

Fučkar, N. S. and G. K. Vallis, 2007: Interhemispheric influence of surface buoyancy conditions on a circumpolar current. *Geophys. Res. Lett.*, **34**, L14 605.

Galbraith, E. D., et al., 2011: Climate variability and radiocarbon in the CM2Mc Earth System Model. *J. Clim.*, **24**, 4230–4254.

Gent, P. R. and G. Danabasoglu, 2011: Response to increasing Southern Hemisphere winds in CCSM4. *J. Clim.*, **24**, 4992–4998.

Gent, P. R., W. G. Large, and F. O. Bryan, 2001: What sets the mean transport through Drake Passage? *J. Geophys. Res.*, **106**, 2693–2712.

Gent, P. R. and J. C. McWilliams, 1990: Isopycnal mixing in ocean circulation models. *J. Phys. Oceanogr.*, **20**, 150–155.

Gille, S. T., 2008: Decadal-scale temperature trends in the Southern Hemisphere ocean. *J. Clim.*, **21**, 4749–4765.

Gnanadesikan, A. and R. W. Hallberg, 2000: On the relationship of the circumpolar current to Southern Hemisphere winds in coarse-resolution ocean models. *J. Phys. Oceanogr.*, **30**, 2013–2034.

Gregory, J. M., 2000: Vertical heat transports in the ocean and their effect on time-dependent climate change. *Clim. Dyn.*, **16**, 501–515.

Gruber, N., et al., 2009: Oceanic sources, sinks, and transport of atmospheric CO_2. *Global Biogeochem. Cy.*, **23**, GB1005.

Hall, A. and M. Visbeck, 2002: Synchronous variability in the Southern Hemisphere atmosphere, sea ice, and ocean resulting from the Annular Mode. *J. Clim.*, **15**, 3043–3057.

Hallberg, R., 1995: Some aspects of the circulation in ocean basins with isopycnals intersecting the sloping boundaries. Ph.D. thesis, University of Washington, Seattle.

Hallberg, R. and A. Adcroft, 2009: Reconciling estimates of the free surface height in Lagrangian vertical coordinate ocean models with mode-split time stepping. *Ocean Modell.*, **29**, 15–26.

Hallberg, R. and A. Gnanadesikan, 2006: The role of eddies in determining the structure and response of the wind-driven Southern Hemisphere overturning: Results from the Modeling Eddies in the Southern Ocean (MESO) project. *J. Phys. Oceanogr.*, **36**, 2232–2252.

Hirabara, M., H. Ishizaki, and I. Ishikawa, 2007: Effects of the westerly wind stress over the Southern Ocean on the meridional overturning. *J. Phys. Oceanogr.*, **37**, 2114–2132.

Hofmann, M. and M. A. Morales Maqueda, 2011: The response of Southern Ocean eddies to increased midlatitude westerlies: A non-eddy resolving model study. *Geophys. Res. Lett.*, **38**, L03605.

Hogg, A. M., 2010: An Antarctic Circumpolar Current driven by surface buoyancy forcing. *Geophys. Res. Lett.*, **37**, L23 601.

Hogg, A. M., H. A. Dijkstra, and J. A. Saenz, 2013: The energetics of a collapsing meridional overturning circulation. *J. Phys. Oceanogr.*, **43**, 1512–1524.

Hogg, A. M. C., M. P. Meredith, J. R. Blundell, and C. Wilson, 2008: Eddy heat flux in the Southern Ocean: Response to variable wind forcing. *J. Clim.*, **21**, 608–620.

Huang, B., P. H. Stone, and C. Hill, 2003: Sensitivities of deep-ocean heat uptake and heat content to surface fluxes and subgrid-scale parameters in an ocean general circulation model with idealized geometry. *J. Geophys. Res.*, **108**, C13 015.

Hughen, K., J. Southon, S. Lehman, C. Bertrand, and J. Turnbull, 2006: Marine-derived ^{14}C calibration and activity record for the past 50,000 years updated from the Cariaco Basin. *Quaternary Sci. Rev.*, **25**, 3216–3227.

Ishii, M., A. Shouji, S. Sugimoto, and T. Matsumoto, 2005: Objective analyses of sea-surface temperature and marine meteorological variables for the 20th century using ICOADS and the Kobe Collection. *Int. J. Climatol.*, **25**, 865–879.

Jones, D. C., T. Ito, and N. S. Lovenduski, 2011: The transient response of the Southern Ocean pycnocline to changing atmospheric winds. *Geophys. Res. Lett.*, **38**, L15 604.

Juranek, L. W., R. a. Feely, D. Gilbert, H. Freeland, and L. a. Miller, 2011: Real-time estimation of pH and aragonite saturation state from Argo profiling floats: Prospects for an autonomous carbon observing strategy. *Geophys. Res. Lett.*, **38**, L17 603.

Karoly, D. J., 2003: Ozone and climate change. *Science*, **302**, 236–237.

Kawano, T., T. Doi, H. Uchida, S. Kouketsu, M. Fukasawa, Y. Kawai, and K. Katsumata, 2010: Heat content change in the Pacific Ocean between the 1990s and 2000s. *Deep-Sea Res. Pt. II*, **57**, 1141–1151.

Kirkman, C. H. and C. M. Bitz, 2011: The effect of the sea ice freshwater flux on Southern Ocean temperatures in CCSM3: Deep-ocean warming and delayed surface warming. *J. Clim.*, **24**, 2224–2237.

Klocker, A. and T. J. McDougall, 2010: Influence of the nonlinear equation of state on global estimates of dianeutral advection and diffusion. *J. Phys. Oceanogr.*, **40**, 1690–1709.

Kouketsu, S., et al., 2011: Deep ocean heat content changes estimated from observation and reanalysis product and their influence on sea level change. *J. Geophys. Res.*, **116**, C03 012.

Latif, M., T. Martin, and W. Park, 2013: Southern Ocean sector centennial climate variability and recent decadal trends. *J. Clim.*, **26**, 7767–7782.

Lauderdale, J. M., A. C. Naveira Garabato, K. I. C. Oliver, M. J. Follows, and R. G. Williams, 2013: Wind-driven changes in Southern Ocean residual circulation, ocean carbon reservoirs and atmospheric CO_2. *Clim. Dyn.*, **41**, 2145–2164.

Le Quéré, C., et al., 2007: Saturation of the Southern Ocean CO_2 sink due to recent climate change. *Science*, **316**, 1735–1738.

Le Quere, C., et al., 2009: Trends in the sources and sinks of carbon dioxide. *Nat. Geosci.*, **2**, 831–836.

Levitus, S., (Ed.) , 2010: *NOAA Atlas NESDIS 68 and 69.* U.S. Gov. Print. Off., Washington, D.C.

Levitus, S., et al., 2012: World ocean heat content and thermosteric sea level change (0-2000 m), 1955-2010. *Geophys. Res. Lett.*, **39**, L10 603.

Lovenduski, N. S., N. Gruber, and S. C. Doney, 2008: Toward a mechanistic understanding of the decadal trends in the Southern Ocean carbon sink. *Global Biogeochem. Cy.*, **22**, GB3016.

Lumpkin, R. and K. Speer, 2007: Global ocean meridional overturning. *J. Phys. Oceanogr.*, **37**, 2550–2562.

Manabe, S. and R. J. Stouffer, 1995: Simulation of abrupt climate change induced by freshwater input to the North Atlantic Ocean. *Nature*, **378**, 165–167.

Marshall, G. J., 2003: Trends in the southern annular mode from observations and reanalyses. *J. Clim.*, **16**, 4134–4143.

Marshall, J., A. Adcroft, C. Hill, L. Perelman, and C. Heisey, 1997: A finite-volume, incompressible Navier Stokes model for studies of the ocean on parallel computers. *J. Geophys. Res.*, **102**, 5753–5766.

Marshall, J. and T. Radko, 2003: Residual-mean solutions for the Antarctic Circumpolar Current and its associated overturning circulation. *J. Phys. Oceanogr.*, **33**, 2341–2354.

Marshall, J. and K. Speer, 2012: Closure of the meridional overturning circulation through Southern Ocean upwelling. *Nat. Geosci.*, **5**, 171–180.

Marsland, S. J., J. A. Church, N. L. Bindoff, and G. D. Williams, 2007: Antarctic coastal polynya response to climate change. *J. Geophys. Res.*, **112**, C07 009.

Martin, T., W. Park, and M. Latif, 2013: Multi-centennial variability controlled by Southern Ocean convection in the Kiel Climate Model. *Clim. Dyn.*, **40**, 2005–2022.

Meijers, A. J. S., N. L. Bindoff, and S. R. Rintoul, 2011: Frontal movements and property fluxes: Contributions to heat and freshwater trends in the Southern Ocean. *J. Geophys. Res.*, **116**, C08 024.

Menviel, L., A. Timmermann, A. Mouchet, and O. Timm, 2008: Climate and marine carbon cycle response to changes in the strength of the Southern Hemispheric westerlies. *Paleoceanography*, **23**, PA4201.

Menviel, L., A. Timmermann, O. E. Timm, and A. Mouchet, 2010: Climate and biogeochemical response to a rapid melting of the West Antarctic Ice Sheet during interglacials and implications for future climate. *Paleoceanography*, **25**, PA4231.

Meredith, M. P. and A. M. Hogg, 2006: Circumpolar response of Southern Ocean eddy activity to a change in the Southern Annular Mode. *Geophys. Res. Lett.*, **33**, L16 608.

Meredith, M. P., A. C. Naveira Garabato, A. M. Hogg, and R. Farneti, 2012: Sensitivity of the overturning circulation in the Southern Ocean to decadal changes in wind forcing. *J. Clim.*, **25**, 99–110.

Morrison, A. K. and A. M. Hogg, 2013: On the relationship between Southern Ocean overturning and ACC transport. *J. Phys. Oceanogr.*, **43**, 140–148.

Morrison, A. K., A. M. Hogg, and M. L. Ward, 2011: Sensitivity of the Southern Ocean overturning circulation to surface buoyancy forcing. *Geophys. Res. Lett.*, **38**, L14 602.

Munday, D. R., H. L. Johnson, and D. P. Marshall, 2013: Eddy saturation of equilibrated circumpolar currents. *J. Phys. Oceanogr.*, **43**, 507–532.

Munk, W. H. and E. Palmen, 1951: Note on the dynamics of the Antarctic Circumpolar Current. *Tellus*, **3**, 4–6.

Nikurashin, M. and G. Vallis, 2012: A theory of the interhemispheric meridional overturning circulation and associated stratification. *J. Phys. Oceanogr.*, **42**, 1652–1667.

Olbers, D., D. Borowski, C. Volker, and J. O. Wolff, 2004: The dynamical balance, transport and circulation of the Antarctic Circumpolar Current. *Antarct. Sci.*, **16**, 439–470.

Olbers, D. and M. Visbeck, 2005: A model of the zonally averaged stratification and overturning in the Southern Ocean. *J. Phys. Oceanogr.*, **35**, 1190–1205.

Petit, J. R., et al., 1997: Four climate cycles in Vostok ice core. *Nature*, **387**, 126.

Purkey, S. G. and G. C. Johnson, 2010: Warming of global abyssal and deep Southern Ocean Waters between the 1990s and 2000s: Contributions to global heat and sea level rise budgets. *J. Clim.*, **23**, 6336–6351.

Purkey, S. G. and G. C. Johnson, 2013: Antarctic Bottom Water warming and freshening: Contributions to sea level rise, ocean freshwater budgets, and global heat gain. *J. Clim.*, **26**, 6105–6122.

Radko, T. and I. Kamenkovich, 2011: On the link between the two modes of the ocean thermohaline circulation and the formation of global-scale water masses. *J. Phys. Oceanogr.*, **41**, 757–780.

Rayner, N. A., D. E. Parker, E. B. Horton, C. K. Folland, L. V. Alexander, and D. P. Rowell, 2003: Global analyses of sea surface temperature, sea ice, and night marine air temperature since the late nineteenth century. *J. Clim.*, **108**, D144 407.

Redi, M. H., 1982: Oceanic isopycnal mixing by coordinate rotation. *J. Phys. Oceanogr.*, **12**, 1154–1158.

Reynolds, R. W., N. A. Rayner, T. M. Smith, D. C. Stokes, and W. Wang, 2002: An improved in situ and satellite SST analysis for climate. *J. Clim.*, **15**, 1609–1625.

Rignot, E., I. Velicogna, M. R. van den Broeke, A. Monaghan, and J. Lenaerts, 2011: Acceleration of the contribution of the Greenland and Antarctic ice sheets to sea level rise. *Geophys. Res. Lett.*, **38**, L05 503.

Rintoul, S. R., C. Hughes, and D. Olbers, 2001: The Antarctic Circumpolar Current System. *Ocean Circulation and Climate*, G. Siedler, J. A. Church, and J. Gould, Eds., Academic, London, chap. 4.6.

Rivas, D., A. Badan, J. Sheinbaum, J. Ochoa, and J. Candela, 2008: Vertical velocity and vertical heat flux observed within Loop Current eddies in the central Gulf of Mexico. *J. Phys. Oceanogr.*, **38**, 2461–2481.

Sabine, C. L., et al., 2004: The oceanic sink for anthropogenic CO_2. *Science*, **305**, 367–371.

Saenko, O. A., J. C. Fyfe, and M. H. England, 2005: On the response of the oceanic wind-driven circulation to atmospheric CO_2 increase. *Clim. Dyn.*, **25**, 415–426.

Saenko, O. A., A. Sen Gupta, and P. Spence, 2012: On challenges in predicting bottom water transport in the Southern Ocean. *J. Clim.*, **25**, 1349–1356.

Saenko, O. A., A. J. Weaver, and J. M. Gregory, 2003: On the link between the two modes of the ocean thermohaline circulation and the formation of global-scale water masses. *J. Clim.*, **16**, 2797–2801.

Sen Gupta, A. and M. H. England, 2006: Coupled ocean-atmosphere-ice response to variations in the Southern Annular Mode. *J. Clim.*, **19**, 4457–4486.

Shimada, K., S. Aoki, K. I. Ohshima, and S. R. Rintoul, 2012: Influence of Ross Sea Bottom Water changes on the warming and freshening of the Antarctic Bottom Water in the Australian-Antarctic Basin. *Ocean Sci.*, **8**, 419–432.

Siegenthaler, U. and T. Wenk, 1984: Rapid atmospheric CO_2 variations and ocean circulation. *Nature*, **308**, 624–626.

Sigman, D. M. and E. A. Boyle, 2000: Glacial/interglacial variations in atmospheric carbon dioxide. *Nature*, **407**, 859–869.

Sigman, D. M., M. P. Hain, and G. H. Haug, 2010: The polar ocean and glacial cycles in atmospheric CO_2 concentration. *Nature*, **466**, 47–55.

Skinner, L. C., S. Fallon, C. Waelbroeck, E. Michel, and S. Barker, 2010: Ventilation of the deep Southern Ocean and deglacial CO_2 rise. *Science*, **328**, 1147–1151.

Sloyan, B. M., S. E. Wijffels, B. Tilbrook, K. Katsumata, A. Murata, and A. M. Macdonald, 2013: Deep ocean changes near the western boundary of the South Pacific Ocean. *J. Phys. Oceanogr.*, **43**, 2132–2141.

Smith, T. M., R. W. Reynolds, T. C. Peterson, and J. Lawrimore, 2008: Improvements to NOAA's historical merged land-ocean surface temperature analysis (1880-2006). *J. Clim.*, **21**, 2283–2296.

Speer, K., E. Guilyardi, and G. Madec, 2000a: Southern Ocean transformation in a coupled model with and without eddy mass fluxes. *Tellus*, **52A**, 554–565.

Speer, K., S. R. Rintoul, and B. Sloyan, 2000b: The diabatic Deacon cell. *J. Phys. Oceanogr.*, **30**, 3212–3222.

Stewart, A. L. and A. F. Thompson, 2012: Sensitivity of the ocean's deep overturning circulation to easterly Antarctic winds. *Geophys. Res. Lett.*, **39**, L18 604.

Stouffer, R. J., D. Seidov, and B. J. Haupt, 2007: Climate response to external sources of freshwater: North Atlantic versus the Southern Ocean. *J. Clim.*, **20**, 436–448.

Straub, D. N., 1993: On the transport and angular-momentum balance of channel models of the Antarctic Circumpolar Current. *J. Phys. Oceanogr.*, **23**, 776–782.

Swingedouw, D., T. Fichefet, H. Goosse, and M. F. Loutre, 2008: Impact of transient freshwater releases in the Southern Ocean on the AMOC and climate. *Clim. Dyn.*, **33**, 365–381.

Takahashi, T., C. Sweeney, B. Hales, D. W. Chipman, T. Newberger, and J. G. Goddard, 2012: The changing carbon cycle in the Southern Ocean. *Oceanography*, **25**, 26–37.

Talley, L. D., 2008: Freshwater transport estimates and the global overturning circulation: Shallow, deep and throughflow components. *Prog. Oceanogr.*, **78**, 257–303.

Talley, L. D., 2013: Closure of the global overturning circulation through the Indian, Pacific, and Southern Oceans: Schematics and transports. *Oceanography*, **26**, 80–97.

Thompson, D. W. J. and S. Solomon, 2002: Interpretation of recent Southern Hemisphere climate change. *Science*, **296**, 895–899.

Thompson, D. W. J., S. Solomon, P. J. Kushner, M. H. England, K. M. Grise, and D. J. Karoly, 2011: Signatures of the Antarctic ozone hole in Southern Hemisphere surface climate change. *Nat. Geosci.*, **4**, 741–749.

Toggweiler, J. R., J. L. Russell, and S. R. Carson, 2006: Midlatitude westerlies, atmospheric CO_2, and climate change during the ice ages. *Paleoceanography*, **21**, PA2005.

Toggweiler, J. R. and B. Samuels, 1993: Is the magnitude of the deep outflow from the Atlantic Ocean actually governed by Southern Hemisphere winds? *The Global Carbon Cycle*, M. Heimann, Ed., Springer, Heidelberg, Germany, 303–331.

Toggweiler, J. R. and B. Samuels, 1995: Effect of Drake Passage on the global thermohaline. *Deep-Sea Res. Pt. II*, **42**, 477–500.

Tschumi, T., F. Joos, and P. Parekh, 2008: How important are Southern Hemisphere wind changes for low glacial carbon dioxide? A model study. *Paleoceanography*, **23**, PA4208.

Viebahn, J. and C. Eden, 2010: Towards the impact of eddies on the response of the Southern Ocean to climate change. *Ocean Modell.*, **34**, 150–165.

Watson, A. J. and A. C. Naveira Garabato, 2006: The role of Southern Ocean mixing and upwelling in glacial-interglacial atmospheric CO_2 change. *Tellus B*, **58**, 73–87.

Waugh, D. W., F. Primeau, T. Devries, and M. Holzer, 2013: Recent changes in the ventilation of the southern oceans. *Science*, **339**, 568–570.

Winton, M., R. W. Hallberg, and A. Gnanadesikan, 1998: Simulation of density-driven frictional downslope flow in z-coordinate ocean models. *J. Phys. Oceanogr.*, **28**, 2163–2174.

Wolfe, C. L. and P. Cessi, 2009: Overturning circulation in an eddy-resolving model: The effect of the pole-to-pole temperature gradient. *J. Phys. Oceanogr.*, **39**, 125–142.

Wolfe, C. L., P. Cessi, J. L. McClean, and M. E. Maltrud, 2008: Vertical heat transport in eddying ocean models. *Geophys. Res. Lett.*, **35**, L23 605.

Xie, P. and G. K. Vallis, 2012: The passive and active nature of ocean heat uptake in idealized climate change experiments. *Clim. Dyn.*, **38**, 667–684.

Zhang, J., 2007: Increasing Antarctic sea ice under warming atmospheric and oceanic conditions. *J. Clim.*, **20**, 2515–2529.